Understanding Basic Mechanisms of Neurovascular Coupling in Physiological Conditions and Hypertension

---

Dissertation

zur

Erlangung der naturwissenschaftlichen Doktorwürde

(Dr. sc. nat.)

vorgelegt der

Mathematisch-naturwissenschaftlichen Fakultät

der

Universität Zürich

von

Novella Calcinaghi

aus

Italien

Promotionskomitee

Prof. Dr. Jean-Marc Fritschy (Vorsitz)

Prof. Dr. Bruno Weber (Leitung der Dissertation)

Prof. Dr. Roland Wenger

Dr. Renaud Jolivet

Zürich, 2012

To my wonderful parents
and to my beloved family,
Francesco and Angelo.

Table of Contents

List of figures

Summary

The brain relies on the continuous supply of energetic substrates through the vascular system. Upon increased neuronal activity, the increase in cerebral blood flow (CBF) is commensurate to a raise in energy needs. This highly regulated link is termed as neurovascular coupling (NVC). CBF modulation occurs at the neurovascular unit (NVU) by means of an orchestrated interplay between neurons, astrocytes and micro-vessels. Yet, the basic cellular mechanisms which underlie this stimulus-dependent CBF increase in NVC have not been fully elucidated and research in this field is currently on-going. Furthermore, NVC is disrupted in pathological conditions associated with cerebrovascular dysfunction such as stroke or Alzheimer's disease.

The experimental work described in this thesis aimed to investigate basic mechanisms of NVC in physiological conditions and NVC impairment in the presence of hypertension.

In the first part of the thesis I investigated if the pathway activated by the metabotropic glutamate receptor $mGluR_5$ is directly involved in the hemodynamic response initiation in the rat somatosensory cortex. Recently, a comprehensive model has been proposed in which astrocytes are activated by glutamate through $mGluR_5$, with a subsequent spread of intracellular Ca^{2+} transients and activation of phospholipase A_2. Phospholipase A_2, in turn, activates a variety of pathways that ultimately lead to the astrocytic release of several vasoactive agents. Using concurrent optical imaging and determination of receptor occupancy with radiolabelled ^{11}C-ABP688, we report that blocking up to 80% of $mGluR_5$ *in vivo* does not impair hemodynamic responses upon brief whisker stimulations while transiently reducing neuronal activity as measured by voltage-sensitive dye imaging. The reported data challenge the model outlining the astrocytes as first responders and principal mediators of functional hyperemia *in vivo*. Furthermore, our data are consistent with other *in vivo* experimental results, demonstrating astrocytic Ca^{2+} waves to be delayed in comparison to the vasodilation onset upon stimulation.

In a second study, NVC mechanisms were investigated in Spontaneous Hypertensive Rats (SHR), a well-established animal model of arterial hypertension. We studied CBF and hemodynamic responses upon whisker stimulation in SHR of different ages (10-20 and 40 weeks) and in age-matched Wystar Kyoto rats (CTRL). We applied a multimodal imaging approach using multiwavelength spectroscopy, laser speckle imaging, and two-photon microscopy. Compared to controls, increased arterial blood pressure in SHRs was associated with a progressive impairment in functional hyperemia in 20 and 40 weeks old SHRs. Baseline capillary red blood cell velocity (RBC) was higher in 40 weeks SHRs compared to CTRLs. Ten weeks treatment with verapamil or losartan did not reverse the hemodynamic impairment in 40 weeks old SHR but restored the RBC velocity measured in the resting condition. Impaired neurovascular coupling in SHR occurs only after a sustained period of increased blood pressure. Hence, monotherapy with verapamil or losartan is not sufficient to abolish this functional impairment.

This thesis contributes to a better understanding of the basic mechanisms underlying NVC in physiological condition. Furthermore, it sheds light on the alteration of functional hyperemia in hypertension, one of the factors that may underlie the cerebrovascular component of important cognitive disorders.

Zusammenfassung

Die kontinuierliche Energieversorgung des Gehirns wird über ein weit verzweigtes Gefässsystem und einen fein regulierten Blutfluss gewährleistet. Bei einer Zunahme der neuronalen Aktivität kommt es zu einer schnellen lokalen Steigerung des zerebralen Blutflusses, um den erhöhten Sauerstoffbedarf des aktiven Nervengewebes zu decken. Dieses orchestrierte Zusammenspiel zwischen neuronaler Aktivität und Hirndurchblutung wird neurovaskuläre Kopplung (NVK) genannt und basiert auf der Interaktion zwischen Astrozyten, Neuronen und Gefässwand (glatte Muskelzellen und Endothelzellen). Obwohl die NVK bereits vor mehr als 100 Jahren zum ersten Mal beschrieben wurde, sind viele der ihr zugrunde liegenden molekularen Mechanismen nicht vollständig geklärt. Gegenwärtig wird dieses Gebiet intensiv erforscht, um die Mechanismen besser zu verstehen. Hinzu kommt, dass die NVK bei vielen pathologischen Zuständen gestört ist, z. B. bei einem Schlaganfall oder degenerativen Hirnerkrankungen, wie der Alzheimer-Krankheit.

In dieser Doktorarbeit wurden zwei grundsätzliche Fragestellungen bearbeitet:

1. Welche Rolle spielt die Aktivierung des metabotropen Glutamatrezeptors mGluR5 für die NVK?
2. Führt die arterielle Hypertonie zu einer Störung der NVK?

In einer ersten Studie wurde untersucht, ob die Aktivierung des metabotropen $mGluR_5$-Glutamat-Rezeptors für die Einleitung einer hämodynamischen Reaktion grundlegend ist. Kürzlich wurde ein umfassendes Modell veröffentlicht, welches postuliert, dass durch neuronaler Aktivität freigesetztes Glutamat astrozytäre $mGluR_5$ aktiviert. Diese Aktivierung setzt eine Kaskade von Prozessen in Gang, welche zu einer Erhöhung und intrazellulären Ausbreitung von Ca^{2+} und nachfolgender Phospholipase A_2-Aktivierung führt. Die Phospholipase A_2 wiederum löst eine Vielzahl von Reaktionen aus, die letztendlich zur Produktion und Freisetzung verschiedener vasoaktiver Substanzen aus den Astrozyten führt. In der vorliegenden Arbeit wurden mittels multimodaler Bildgebung hämodynamische Signale, neuronale Aktivität und die mGluR5 - Rezeptorbelegung gemessen. Es konnte gezeigt werden, dass eine 80%-ige Blockierung des $mGluR_5$ die

hämodynamische Antwort im somatosensorischen Kortex bei kurzer Stimulation der Schnurrhaare *in vivo* nicht beeinträchtigt. Hingegen wurde mittels spannungsabhängigen Farbstoffen eine transiente Verringerung der neuronalen Aktivität beobachtet. Diese Ergebnisse stellen das zuvor postulierte Modell in Frage, welches die Astrozyten als ″first responders″ und Hauptmediatoren der funktionellen Hyperämie beschreibt.

Im zweiten Teil dieser Arbeit untersuchte ich den Einfluss von erhöhtem Blutdruck auf die NVK-Mechanismen bei spontan hypertensiven Ratten (SHR), einem gut etablierten Tiermodell für arterielle Hypertonie. Dazu wurden verschiedene hämodynamische Parameter sowie die Blutflussantwort auf sensorische Stimulation im somatosensorischen Kortex bei spontan hypertensiven Ratten unterschiedlichen Alters (10, 20 und 40-Wochen) gemessen und mit entsprechenden Kontrolltieren verglichen. Dazu wurde eine breite Palette von Imaging-Methoden eingesetzt: ″multiwavelength spectroscopy“, „laser speckle imaging“ und Zwei-Photonen Mikroskopie. Bei 20 und 40 Wochen alten SHR ging die Zunahme des arteriellen Bluthochdrucks einher mit einer deutlichen Beeinträchtigung der funktionellen Hyperämie, bei 10 Wochen alten SHR wurde diese Veränderung der Hyperämie nicht beobachtet. Zusätzlich war die kapillare Ruhedurchblutung in 40 Wochen alten SHR erhöht. Interessanterweise konnte eine 10-wöchige Monotherapie der SHR mit Antihypertensiva (Verapamil und Losartan) die Beeinträchtigung der sensorischen hämodynamischen Antwort bei 40 Wochen alten Tieren nicht rückgängig machen. Der Ruheblutfluss hingegen wurde so pharmakologisch normalisiert. Zusammenfassend kann gesagt werden, dass die Beeinträchtigung der neurovaskulären Kopplung bei arterieller Hypertonie erst nach einem länger andauernden Zeitraum mit erhöhten Blutdruckwerten eintritt. Ausserdem reicht eine Monotherapie mit Verapamil oder Losartan nicht aus, um die funktionelle Einschränkung zu verbessern.

Diese Arbeit hinterfragte die Rolle von astrozytären Calciumwellen für die NVK im gesunden Organismus. Im zweiten Teil wurde der Einfluss einer systemischen hämodynamischen Störung (arterielle Hypertonie) auf die lokale zerebrale Perfusion

untersucht. Sie soll zu einem besseren Verständnis der zerebralen Blutflussantwort sowohl in physiologischen als auch pathologischen Situationen beitragen.

Acknowledgements

This work was carried out during my employment as a PhD Student in Prof. Bruno Weber's laboratory at the institute of Pharmacology and Toxicology, University of Zürich.

My sincere gratitude goes to all of the people who supported me during my PhD.

I would like to thank my supervisor, Prof. Bruno Weber, who gave me the opportunity to work in his laboratory and to complete a PhD at the University of Zürich. Directly from him, I learnt some of the most modern and sophisticated techniques in the *in vivo* brain imaging field. This provided me with an exciting working experience and widely opened my research prospective. I am very grateful to him for the advice and guidance in the experimental activity and for the scientific support in the different phases of the all projects.

I would like to thank Prof. Jean-Marc Fritschy, Prof. Roland Wenger and Dr. Renaud Jolivet for being in my PhD steering committee and for their scientific supervision. In particular, I would like to thank Prof. Jean-Marc Fritschy for giving me the opportunity to learn directly from him and to perform experiments in his laboratory. It was an honor, a big pleasure, and a good time. Special thanks go to Dr. Renaud Jolivet for the fruitful scientific discussions, constant support and for helping me to develop my own scientific thinking.

Thanks to Dr. Matthias Wyss, who was an important reference point for my every day activity in the lab (including the unplanned emergency calls) and for thoroughly reviewing this manuscript. Thanks also to Prof. Freddy Buck and Dr. Anna Keller.

I thank PD Dr. Christian Matter and MD. Stephan Winnik for the interesting collaboration of the SHR project and the Zurich Center for Integrative Human Physiology (ZIHP) for founding it. Thanks to Dr. Fabrizio Gasparini for providing the compound M-MPEP.

Grazie mille to all my colleagues who created a nice working environment and were always available to help me when I asked: Johannes Mayrhofer, Wolfger von der Behrens, Florent Haiss, Vida Skreb, Anand Singh and Philipp Machler. Special Thank belongs to Cristina Zunzunegui for the help in the first months of PhD. Thanks for the nice time spent together to the friends I met at the Pharmacology Institute (Alessandra, Ako, Gonzalo), at the University Hospital (Katrin, Ela, Martina, Nicole, Nadja, Dani, Colette, Nadia, Ola) and thanks to Miriam.

A big grazie goes to my family: to my father and mother, who will be always with me and supported me in any life step with unlimited energy. Grazie for your big and always warm love. Thanks to my brother Mario. I thank my family-in-law for the generous love and help.

Finally, the biggest thank you goes to my husband Francesco, who shared with me the excitement of these years. Thanks to my little son Angelo, who tried hard to study with me during these last months. You are our greatest joy!

Chapter 1. Introduction

Neurovascular coupling: a historical perspective

The human brain has a high energy demand. Although it constitutes only 2% of the body weight, it is responsible for approximately 25% of total body glucose utilization and 20% of total oxygen consumption. Given the brain has limited capacity for energy storage, it is heavily dependent upon the continuous blood supply of energetic substrates (Sokoloff 1960). All brain functions require adequate supply of oxygen and glucose, which are provided through the blood circulation with tight spatiotemporal control. An inadequate supply of energetic substrates leads to neuronal and glial damage, and ultimately cell death. These phenomena have been reported in some pathological conditions such as ischemic stroke and vasospasm following sub-arachnoid hemorrhage (Attwell et al. 2010). In physiological conditions, astrocytes, neurons, microvessels and pericytes tightly interact to induce a rapid and localized increase in cerebral blood flow (CBF), providing the sufficient energy supply to active cells. This process is defined as neurovascular coupling (NVC).

The first observations of NVC were performed more than a century ago by the eminent Italian physiologist Angelo Mosso (Mosso 1881). He performed measurements in patients with skull defects. In particular, Michele Bertini, a 37 year old male, reported a round defect of about 20 mm diameter in his right frontal skull after an accident. This defect represented a suitable brain window to attach Mosso's apparatus containing a sensitive pressure transducer. He continuously measured pulsations and volume changes from the brain window and from the forearm in parallel. This was done in order to separate local brain processes from systemic responses to a task. When either the subject was asked to make a simple calculation or when he reported the result, cerebral blood volume and pulse height increased, whereas the systemic measurements from the forearm were unchanged (Figure 1). Mosso observed for the first time blood flow pulsations variations during certain cognitive events. According to Mosso's notes, this key experiment was performed on September 23rd, 1878, and since then, innumerable experiments have confirmed this initial observation (Raichle and Mintun 2006a). In

1890, the seminal work *On the regulation of the blood-supply of the brain* was published by the British scientists Charles Roy and Charles Sherrington (Roy and Sherrington 1890). By means of oncographic measurements from the parietal cortex of anesthetized dogs, localized increases in blood flow were shown to be coupled to specific stimulation of sensory nerves. Their experimental approach allowed them to extend Mosso's conclusions about regional variations of blood flow corresponding to localized changes in brain activity. One of their key findings was:

> *"Bearing in mind that strong evidence exists of localization of function in the brain, we are of opinion that an automatic mechanism … is well fitted to provide for a local variation of the blood-supply in accordance with local variations of the functional activity".*

These first experimental observations outlined basic concepts in the NVC field that are still the object of investigation today.

Roy and Sherrington also used pharmacological manipulations to assess the importance of vasoactive agents in the initiation and control of NVC. They reported (Roy and Sherrington 1890):

> *"The blood supply of any part of the cerebral tissue is varied in accordance with the activity of the chemical changes which underlie the functional action of that part".*

Since these first pioneering studies, CBF changes evoked by neuronal activity have been extensively used to explore brain function.

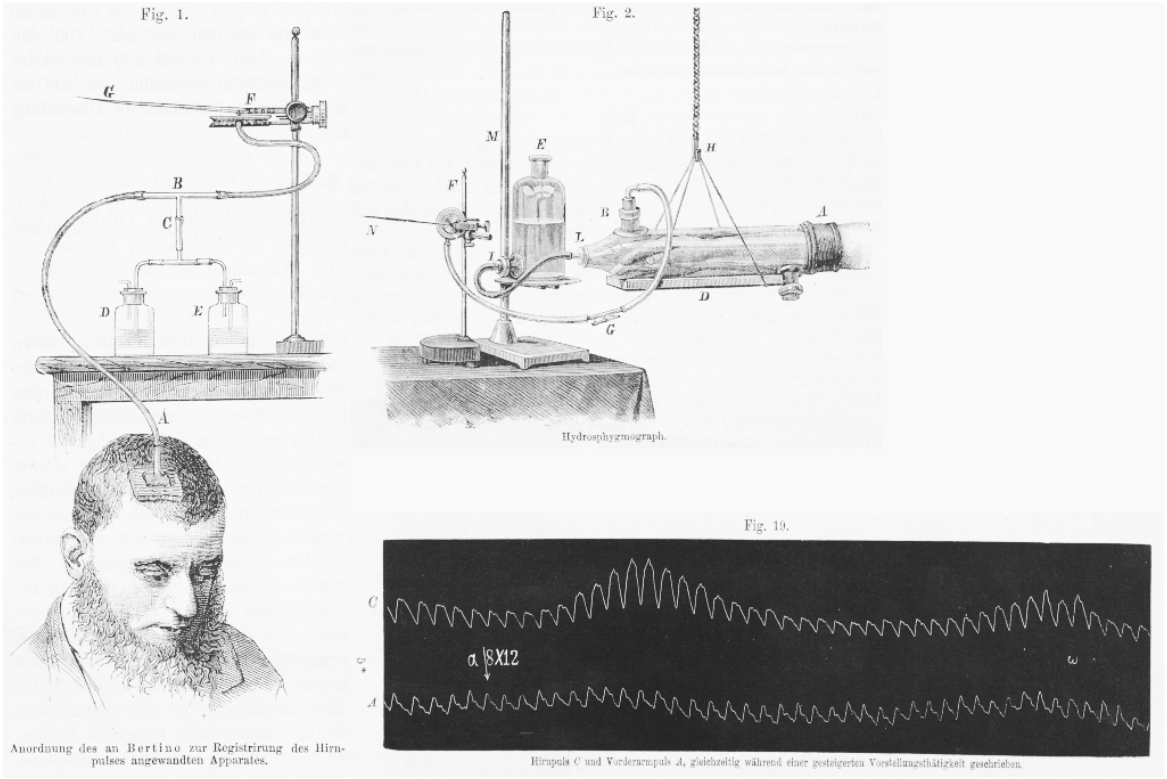

Figure 1. A first open window to investigate neurovascular coupling; Angelo Mosso's experiment in the 1880s.

On the left, drawing of the instrument used to detect cerebral blood pulsations and volume changes from the cranial window of the patient Michele Bertini. On the top right, the instrument used to measure the pressure variations at the forearm is shown. On the bottom right, example traces recorded before and after a calculation task (indicated with α=8x12). Note the increase of cerebral blood pulsations (upper tracer) after the task whereas no change at the forearm level was reported, representing the systemic situation (bottom trace).

In the last century, important progress was made in the field of human brain imaging through the development of new techniques relying on the tight coupling between local neuronal activity increase and subsequent changes in CBF. These brain imaging techniques continue to be refined. One of the most commonly used techniques in basic research is functional magnetic resonance imaging (fMRI). When brain tissue is activated, the fMRI Blood-Oxygenation-Level-Dependent (BOLD) signal increases in response to a decreased amount of deoxyhemoglobin (HbR) in a given region, and is used as a surrogate for neuronal activity.

However, despite significant progress in neuro-imaging, the basic mechanisms underlying the relationship between neuronal activity and CBF are not yet fully elucidated. A better understanding of NVC is essential to properly interpret functional imaging data, now routinely used in patients, and may contribute to the development of new treatments for central nervous system (CNS) disorders.

The vascular organization of the brain and the neurovascular unit

The human brain continuously receives blood at the rate of approximately one liter per minute through two arterial roots: the vertebral arteries and internal carotid arteries. The vertebral arteries band together into the basal artery that, together with the carotid and the posterior communicating arteries, creates a vascular circle at the base of the human brain, known as the circle of Willis, and named after Sir Thomas Willis who described the arterial circle (*circulus arteriosus cerebri*) (Purves et al. 2004). This structure surrounds the base of the hypothalamus and pituitary gland stalk. Due to the numerous anastomoses, it essentially creates redundancy in the vascular system because of the ability to preserve cerebral perfusion to the brain. This occurs even if one of the main input arteries supplying the circle becomes occluded. There are numerous anastomoses within the pial network, but within the cerebral cortex, there is a significant reduction in anastomoses between arteries as well as arterioles.

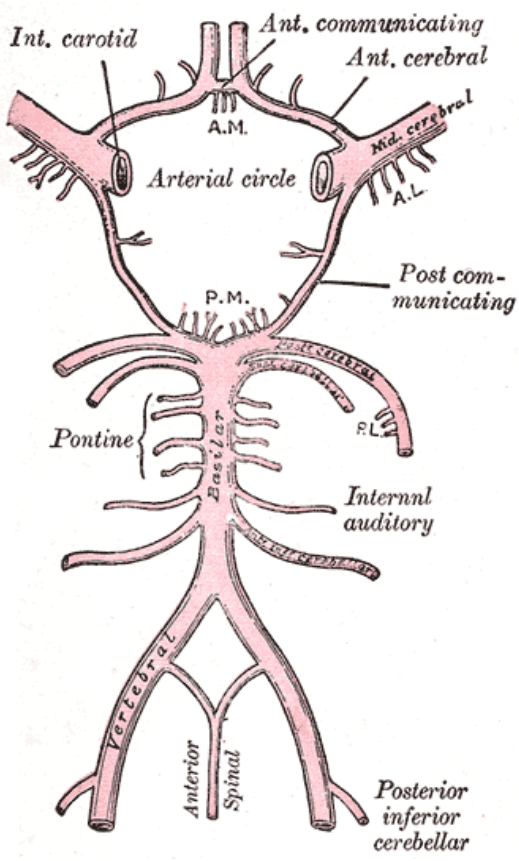

Figure 2. Diagram of the arterial circulation at the base of the brain.

Reproduction of a lithograph plate from Gray's Anatomy of the human body (1918).

As a consequence, even a small arteriolar occlusion can rapidly lead to oxygen deprivation and cause stroke.

For our research, rats were employed as a laboratory animal model. Although the gross anatomical organization of the cerebro-vascular system is largely similar between humans and rats, there are some important differences. These are: (i) the anterior communicating artery is present in humans but not in rats, and (ii) the olfactory artery is present only in rats (Lee 1995).

Large cerebral arteries divide progressively into smaller arteries that run along the surface of the brain, named pial arteries (Figure 3). Pial arteries penetrate deeper into the brain, oriented perpendicular to the surface (cortical arteries). These give rise to cerebral parenchymal arterioles and eventually to capillaries, forming the capillary bed (Jones 1970). The Virchow-Robin, a perivascular funnel-shaped space, is the continuation of the subarachnoid space, surrounding pial arteries, veins and penetrating arterioles. It separates the vessels from the brain parenchyma (Weber et al. 2008; Zhang et al. 1990).

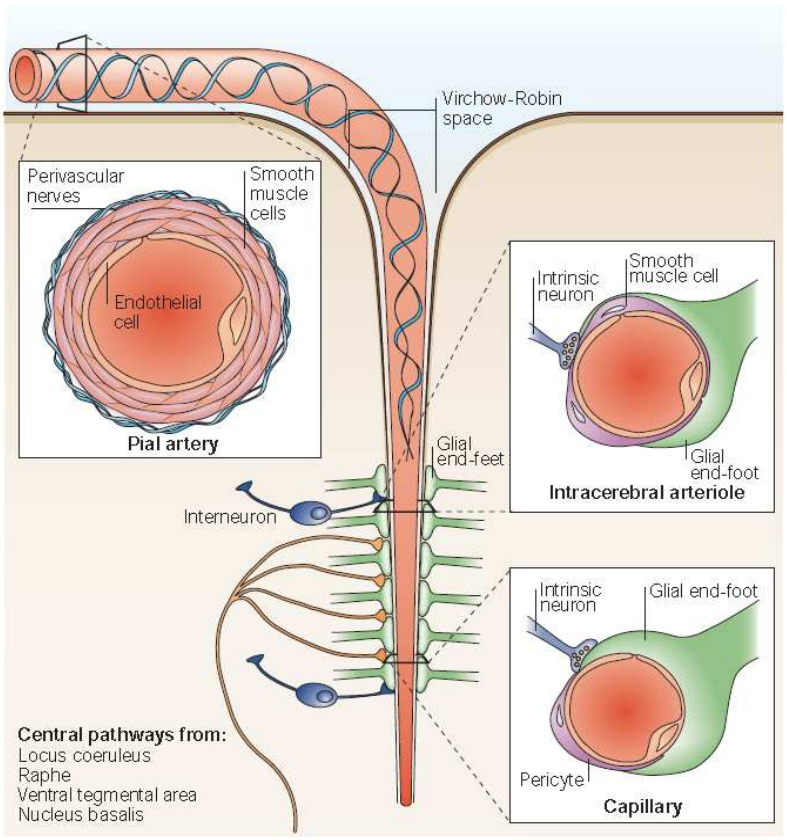

Figure 3. The neurovascular Unit.

Pial arteries penetrate perpendicular to the cortical surface (as so-called cortical arteries) and then divide into intracerebral arterioles and capillaries. SMCs modulate the vessel diameter of arteries and arterioles but are absent in capillaries. At the capillary level, astrocytic endfeet enwrap the vessel wall together with pericytes and perivascular neurons. From Iadecola C. "Neurovascular regulation in the normal brain and in Alzheimer's disease." Nature Reviews Neuroscience, (Iadecola 2004).

As soon as the Virchow-Robin space disappears, parenchymal arterioles and capillaries run within the neuropil, in direct contact with neuronal processes and astrocytic endfeet (Figure 3). At the capillary network level, a tight exchange of energetic substrates and oxygen between tissue and blood occurs.

The capillary bed consists of a dense network of intercommunicating vessels, that totals 400 miles in length in the human brain (Zlokovic 2005), and at this level the exchange of oxygen and nutrients occur. It has been estimated that each neuron has its own capillary, further confirming the importance of the link between vascular compartment and neurons (Cipolla 2009). The venous system ensures that the blood is drained from the capillary bed up to the surface of the brain by ascending vessels, which converge into sinuses.

Generally, the wall of cerebral arteries and arterioles is comprised, from the innermost to the outermost layer, of; the *tunica intima*, with a layer of endothelial cells and the internal elastic lamina, the *tunica media* consisting of smooth muscle cells (SMC), and the *tunica adventitia*, made up of collagen fibers, perivascular nerves and connective tissue. However, between the different vessel types some structural variations in the vessel architecture can be detected. Firstly, perivascular nerves are entwined around the outermost layer of pial arteries (extrinsic innervation) whereas pericytes and astrocytes enwrap the smallest arteries such as arterioles and capillaries. Secondly, the number of SMC layers varies with the size of the vessels, from two to three for pial arteries to only one for arterioles and none in capillaries. Despite these differences, all cerebral vessels have endothelial cells which are sealed by tight junctions and form, together with the basal lamina and pericytes, the Brain Blood Barrier (BBB). The BBB is a physical barrier capable of ensuring neuronal homeostasis and achieves this via strictly regulating the exchange of solutes, water, and nutrients between the blood and the brain (Zlokovic 2008).

The endothelium is supported by the basement membrane and enwrapped by pericytes, astrocytic endfeet and neuronal synapses. Together this constitutes a functional unit, denoted as the neurovascular unit (NVU). Dynamic communication between the cells of the NVU controls different functions such as CBF increase after a

specific stimulation, BBB permeability and homeostatic maintenance during stress response.

Pericytes surround almost all capillaries, small arterioles and venules, sending processes around and along the capillaries. More specifically, they are separated from the endothelial cells layer and the parenchyma by a basal lamina layer. In addition to being part of the NVU, pericytes support several functions such as angiogenesis, vessel stabilization and endothelial cell regulation. Furthermore, anatomical and morphological evidence (e.g. pericytes surround capillaries which lack SMC) suggests that pericytes might have an active role in CBF regulation via capillary lumen modulation, but this topic is highly debated (Hamilton et al. 2010).

Astrocytic endfeet not only partially surround the vessel walls but constitute a complete covering of the brain microvessel walls. The endfeet interdigitate and overlap without leaving slits between them, as observed by electron microscopy 3D reconstruction in the rat hippocampus (Mathiisen et al. 2010).

Following from the above, it is clear, why research in the NVC field has focused primarily on the complex cross-talk between all cell types of the NVU. Following anatomical description of NVU members, their functional contribution to blood flow regulation is described in the “Functional Hyperemia” chapter.

Much of the morphological knowledge of cerebral microvasculature has come from electron microscopy studies of vascular corrosion casts and histochemistry (Weber et al. 2008). In short, Weber et al. (2008) have quantified the vasculature in the macaque visual cortex and report that: (i) vascular density is much higher in gray than in white matter and is highest in layer IV; and (ii) that the relationship between vascular and neuronal density is weak but with a strong correlation between patterns of oxidative metabolism and microvascular density. More recently, two-photon laser scanning microscopy (2PLSM) has been employed to specifically study three-dimensional microvascular topology (Tsai et al. 2009). 2PLSM technology has been utilized also by our group and is further outlined in Chapter 3. In these 2PLSM experiments, the plasma

was labeled with a fluorescent dextran enabling subsequent imaging of the vasculature and the determination of vascular density and vessel lumen diameter in the cortex.

Brain metabolism

Until relatively recently, blood-borne glucose was considered the unique energy substrate supporting neuronal activity in the healthy brain (Sokoloff 1989). Glucose is transported from blood across the BBB and enters the brain via specific glucose transporters (Vannucci et al. 1997). Glucose Transporter 1 (GLUT1) is primarily found on endothelial cells and glia and GLUT3 is found on neurons. After entering the brain cell, glucose is metabolized to CO_2 and water. This occurs via: i) glycolysis, providing 2 mol of adenosine triphosphate (ATP) per mol of glucose; and ii) the tricarboxylic acid (TCA) cycle, providing 30 mol of ATP/mol of glucose.

In 1986, Fox and Raichle used Positron Emission Tomography (PET) to show that activity-dependent increases in CBF and glucose consumption outstrip the concomitant changes in oxygen consumption (Fox and Raichle 1986). Indeed, they challenged the assumption that the majority of energy used by active neurons comes from oxidative phosphorylation rather than glycolysis as the predominant energy source during neuronal activity. The reported mismatch between CBF increase and oxygen consumption causes a restricted hyperoxygenation with decreased HbR which provides the basis for the BOLD signal used by the functional MRI.

In the mid-1990s, Pellerin and Magistretti (1994) observed a stimulation of glucose uptake into astrocytes and subsequent predominant metabolism to lactate. Starting from this experimental evidence, the astrocyte-neuron-lactate shuttle hypothesis (ANLSH) was proposed. According to the ANLSH, the glutamate released from neurons during activation is taken up by astrocytes, leading to an activation of the astrocytic Na^+-K^+ ATPase, which in turn consumes ATP. The reduction in ATP levels stimulates astrocytic glycolysis leading to lactate production. Lactate produced by astrocytes is released to the extracellular space and taken up by neurons to fuel their energetic needs. Furthermore, several reports demonstrated that lactate may constitute the preferred energy substrate for neurons over glucose (Hyder et al. 2006; Jolivet et al. 2009; Wyss

et al. 2010). In addition, various important roles have been attributed to lactate recently. For example, it was shown that lactate released from astrocytes modulates the activity of neighboring GABAergic neurons in the subfornical organ (SFO) (Shimizu et al. 2007) and that lactate dictates the vascular response by controlling the vessel diameter (Gordon et al., 2008). Finally, the flow of extracellular lactate through pericytes was shown to directly control the contractile force exerted on retinal capillaries (Yamanishi et al. 2006). These results suggest that lactate could be at the center of metabolic regulation of brain activity affecting both local blood flow and the energy state of neurons and thus the activity of the local network.

Functional hyperemia

When brain regions are activated by a specific stimulus, CBF increases in the corresponding area. This close coordination between neuronal activity and CBF is denoted as functional hyperemia. To allow CBF increase in a defined area, members of the NVU act in concert to elicit vasodilation at the capillary level, and to regulate the maintenance and termination of the functional hyperemic response. The first hemodynamic response is initiated in the parenchyma, and shortly after (200 ms) spreads to the surface arterioles supplying the activated area (Chen et al. 2010). The blood flow increase is associated with a reduction of vascular resistance that, in arteries and arterioles, is controlled by SMCs.

SMCs are also capable of maintaining constant CBF within a certain blood pressure range (60-150 mm Hg). This process is known as cerebrovascular autoregulation. SMCs contract when the intravascular pressure increases and constrict in response to reduced pressure (Bayliss 1902). The myogenic response is initiated by an increase in blood pressure which depolarizes the SMC membrane and triggers calcium influx via voltage-gated ion channels. Higher intracellular calcium concentration increases myosin light chain phosphorylation and induces vasoconstriction (Brayden et al. 2008). However, SMC vasodilation could be due to hyperpolarization through K^+ channel activation and reduced phosphorylation of myosin light chain upon PGE_2 release (Attwell et al. 2010).

Major hypotheses: metabolic and neurogenic hypotheses

To date, an unanswered question has been: why and how does CBF change with the changes in brain activity? This question has attracted the attention of many scientists in the NVC field during the last century. In examining the literature produced from these investigations, two main theories have arisen attempting to explain the link between CBF and neuronal activity. According to the traditional metabolic hypothesis, CBF increases in order to compensate for the increased need of glucose and oxygen in activated neurons (Raichle and Mintun 2006b). In other words via a negative feedback system, a localized decrease of energetic substrates (Oxygen (O_2) or glucose) or the production of carbon dioxide (CO_2) elicits a compensatory CBF increase. This paradigm may represent an oversimplification of a more complex process. Indeed, the negative feedback mechanism theory is unable to explain compelling evidence such as: (i) blood oxygenation and CBF decrease occur concurrently with an increase in glucose uptake and neuronal activity (Devor et al. 2008); and (ii) stimulus-evoked CBF increases have been recorded also in the absence of deoxygenated hemoglobin (Lindauer et al. 2010). Alternatively, the more recent neurogenic hypothesis has been proposed to explain increased CBF via a feed-forward mechanism. This proposes either active neurons or astrocytes release vasoactive agents into the vessels, eliciting a vascular response without involving metabolic substrates (Attwell et al. 2010) (Figure 4).

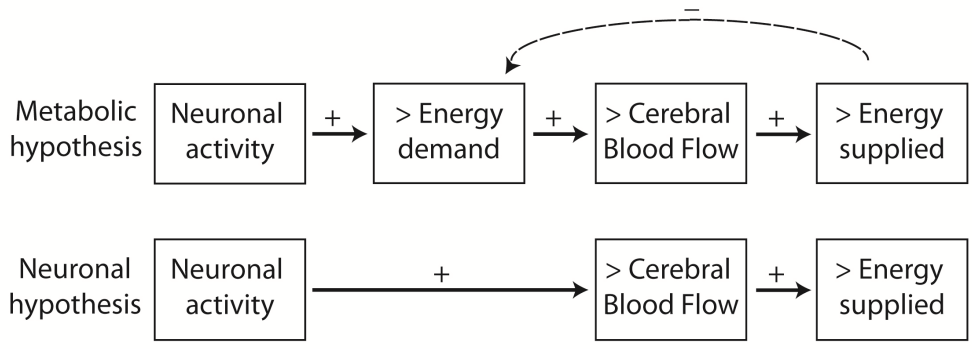

Figure 4. Metabolic and neurogenic hypotheses.

Adapted from Attwell et al. 2010.

Neuronal control of CBF

Current evidence suggests that neurons and astrocytes are both important contributors in the signaling process that links vascular responses to changes in neuronal activity. Focusing first on neurons, hemodynamic responses in the somatosensory cortex have been shown to correlate with local field potentials, indicating that vascular changes are directly linked to incoming neuronal inputs in a specific area (Logothetis et al. 2001).

Here, I briefly describe the perivascular innervations, for a better understanding of the neuronal contribution to cerebrovascular tone.

Extrinsic innervations. Pial arteries and arterioles on the brain surface contain perivascular nerves that originate in the peripheral nervous system (PNS). More specifically, the extrinsic innervation has its origin from different ganglia (Hamel 2006):

(i) The superior cervical ganglion (SCG), from where sympathetic innervations arise releasing neuropeptide Y (NPY) and norepinephrine (NE), both vasoconstrictors;
(ii) The sphenopalatine (SPG) and otic (OG) ganglia, from where parasympathetic nerves originate releasing vasoactive intestinal peptide (VIP), acetylcholine (ACh) and nitric oxide (NO); and
(iii) The trigeminal ganglion (TG), starting point for sensory nerves containing substance P (SP) and calcitonin gene related peptide (CGRP), both vasodilators.

Intrinsic innervations. Parenchymal arterioles and cortical microvessels are innervated from neurons that originate in the CNS. The main vasoactive pathways arise from:

(i) Nucleus basalis with cholinergic projections;
(ii) Raphe nucleus with serotoninergic projections; and
(iii) Locus coeruleus with noradrenergic fibers.

Activation of cholinergic fibers from the basal forebrain (BF) induces significant increases in cortical perfusion together with a dilation of intracortical microvessels (Lecrux et al. 2012). The NVC response following BF stimulation is mediated by glutamate from pyramidal neurons, by EETs, likely released by astrocytes, and possibly by GABA from specific subsets of interneurons. Following stimulation of the locus coeruleus, the observed CBF decrease has been described to be mediated by astrocytes, whereas bidirectional changes in vascular tone have been reported upon raphe nucleus activation (Cohen et al. 1996).

An additional neuronal pathway for the modulation of cortical blood flow occurs via the rostral ventrolateral medulla, whose projections to the cortex are relayed by the interlaminar thalamic nucleus (Golanov and Reis 1996).

Furthermore, other important local pathways involve local inhibitory and excitatory neurons that integrate the signal within the NVU.

GABA interneurons. Inhibitory GABA interneurons have been described to act as "local integrators" of NVC for subcortical regions (Cauli et al. 2004), able to convert neuronal signals into vascular responses. They are indeed positioned in close contact with pyramidal cells and project to neighboring microvessels and astrocytic endfeet.

Different GABA interneurons release vasodilating transmitters such as NO (see below) and vasoactive intestinal peptide (VIP) or vasoconstricting factors, such as the neuropeptide somatostatin (SOM), and NPY (Lecrux and Hamel 2011) (vasoactive molecules collected in the summary table 1). Evidence for the active role of GABA interneurons in NVC was first provided by *in vitro* experiments in brain slices (Cauli et al. 2004). More recently and tellingly, *in vivo* studies (Kocharyan et al. 2008; Lecrux et al. 2011) have suggested that specific GABA interneurons are employed according to the nature of the stimulus. In this connection, GABA interneurons expressing VIP or choline acetyltransferase (ChAT) shape the hemodynamic responses to whisker stimulation via GABA-A mediated synchronization of the cortical network (Lecrux et al. 2011).

Excitatory pyramidal neurons. Glutamate is the primary excitatory neurotransmitter in the CNS (Attwell and Laughlin 2001), activating ionotropic receptors (N-methyl-D-aspartate (NMDA), α-amino-3-hydroxy-5-methyl-4-isoxazolepropionic acid (AMPA), and kainate receptors) and mGluR. Thalamocortical glutamatergic afferent fibers release glutamate at the barrel cortex level and recruit excitatory pyramidal neurons through NMDA activation. This leads to: (i) calcium entry into neurons, nNOS activation and release of the vasodilating NO; (ii) glutamate release which can also directly interact with astrocytes; and (iii) release of prostanoids, the dilatory cyclooxygenase-2 (COX2) derived products (Lecrux et al. 2011).

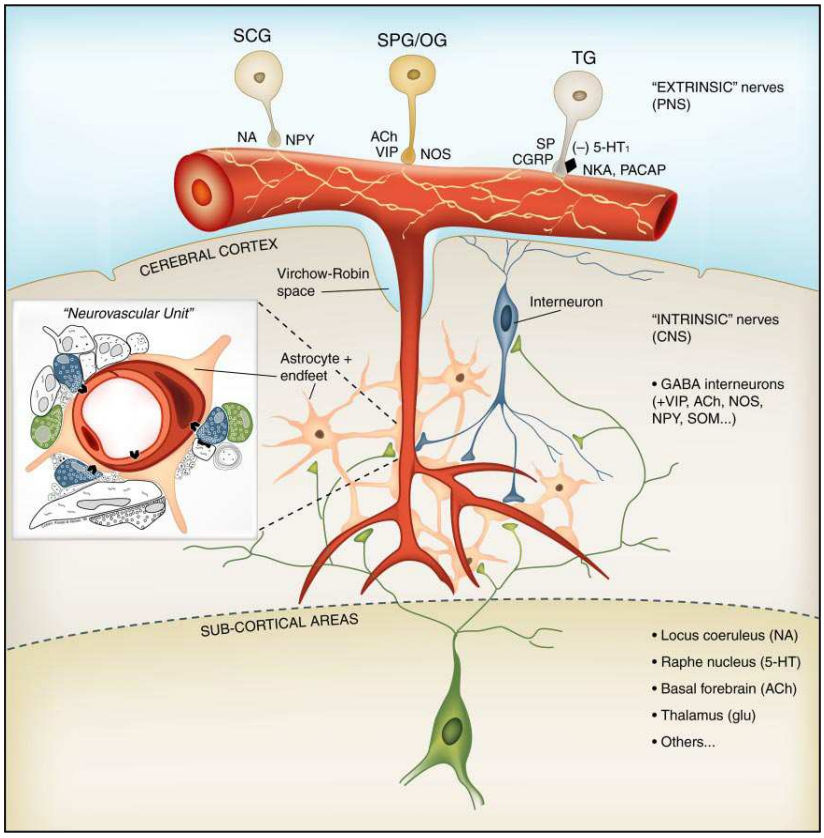

Figure 5. Scheme of the different perivascular nerves.

Extrinsic nerves originate from the peripheral nervous system (superior cervical, sphenopalatine, otic or trigeminal ganglion). Intrinsic nerves from CNS innervate arterioles within the parenchyma. Cortical microvessels receive NA, 5-HT, ACh, or GABAergic afferents from neurons from the locus coeruleus, raphe nucleus, basal forebrain, or local cortical interneurons. From Hamel, E. "Perivascular nerves and the regulation of cerebrovascular tone." J Appl Physiol.(2006).

Nitric Oxide. NO is also an important vasoactive molecule released from neurons. NO is produced by neuronal NO synthase (nNOS) upon NMDA receptor activation and diffuses to vascular SMC where vasodilation is induced by guanylate cyclase stimulation. It has been shown that NO acts as a permissive factor or modulator, rather than a main signaling factor. This is because NO donors can restore completely the attenuation of evoked CBF signals due to nNOS inhibition (Lindauer et al. 1999).

Astrocytes as intermediaries of the neurovascular coupling response

For a long time astrocytes were regarded to be only supportive cells. However, over the last 20 years this view has changed. Accumulating data has corroborated the view that astrocytes act as active partners in the so called “tripartite synapse,”(Perea et al. 2009) and in serving as bridges between active neurons and capillaries (Attwell et al. 2010). From a morphological point of view, astrocytes are in a strategically ideal position. On the one hand, they surround synaptic processes and with their endfeet enwrap blood vessels. Moreover, the processes from a single rodent astrocyte can sense the activity of about 90,000 synapses (Oberheim et al. 2006). Furthermore, each astrocytic domain has minimal overlap with neighboring astrocytic domains, creating glially-defined synaptic islands (Halassa et al. 2007). Additionally, by *in vivo* 2PLSM experiments, peaks of astrocytic laminar density have been shown to mirror the density of capillaries (at 40 µm and at 500 µm below the cortex), (McCaslin et al. 2010) and the neuronal density (peaking at 600 µm), (Tsai et al. 2009) in the mouse somatosensory cortex. This suggests strong physiological interactions between neurons, vessels and astrocytes.

Regarding the role of astrocytes in NVC, Zonta and colleagues (2003) described in acute cortical slices, that arteriolar dilation evoked by electrical stimulation of neuronal afferents, depends on astrocytic calcium wave propagation. After blockade of $mGluR_5$, the CBF response was impaired leading to the conclusion that activation of mGluRs is a key step in evoking astrocytic calcium waves. Furthermore, the authors showed that Ca^{2+} increases in glial cells elicited vasodilation mediated by COX production. However, other *in vitro* experiments have reported conflicting results: Mulligan and colleagues

(2004) observed vasoconstriction mediated by production of the ω-hydroxylase metabolite 20-HETE. Metea and Newman (2006) found that in isolated mammalian retina the different vasomotor responses can be modulated by NO. This plethora of *in vitro* data clearly pointed out the need for *in vivo* studies in which physiological vascular tone is maintained and in which all NVU elements are intact. In the highly cited *in vivo* study by Takano et al. (2006) vasodilation was observed to be associated with elevation of endfoot Ca^{2+} and reduced by a selective COX-1 inhibitor. This suggests that prostaglandin E_2 (PGE_2), a product of COX metabolism, is likely to be involved in CBF regulation. Interestingly, conflicting results have been reported regarding astrocytic activation via $mGluR_5$ in the olfactory bulb. Whereas Petzold and colleagues could replicate a reduction in hemodynamic signal upon $mGluR_5$ blocker application (Petzold et al. 2008), other researchers found the odor evoked signals were independent of ionotropic or metabotropic receptor activation but were affected by blockade of astrocytic glutamate transporter (Gurden et al. 2006). In chapter 3, our research data addressing this question are described.

In addition to the activation of the arachidonic acid metabolites pathway, astrocytic Ca^{2+} increases can also induce potassium ion (K^+) release through activation of large conductance Ca^{2+} sensitive K^+ channels (BK), located on astrocytic endfeet. The K^+ induces vasodilation in SMC by hyperpolarization via inward rectifier K_{ir} channels (Filosa et al. 2006; Girouard et al. 2010).

What determines whether arterioles dilate or constrict upon a high Ca^{2+} concentration in astrocytes? Gordon and colleagues (2008) have shown in acute hippocampal brain slices that the metabolic state of rat brain tissue altered by O_2 availability is the factor responsible for inducing either a vasodilation or vasoconstriction via indirectly modulating lactate production. Nevertheless, these results were not confirmed in a recent *in vivo* study (Lindauer et al. 2010), suggesting that changes in O_2 level in the cortex do not directly regulate NVC. The rat cortex was kept at high O_2 concentration by perfusion with hyperbaric oxygen, but the blood flow response to forepaw stimulation was not affected.

Overall, astrocytes appear undoubtedly to have an important role as intermediaries between neurons and blood vessels. However, further investigations are needed to answer many unresolved questions, for example: What is the temporal sequence in the recruitment of neurons and astrocytes? And, is activation of astrocytes triggered by specific neuronal cell population?

CBF control at the capillary level: role of pericytes

Pericytes have recently been a focus of interest in the neuroscience field due to their potentially important role in modulating vascular resistance at the capillary level. The anatomical features of pericytes have sustained research interest in the NVC field. Beyond their morphology and location, the number of pericytes in the brain is greater than in any other areas of the body, and they express contractile proteins (Hamilton et al. 2010).

Pericytes have been shown to control the capillary diameter in retina and cerebellar brain slices via constriction of capillary diameter in response to NE stimulation and GABA receptor inhibition and via dilation of capillaries in response to glutamate (Peppiatt et al. 2006). Recently, *in vivo* studies have investigated pericyte's role in the intact brain. Using transgenic mice expressing GFP in endothelial cells and pericytes, the capability of pericytes to contract capillaries *in vivo* has been shown by Fernandez-Klett and colleagues (2010). In this study, pericytes induced a constrictive response to a thromboxane A_2 analogue but did not show any induced dilation upon bicuculline application (GABA receptor antagonist). Dilation was only observed in precapillary arterioles, penetrating and pial arterioles, interestingly, indicating that relaxation of capillaries is not required for the development of a functional hyperemic response. Furthermore, the availability of adult viable pericyte-deficient mice allowed to study the effect of pericyte loss. Vascular damage was observed through: (i) reduction in brain microcirculation with consequent reduced CBF responses; and (ii) BBB breakdown (Bell et al. 2010). The importance of pericytes in disease has also been described; after ischemia, pericytes are involved in acute microcirculatory disturbance by contracting in response to oxidative-nitrative stress (Yemisci et al. 2009)

Concerning pericytes function in NVC, *in vivo* research is very recent. Further efforts are required to precisely define the importance of these unique cells in the complex blood flow regulation process both in physiological and pathological conditions (Yemisci et al. 2009).

Table 1. Summary table of vasoactive molecules.

Origin	Effect on vessels	Vasoactive molecule	Mediator
Neurons	Vasodilating	Nitric oxide (NO)	NOS and NPY interneurons (Endothelial cells eNOS)
		Vasoactive intestinal peptide (VIP)	VIP interneurons
		Prostaglandins (PG) and prostaglandin E_2 (PGE_2)	COX_2 pyramidal neurons
		Acetylcholine (Ach)	Subcortical neurons
		Substance P	Peripheral neurons
		γ-aminobutyric acid (GABA)	Interneurons
		Adenosine	
		Calcitonin gene-related peptide (CGRP)	Peripheral neurons
	Vasoconstricting	Somatostatin (SOM)	Somatostatin neurons
		Serotonin (5-HT)	Raphe nucleus neurons
		Noradrenalin (NA)	Locus coeruleus neurons
		Dopamine	Interneurons
		Neuropeptide Y (NPY)	
Astrocytes	Vasodilating	Prostaglandins (PG) and prostaglandin E2 (PGE_2)	COX_1
		Epoxyeicosatrienoic acids (EETs)	P450 epoxygenase
		Adenosine	
	Vasoconstricting	20-HETE	
Vasoactive ions	Vasodilating	High Extracellular $[K^+]$	
		Decreased pH, > $[H^+]$	
	Vasoconstricting	Increased pH, <$[H^+]$	
Blood metabolites	Vasodilating	Lactate	
	Vasoconstricting	CO_2	

The whisker to barrel system

Many nocturnal animals including rodents explore the surrounding environment using their whiskers to detect and spatially locate objects. This so-called whisking, is a backwards and forwards whisker motion used to acquire information from the environment and to identify objects, shapes and textures (Lubke and Feldmeyer 2007).

Whiskers in the rat snout are organized in a grid with 5 different rows, named from A to E, and arcs, numbered from 1 to 5 or up to 9. Consequently, each whisker is uniquely denoted by the coordinates of a row and an arc, e.g C2. This layout of the whiskers is reproduced in all rat snouts. Each whisker is attached to the skin by a follicle, innervated by the peripheral branches of 200 cells of the trigeminal ganglion. At the follicle level, each whiskers mechanical movement is converted into an action potential of these nerve endings, bearing the sensory information from the whisker follicles to the brain stem nuclei. The trigeminal nuclei convey afferent vibrissal information to the thalamus via parallel pathways that then reach the barrel field of the somatosensory cortex. Every single whisker is strongly connected to a single barrelette at the brain stem level, to a barreloide at the thalamus, and to a single barrel at the somatosensory cortex. Barrelettes, barelloides, and barrels are arranged as a topographic projection of the whiskers themselves. There is a clear layout of the barrels at the somatosensory cortex that mirrors the whisker map on the rat's snout (Diamond et al. 2008).

Each barrel appears as a 300 μm diameter column that contains 10,000-20,000 neurons, arranged in six layers. These neurons are primarily excitatory neurons providing most of the local, cortico-cortical, and extracortical projections, as well as inhibitory GABA interneurons (Lubke and Feldmeyer 2007). Additionally, the glutamatergic neurons form cortico-cortical synapses and reciprocally connect the primary somatosensory cortex to the secondary somatosensory corte and primary motor cortex on the same hemisphere.

Given the glutamatergic pathway from the whisker to the barrel cortex has been so well described, the whisker to barrel system in rodents constitutes an ideal model to

explore NVC mechanisms. For this reason it has been extensively used since pioneering experiments in this field (Orbach et al. 1985).

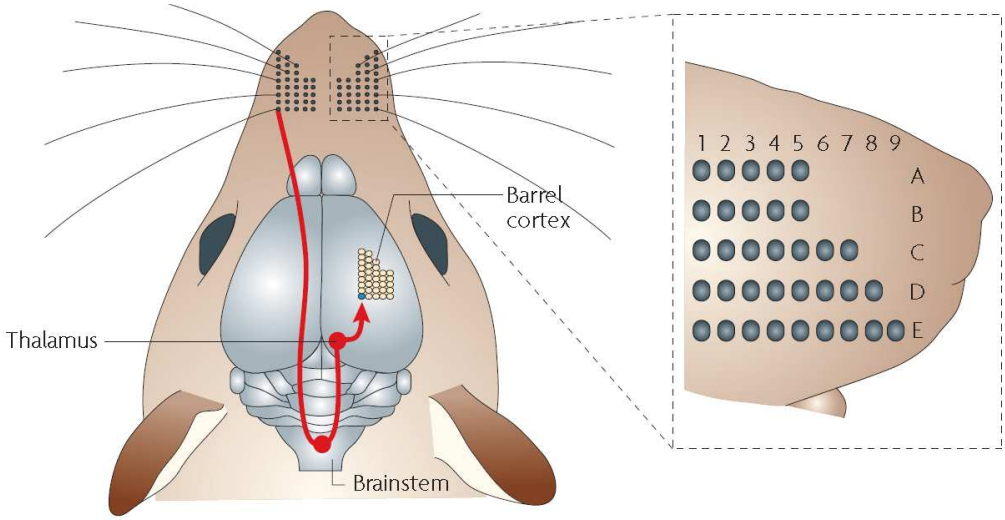

Figure 6. From whisker to barrel cortex: a system often used for NVC studies.

The vibrissae of each side of the rat snout are organized in a grid, formed of 5 rows, each of these containing from 5 to 9 whiskers. Nerve endings bring the information from each whisker to the brain stems, after that neurons project to the thalamic somatosensory nuclei and finally to the barrels of somatosensory cortex. From Diamond, M. E., M. von Heimendahl, et al. "'Where' and 'what' in the whisker sensorimotor system." Nat Rev Neurosci (2008).

Neurovascular coupling in disease: the hypertension example

The effect of hypertension (HT) on NVC is one of our research topics, and is reported in chapter 3. Here, I would like to briefly introduce the main research findings published to date relating to hypertension and NVC.

HT is one of the most widespread health issues facing Western countries and is defined as an elevation of blood pressure above 140 mm Hg systolic or 90 mm Hg diastolic. HT has known deleterious effects on blood supply to the brain and is a strong risk factor for stroke and over time a significant cause of cognitive decline (Dahlof 2007).

From a structural point of view, HT may lead to numerous changes in cerebral arteries and arterioles (e.g. atherosclerosis, hypertrophic remodeling and vascular stiffening), resulting in vascular occlusions, alteration of the mechanical properties of the

vessels, and changes in the composition of the vessel wall. These structural changes have several functional implications. Whereas resting CBF has been reported to be unchanged or slightly reduced, functional hyperemia in HT is attenuated in several animal models and human studies. Overall, structural and functional changes in HT induce an impaired compensatory capacity of the cerebral circulation and increased brain susceptibility to vascular insufficiency (Iadecola and Davisson 2008). Furthermore, oxidative stress is considered a critical factor for HT's cerebro-vascular effects. Reactive oxygen species (ROS) production, increased in cerebral vessels in a model of angiotensin II-induced hypertension, and, more specifically, peroxynitrite, the product of NO and the radical superoxide, constitutes one of the main pathways responsible for deleterious effects of HT (Girouard et al. 2007).

Therefore, although the effect of HT on the brain has recently become an object of increased research interest, many open questions remain. For example, how much does blood pressure need to be reduced to prevent brain damage? What are the possible cognitive deficits? Also, which is the best anti-hypertensive treatment able, not only to reduce blood pressure, but also to protect brain circulation and function? Finally, how do HT and aging interact in the development of cerebro-vascular impairments?

Optical imaging: state of the art

In the last few decades, technological advancement has enabled a broad array of significant findings in the NVC field. Digital cameras and the advent of laser sources have provided new tools for a multifaceted approach to studying *in vivo* CBF regulation with previously unreached spatial and temporal resolution. Despite these advancements, numerous questions remain which may now begin to be answered with recently improved imaging tools. Here, I will focus on recent developments in optical microscopy technologies for *in vivo* studies on NVC and neurometabolism. Some of these developments are described in more detail in the methods section of chapter 3.

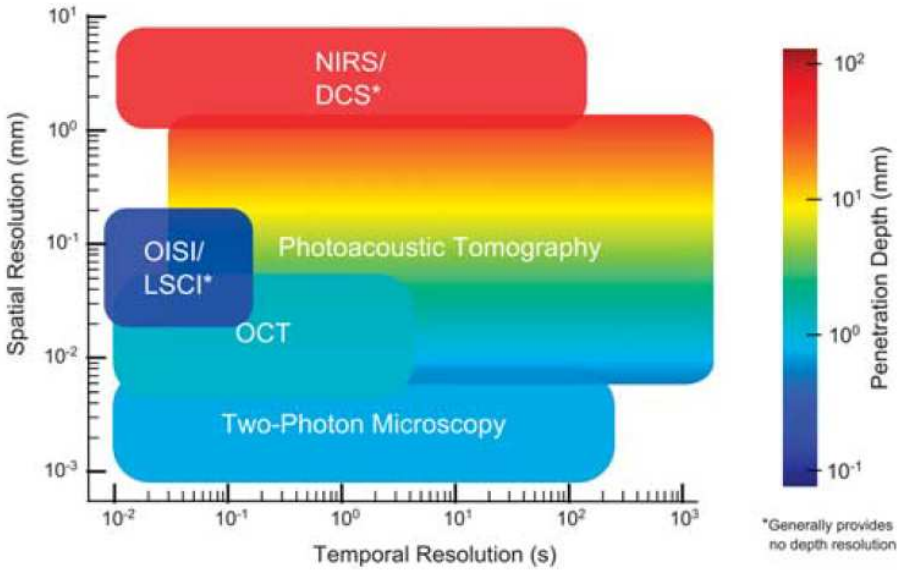

Figure 7. Comparison of optical images technologies.

Comparison of spatial resolution, temporal resolution and penetration depth of neurovascular and neuro metabolic optical imaging techniques. From Devor, A., S. Sakadzic, et al. "Frontiers in optical imaging of cerebral blood flow and metabolism." J Cereb Blood Flow Metab. (2012).

Vascular and hemodynamic imaging

Hemoglobin concentration and oxygenation

Optical intrinsic imaging. 25 years ago, Grinvald and colleagues introduced intrinsic optical imaging (IOI) for studying cerebral functions *in vivo*. The absorption spectra of oxy- hemoglobin (HbO) and HbR have different profiles in the visible and near-infrared spectrum. Thus measurements at different wavelengths provide temporal and spatial variations of HbO and HbR concentrations subsequent to sensory stimulation (Lieke et al. 1989). IOI requires a cranial window or thinned skull preparation which is illuminated by light and images of the reflected light are taken by a camera. Most of the signal detected with this method originates from the top 500 µm of cortex. IOI signals were extensively used to characterize the functional organization of the cerebral cortex (Grinvald et al. 1991) and the temporal profile of the hemodynamic response. Details of this methodology are further described in Paper 1.

Near Infrared spectroscopy. Near infrared spectroscopy (NIRS) is based on the same principle as IOI, namely, near infrared light monitors changes in hemoglobin

concentration via absorption spectroscopy. The main advantage of NIRS lies in the ability to perform measurements through the intact skull and scalp. Therefore, NIRS enables bedside analysis as well as neurodevelopmental assessments in developing infants (Lloyd-Fox et al. 2010).

Blood Flow

Laser Speckle Contrast Imaging. Introduced in 1980, laser speckle contrast imaging (LSCI) is a powerful tool to study blood flow changes in the brain. When laser light is projected onto a brain area a speckle pattern is produced. This speckle pattern can be recorded with the use of a camera. The temporal and spatial intensity fluctuations of the speckle pattern contain information about movements of the scattering particles, in this case red blood cells (RBC). In case of no RBC movement, the speckle pattern appears homogeneous in the entire field and the contrast is maximal. In the presence of moving RBCs the speckle pattern is blurred, i.e. the speckle contrast is reduced. Spatial maps of relative blood flow are obtained by quantification of the contrast of the speckles. In terms of spatial and temporal resolution, LSCI is comparable to IOI (Dunn et al. 2001). Due to the ease of implementation, LSCI has been extensively used to study CBF response to spreading depression, in the retina and in the somatosensory cortex (Devor et al. 2012).

Two-photon laser scanning microscopy. The introduction of 2PLSM has enabled scientists to measure CBF with a notably new approach. It allows depth-resolved monitoring of RBC velocities and vascular diameters in a microscopic fashion. Brain RBC velocity monitoring is obtained through a cranial window by labeling the blood plasma with a fluorescent dye (following *intravenous* injection). When the serum is labeled, RBCs appear as dark objects and by linear scanning along single vessels, temporal-spatial images are acquired. The individual scan lines are stacked upon each other, and from the slope of these black stripes, RBC velocity is calculated as shown in the figure 3 from Paper 2. 2PLSM studies have provided important results in the NVC field. For example, studies of the vascular architecture and of CBF reorganization upon experimental disruptions of the vascular network have been demonstrated (Kleinfeld et al. 1998).

Neuronal Imaging

Voltage Sensitive Dye (VSD) imaging provides a visualization of brain cortical activity with 20-50 µm spatial resolution and a temporal resolution down to 1 millisecond (Chemla and Chavane 2010). The dye molecules, applied to the cortex surface through a cranial window, bind to the external membranes of neuronal and non-neuronal cells. Upon light excitation (630 nm) these cells emit fluorescent light, which is proportional to the changes in membrane potential. Due to its unique temporal resolution, VSD is ideal to monitor dynamics of cortical activity. However, the main limitation of this technique lies in the inability to identify the exact signal origin in different neuronal populations (excitatory or inhibitory) and non-neuronal cells (e.g. glia).

Metabolic Imaging

Phosphorescence lifetime imaging of oxygenation. Phosphorescence lifetime imaging of partial pressure of O_2 ($PLIO_2$) monitors oxygen-dependent phosphorescence lifetimes of an exogenous contrast agent. This technology has been used to measure cerebral intravascular and tissue oxygenation *in vivo*. Recently, $PLIO_2$ has been combined with TPM (Sakadzic et al. 2009) in order to monitor cortical O_2 delivery in tissue and deep microvasculature with unprecedented high spatial resolution. This cutting edge technology has been employed to measure partial pressure of O_2 during sustained neuronal activation. The findings from Devor and colleagues (2011) indicate that the described overshoot in O_2 (Raichle and Mintun 2006b) concentration during sustained stimulus-evoked activation may be a survival mechanism preventing hypoxia at the tissue level, where it is far away from the vascular feeding sources.

Chapter 2. Aims

The study of basic mechanisms underlying NVC is a fascinating topic of research in neuroscience. Understanding how the active brain matches energy demands with local increases of blood flow is important for several reasons. Firstly, brain imaging techniques such as MRI and PET are now widely used in basic and clinical research. These techniques rely on NVC as a surrogate marker of brain activity. However, better understanding of the basic mechanisms of NVC is crucial to allow for clearer interpretation of obtained data. Secondly, NVC is disrupted in numerous neurological disorders and diseases such as hypertension. Better identification of the involved pathways could help to optimize treatments and improve patient outcomes.

The research undertaken for this thesis is divided into two parts. The specific investigation of the involvement of astrocytes in normal NVC forms the first part. Secondly, we examined potential changes of the cerebral hemodynamic responses in hypertension.

More specifically, in the first part, we wanted to investigate the following questions:

1) Does activation of $mGluR_5$ play a major role in the initiation of the hemodynamic response in the rat somatosensory cortex as postulated by earlier studies?
2) What is the effective $mGluR_5$ receptor occupancy upon specifically blocking the receptors?
3) What is the effect of $mGluR_5$ blockade on the evoked neuronal activity?

In the second part, effects of hypertension on NVC were investigated. Hypertension has been shown to impair NVC in animal and human studies. Hence, in our project we were interested in investigating the following questions:

1) What is the influence of arterial HT on evoked hemodynamic responses?
2) Does antihypertensive treatment with losartan or verapamil reverse possible alterations found in hypertensive animals?

3) How does chronically increased blood pressure influence resting CBF at the capillary level? What is the effect of losartan or verapamil treatment on CBF at the capillary level?
4) Is there any evidence of structural or biochemical alterations as a consequence of arterial hypertension?

Chapter 3. Publications

This chapter presents a compilation of the publications of the research performed during the PhD. Each paper is presented as published (or submitted). Papers are presented with their own introduction, methods, results and discussion sections.

For each paper, I report at the beginning:

- The publication journal (or if the manuscript has been submitted, the journal to which it is submitted to),
- A list of citing papers, and
- A list of congresses where the study was presented in poster format or as a talk.

Paper 1

Metabotropic glutamate receptor mGluR5 is not involved in the early hemodynamic response

Novella Calcinaghi[1], Renaud Jolivet[1,*], Matthias T. Wyss[1,2,*], Simon M. Ametamey[3], Fabrizio Gasparini[4], Alfred Buck[2] and Bruno Weber[1]

[1] Institute of Pharmacology and Toxicology, University of Zurich, CH-8091 Zurich, Switzerland

[2] PET Center, Division of Nuclear Medicine, University Hospital Zurich, CH-8091 Zurich, Switzerland

[3] Center for Radiopharmaceutical Science of ETH, PSI, and USZ, Department of Chemistry and Applied Biosciences of ETH, CH-8091 Zurich, Switzerland

[4] Novartis Institutes for Biomedical Research, CH-4001 Basel, Switzerland

* These authors contributed equally to this work.

Published in the *Journal of Cerebral Blood Flow and Metabolism*, (2011), Vol 31 (9), pag: 1967; e1-e10. (Calcinaghi et al. 2011).

Cited, so far, by:

- Lecrux et al. (2012)
- Liu et al. (2012)
- Scott and Murphy (2012)
- Duchemin et al. (2012)
- Milicevic Sephton et al. (2012)

Presented in poster form at the following conferences:

- Swiss Society of Neuroscience, Fribourg, (Switzerland),March 2009

- Zentrum für Neurowissenschaften Zürich (ZNZ) meeting, Zürich (Switzerland), September 2009
- Gordon Research Congress, Ventura (CA),March 2009
- 9th European Meeting on Glial Cells in Health and Disease, Paris (France), September 2009
- Society for Neuroscience (SfN), Chicago (IL), October 2010
- 10th European Meeting on Glial Cells in Health and Disease, Prague, September 2011.

Summary

Recent years have seen a surge in research on the physiology of astrocytes. Several studies have suggested a role for astrocytes in the local control of cerebral blood flow and a comprehensive model has emerged in which neuronal processing activates the metabotropic glutamate receptor $mGluR_5$ on astrocytes, triggering intracellular Ca^{2+} transients and leading to the activation of phospholipase A_2. Phospholipase A_2, in turn, activates a variety of pathways that ultimately leads to the astrocytic release of various vasoactive agents. Using concurrent optical imaging and determination of receptor occupancy with radiolabelled ^{11}C-ABP688, we report here that blocking up to 80% of $mGluR_5$ *in vivo* does not affect hemodynamic responses upon brief whisker stimulations while transiently reducing neuronal activity as measured by voltage-sensitive dye imaging. The results presented here strongly suggest that $mGluR_5$ does not play a crucial role in the transient phase of the hemodynamic response. This conclusion is supported by a large body of literature showing that: [i] expression of $mGluR_5$ is mostly neuronal in physiological conditions and that it is significantly expressed in reactive glia; [ii] metabotropic receptors are in general responsible for slow postsynaptic signaling and it is still unclear whether this is compatible with the speed of early neurovascular events. Finally, other seemingly contradictory results have been reported, notably that spontaneous astrocytic Ca^{2+} surges are independent from metabotropic glutamate or purinergic receptors and that astrocytic Ca^{2+} increases are infrequent and delayed compared to the onset of vasodilation upon a variety of stimulation types in the rat or mouse somatosensory cortex. Thus, the exact mechanism by which astrocytes sense the extracellular glutamate concentration and trigger intracellular events for regulation of the vascular response remains unclear and research on this topic must continue.

Abstract

Activation of astrocytic $mGluR_5$ is postulated to elicit calcium transients, triggering a chain of events that ultimately regulates cerebral blood flow by changing the tone of SMCs of nearby arterioles. Using concurrent *in vivo* optical imaging and determination of receptor occupancy with ^{11}C-ABP688, we report here that blocking up to 80% of

$mGluR_5$ *in vivo* does not affect transient hemodynamic responses upon brief whisker stimulations while transiently reducing neuronal activity as measured by voltage-sensitive dye imaging. Our results demonstrate that mechanisms other than activation of $mGluR_5$ are required to trigger the initial hemodynamic response in normal physiological conditions.

Keywords

astrocytes, neurovascular coupling, glutamate, G-protein-coupled receptor, metabotropic glutamate receptor $mGluR_5$

Introduction

Neurovascular coupling (NVC) refers to the relationship between local neural activity and subsequent changes in cerebral blood flow (CBF). First described by Mosso in 1881 (1881), NVC ensures the proper supply of oxygen and nutrients to active brain regions and was subsequently shown to reflect the relaxation of vascular SMCs – and perhaps pericytes– of a specific brain area in response to a localized enhancement of neuronal activity. NVC is mediated by a complex flow of information among neurons, astrocytes, pericytes and the vasculature, which act in concert to maintain proper cerebral perfusion.

Research in the field of NVC is highly relevant because it provides the basis for a better understanding of widely used functional imaging modalities based on CBF as a surrogate of neuronal activity. Furthermore, many of the most severe neurodegenerative diseases involve the vascular system as well as the supply of blood-borne substrates and oxygen. Although the complex processes governing the regulation of local CBF are not completely understood and many important questions still unanswered, astrocytes have been identified in the last few years as key players in controlling local blood flow. Strategically located in an ideal position between neurons and vessels, astrocytes can integrate neurotransmitter signals from thousands of synapses (Bushong et al. 2002) and relay this information to the arterioles (Metea and Newman 2006). The specific close interactions among these different cell populations have led to the concept of a neuron-astrocyte-vasculature tripartite functional unit (Vaucher and Hamel 1995).

One astrocytic pathway in particular has recently attracted a lot of attention. It has been reported that activation of the astrocytic metabotropic glutamate receptor $mGluR_5$ triggers Ca^{2+} transients in astrocytes (Wang et al. 2006) and affects NVC (Zonta et al. 2003). Antagonists of group I metabotropic glutamate receptors ($mGluR_1$ and $mGluR_5$) were found to inhibit Ca^{2+} elevation in astrocytic endfeet and to reduce CBF increase in the somatosensory cortex of rodents upon forepaw stimulation (Zonta et al. 2003). It is postulated that these astrocytic Ca^{2+} transients lead in turn to the production and release of vasoactive prostaglandin E_2 by astrocytes (Takano et al. 2006). The enzyme

phospholipase A_2 mediates this mechanism. In the mouse olfactory bulb, the role of mGluRs in the regulation of NVC is still controversial. Gurden and colleagues (2006) discarded any involvement of metabotropic receptors in intrinsic signals evoked by odors and the local odor-evoked CBF functional increase was not affected by LY367385 application to one glomerulus (Chaigneau et al. 2007). On the other hand, Petzold et al. (Petzold et al. 2008) have described a reduction of glomerular functional hyperemia upon topical application of MPEP and MCPG, respectively selective $mGluR_5$ and unselective group I/II mGluR antagonists.

$mGluR_5$ is a G-protein-coupled receptor (GPCR) that plays a key role in the release of Ca^{2+} from internal stores via inositol triphosphate mobilization. It is highly expressed mainly in telencephalic regions, including the cerebral cortex, hippocampus, subiculum, olfactory bulbs and nucleus striatum (Ferraguti and Shigemoto 2006). High levels of astrocytic $mGluR_5$ expression have also been observed in reactive glia and are thus often associated with non-physiological conditions (Aronica et al. 2000; Notenboom et al. 2006). Here, we report that pharmacological blockage of $mGluR_5$ and $mGluR_1$ does not affect NVC in the somatosensory cortex of adult anesthetized rats upon brief whisker stimulation of 4 and 24 seconds. Concurrent beta-probe measurements using the radiotracer ^{11}C-ABP688, which binds with high specificity to the allosteric site of $mGluR_5$ (Wyss et al. 2007), show that our protocol leads to a pharmacological receptor blockage of up to 80% in the somatosensory cortex, confirming blood-brain barrier passage and binding action of the drug. Under the same conditions, voltage-sensitive dye (VSD) imaging shows a transient reversible reduction of neuronal activity upon $mGluR_5$ blockage within the first minutes. Taken together, these results suggest that $mGluR_5$ activation does not play a significant role in the onset and possibly in the short-term maintenance of the hemodynamic response in adult rats, and thus call for a revision of the current astrocytic model of NVC at these time scales.

Materials and Methods

Animals

The experiments were performed by licensed investigators and were approved by the local veterinary authorities. The animals (40 male Sprague Dawley rats weighing 200 to 300 g) were provided by Harlan Laboratories (Netherlands) and were kept in cages in a ventilated cabinet with standardized conditions of light (night/day cycle: 12 h/12 h) and temperature, and free access to food and water was permitted. To exclude a strain effect, additional experiments were conducted using Wistar rats (n=3); no difference was observed between the two strains (data not shown).

Surgical preparation

All surgical procedures were performed under isoflurane anesthesia (2.5% to 3.5%). Catheters (PE-50) were inserted into the right femoral artery and vein. For radiotracer measurements, the vessels of the left hindlimb were also cannulated for the placement of an arteriovenous shunt (av-shunt). The animals were tracheotomized and artificially ventilated. The skull above the barrel cortex (1 mm caudal and 3 to 6 mm lateral from Bregma) was carefully thinned using a dental drill (Bien Air Medical Technologies, Bienne, Switzerland). The thinned area was then covered with 2% agarose type III-A (Sigma, St Louis, MO, USA) in Ringer's solution (in g/l: NaCl 8.6, $CaCl_2$ 0.30, KCl 0.30) and with a circular glass coverslip of 5-mm diameter. The animals' temperature was kept at 37℃ with a heating blanket and blood gases were maintained within physiological ranges by adjusting the ventilation when necessary. After surgery, isoflurane was discontinued (or reduced to a maximum of 0.5% when necessary) and anesthesia was maintained with a first subcutaneous injection of α-chloralose (44 mg/kg; Sigma) followed by continuous subcutaneous infusion (22 mg/kg/h). This anesthetic regime is considered ideal for studies of neurovascular and neurometabolic coupling (Bonvento et al. 1994). The level of anesthesia was controlled by observing arterial blood pressure during stimulation and by tail pinch. Experiments were performed after a postoperative recovery period of at least one hour to obtain a stable level of α-chloralose anesthesia and stable imaging signals.

Sensory stimulation

Following a baseline of 2 seconds, the vibrissae contralateral to the thinned skull were deflected using air puffs for 4 seconds at a frequency of 4 Hz. Ten trials were averaged for each sub-experiment. In an additional subset of experiments, after a baseline of 4 seconds, vibrissae were deflected for 24 seconds and five trials were averaged for each recording. For VSD experiments, a single whisker was deflected once and 10 trials were averaged for each condition.

Intrinsic optical imaging

Cortical images were acquired using two 12-bit CCD cameras (Pixelfly VGA, PCO Imaging, Kelheim, Germany) attached to a motorized epifluorescence stereomicroscope (Leica MZ16 FA, Leica Microsystems, Heerbrugg, Switzerland) focused 0.5 mm below the cortical surface. Two-dimensional optical spectroscopy was performed using the method described by Dunn et al. (2003a). The six wavelengths (560, 570, 580, 590, 600 and 610 nm, 10 nm FWHM) were produced with a monochromator (Polychrome V, Till Photonics, Grafelfing, Germany) and coupled in the microscope using an optical fiber. Images were acquired with 30 Hz and the monochromator was synchronized with the image acquisition (each frame was acquired with a different illumination wavelength). The second camera was used to simultaneously measure CBF employing dynamic laser speckle imaging. The method is described in detail elsewhere (Zakharov et al. 2009). 785-nm laser light (TuiOptics, Munich, Germany) was shone onto the cortex and images were acquired at 30 Hz with an exposure time of 10 ms.

Pharmacological interventions

6-Methyl-2-(phenylethynyl)-pyridine (MPEP) and LY367385 were supplied by Tocris Bioscience and injected i.v. at 1.2 mg/kg body weight or 4.0 mg/kg as specified in the text (dissolved in DMSO, DMSO reaching a maximum of 2% of the final concentration in NaCl). 6-Cyano-7-nitroquinoxaline-2,3-dione (CNQX, Tocris Bioscience) was injected at 15 mg/kg body weight (1:1 polyethylene glycol:NaCl). 2-(3-Methoxy-phenylethynyl)-6-methyl-pyridine (M-MPEP), provided by Dr. Fabrizio Gasparini, was administered i.v. at different concentrations (in a range from 1 to 8 mg/kg, as specified in the text; 1:1

polyethylene glycol:NaCl). Both the MPEP and M-MPEP infusions were delivered at a very slow rate (approximately 0.2 ml/min).

Radiotracer experiments

^{11}C-ABP688, a PET ligand for the study of mGluR$_5$ (Wyss et al. 2007), was used for the determination of receptor density (B_{max}) before and 10 minutes after injection of M-MPEP. Radiotracer experiments included measurements of time courses of tracer accumulation in the left somatosensory cortex using a beta scintillator for surface acquisitions (Wyss et al. 2009) and the online acquisition of total arterial ^{11}C activity in the av-shunt. For the latter purpose, the shunt was run through a coincidence counter (GE Medical Systems). The online arterial sampling procedure is described in detail elsewhere (Weber et al. 2002). Whole blood activity was then corrected for [i] the relative concentration of ^{11}C-ABP688 in plasma versus whole blood and [ii] the concentration of labeled metabolites.

For the tissue acquisitions, the scintillator was adjusted just above the thinned skull covering the somatosensory cortex. The count rate was stored on a personal computer using a bin width of 1 second, yielding tissue time-activity curves. During both conditions (baseline/blockage), data were acquired for 20 minutes. Following each experiment, the beta scintillator was calibrated with a known concentration of ^{11}C activity. Injected activities were in the range of 40–104 MBq throughout all experiments and the injected mass of ABP688 was 0.49–4.08 pmol/g body weight. This methodology used to quantify mGluR5 using ^{11}C-ABP688 is described in detail elsewhere (Wyss et al. 2007).

VSD imaging

For VSD imaging, the dye RH1691 was dissolved at 1 ml/ml in Ringer's solution. A cranial window was drilled on the right hemisphere above the whisker barrel cortex (Bregma, 0 to -5 mm; lateral, 2–7 mm). After removal of the bone, dura was left intact to reduce movement artifact and tendency to edema. Around the craniotomy, a few layers of dental cement were applied to form a trough to prevent dye leakage during the staining process. The dye was topically applied and was allowed to diffuse into the

cortex for 90 minutes. During staining, the dye was continuously circulated by a peristaltic pump (Reglo digital, Ismatec SA, Glattbrugg, Switzerland). Thereafter, the unbound dye was removed and the area was washed with dye-free Ringer's solution for more than 15 minutes. The fluid-filled chamber was then covered with a glass coverslip. For imaging, the dye was excited with 630-nm light from a LED lamp (Thorlabs GmbH, Dachau/Munich, Germany). The excitation light was reflected by a 650-nm dichroic mirror and focused onto the cortical surface with a camera lens. Fluorescent emission light was collected via the same optical pathway, but without mirror reflection, long-pass filtered (>670 nm) and focused onto the sensor of a high-speed Micam Ultima camera (Scimedia, California, USA). This high-speed CMOS-based camera has a detector of 100 × 100 µm. Images were collected with 1-ms temporal resolution. Acquisitions were performed before and 5, 15, 30, 45 and 60 minutes after the i.v. injection of 4 mg/kg M-MPEP. Due to the high sensitivity of the VSD method, the VSD signal was elicited by a single whisker deflection.

Data analysis

Image analysis and radiotracer kinetic analysis were performed using custom-written Matlab routines and the software package PMOD (Mikolajczyk et al. 1998b).

Optical imaging. The analysis of the multiwavelength spectroscopy followed the protocol of Dunn and colleagues (2003a). Baseline values for total hemoglobin concentrations were set to 100 µM with 70% oxygen saturation, which implies $C_0^{\mathrm{HbO}} = 70$ µM and $C_0^{\mathrm{HbR}} = 30\,\mu\mathrm{M}$. To quantify CBF, speckle images were processed as described recently (Zakharov et al. 2009) using 5 × 5 spatial and 25 temporal binning. Circular regions of interest (0.5 mm^2) were drawn manually over the area of maximal signal increase to extract the signal time courses. The 10 trials (5 in long-term stimulation experiments), that were carried out within 12 minutes in each animal, were averaged. All data represent the mean ± standard error of the mean used for each experimental condition. Spectroscopic and CBF maximum signals in the presence of pharmacological intervention were normalized to the control condition.

^{11}C-ABP688 radiotracer kinetic modeling. The applied methods consisted of standard compartmental modeling using an arterial input function. Tracer kinetics were modeled using a two-tissue compartment model with rate constants K_1–k_4, which has been shown to be suitable for the description of ^{11}C-ABP688 data (Wyss et al. 2007). To achieve stable fits, K_1/k_2 and k_4 were fixed at 1.6 and 0.05 min^{-1}, respectively, for both conditions (baseline/blockage), corresponding to mean values of free fitting using two tissue compartments. For data analysis, background counts were subtracted and all time-activity curves were decay corrected (physical half-life = 20.38 minutes) to the time point of injection and converted to kBq/ml taking into account a determined calibration factor (see above). For details of the analysis procedure, see the previous description of the approach (Wyss et al. 2007).

VSD. Bleaching of fluorescence was corrected by subtraction of a best-fit double-exponential. Time courses of fluorescence changes were quantified as $\Delta F/F_0$ from circular regions of interest of constant diameter adjusted to the activation area. In order to compare VSD signals from different animals, regions of interest were centered on the location of the earliest response. Amplitude was defined as the difference between the maximal response and the baseline signal just before the onset of whisker stimulation. Within single studies, amplitude changes across acquisitions were normalized to the signal amplitude of the baseline examination (=acquisition before M-MPEP injection).

Statistics. The required sample size was estimated prior to the study based on published data (Zonta et al. 2003), where a CBF response of 23 ± 7.0% (mean ± standard error of the mean; n=5) was reduced to 8 ± 1.8% by mGluR blockage. The authors report that a t-test for paired samples yielded $p<0.01$, from which follows $t\geq4.6$ ($df=4$) and effect size $d\geq2.05$. Based on these parameters, a minimum sample size of n=8 was determined (Software G*power, University of Düsseldorf, Germany). Differences between hemodynamic responses before and after receptor blockage were statistically analyzed using the Wilcoxon signed-rank test.

Results

To control for the role of $mGluR_5$ in the regulation of CBF, we assessed NVC before and after pharmacological manipulations of the receptor. More specifically, we used multiwavelength spectroscopy to reveal quantitative spatiotemporal changes of deoxyhemoglobin (HbR), oxyhemoglobin (HbO) and total hemoglobin (HbT) concentrations. Concurrently, we used laser speckle contrast imaging maps to measure relative CBF changes (Zakharov et al. 2009).

Transient hemodynamic responses of the somatosensory cortex are not affected by $mGluR_5$ blockage

Figure 1A shows a typical hemodynamic response of the somatosensory cortex upon brief whisker stimulation with co-localized changes in HbR, HbO, HbT and CBF. Spatiotemporal hemodynamic and metabolic responses were measured in a series of (i) control experiments (n=5 animals), and in the absence and presence of pharmacological intervention using (ii) MPEP and LY367385 (n=7 animals), (iii) M-MPEP (n=8 animals) and (iv) CNQX (n=6 animals). To investigate the effect of group I mGluR block on NVC, MPEP and LY367385 ($mGluR_5$ and $mGluR_1$ blockers, respectively) were administered i.v. (1.2 mg/kg). These compounds readily pass through the blood-brain barrier (Gasparini et al. 2002; Gasparini et al. 1999). Surprisingly, no significant changes were observed in the evoked hemodynamic responses following blockage of these mGluRs (Fig. 1B and C). To further confirm these results, we studied the effect of a more effective $mGluR_5$ blocker, M-MPEP, which is five times more potent than MPEP (Gasparini et al. 2002; Gasparini et al. 1999). Again, no significant reduction of evoked hemodynamic signals was observed between baseline condition and 10 minutes after M-MPEP pharmacological intervention (Fig. 1B and C). On the other hand, the CBF signal was slightly but significantly increased by M-MPEP injection. In a separate set of animals, hemodynamic responses were evaluated before and 10 minutes after systemic injection of CNQX, an AMPA/kainate receptor antagonist. The neuronal activity block elicited a significant reduction in all hemodynamic parameters and in CBF.

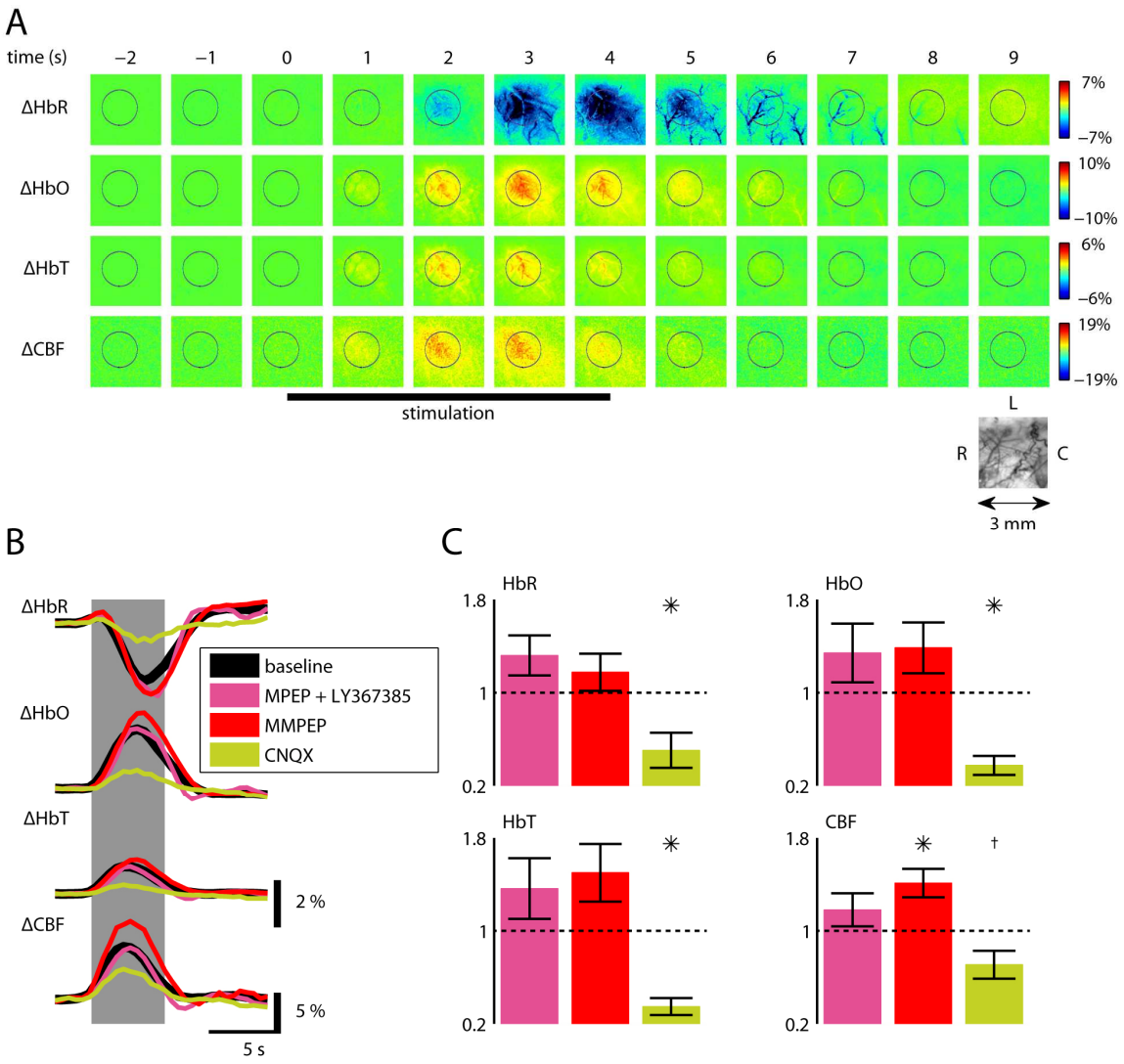

Paper 1 Figure 1. Application of group I mGluR antagonists does not affect NVC upon brief whisker stimulation.

Relative changes of deoxy- (HbR), oxyhemoglobin (HbO) and blood volume (HbT) upon brief whisker stimulation were measured by optical spectroscopy in the activated barrel cortex while CBF was measured by laser speckle imaging. (B) Average responses after i.v. injection of the $mGluR_5$ and mGluR1 antagonists MPEP and LY367385, respectively (1.2 mg/kg; pink), and after injection of M-MPEP (four animals at 1 mg/kg; one animal at 2 mg/kg; one animal at 3 mg/kg and two animals at 4 mg/kg; red) compared to baseline (black). Data shown were recorded 10 minutes after drug injection. No significant decrease of the response was observed after these treatments (statistical testing either for the MPEP-LY367385 and M-MPEP groups separately or for the two groups pooled together, n=15). In contrast, after treatment with CNQX (15 mg/kg; green; n=6), a strong reduction in the hemodynamic signals was evident. (C) Peak deviations normalized to baseline (mean ± sem; *$p<0.05$, $^{\dagger}p=0.075$, Wilcoxon signed-rank test). In total MPEP-LY367385, MMPEP and CNQX were tested, respectively, in 7, 8, 6 rats. Measurements at the later time points (30 and 45 minutes) did not show any significant decrease of the peak response (data not shown).

Steady-state hemodynamic responses are not affected by blockage of group I mGluRs

After demonstrating that group I mGluR block does not affect NVC mechanisms during brief whisker stimulation, we wanted to explore the contribution of $mGluR_5$ to more sustained blood flow responses. Hemodynamic responses before and after injection of group I mGluR antagonists were evaluated in four animals during 24 seconds of whisker stimulation. Stimulus-evoked responses exhibited an initial peak followed by a steady-state component that lasted until the stimulation was discontinued (Fig. 2A). Similar responses have been previously reported (Berwick et al. 2008). Both the initial peak and the steady-state component did not exhibit any change after MPEP and LY367385 i.v. injection (4.0 mg/kg) as reported in CBF example curves (Fig. 2A). On the contrary, a brief systemic increase in mean arterial blood pressure was recorded (significantly different only during the first 5 minutes after systemic injection; $p<0.05$,

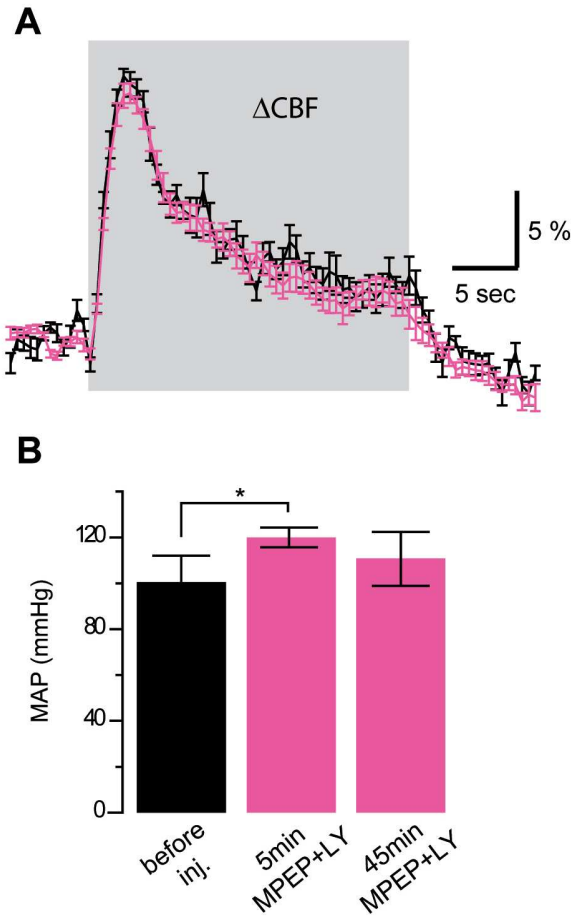

Paper 1 Figure 2. The NVC response during longer stimulation is also not affected by group I mGluR antagonists MPEP and LY367385.

(A) Example of CBF recordings during 24-second whisker stimulation before (black) and 10 minutes after (pink) MPEP and LY367385 i.v. injection (4.0 mg/kg). (B) Systemic effect on mean arterial blood pressure (MAP) evoked by MPEP and LY367385 i.v. injection (4.0 mg/kg). Five minutes after drug injection, a significant increase was observed (MAP before injection: 101 ± 11 mmHg; 5 min after injection: 120 ± 4; 45 min after injection: 111 ± 11; mean ± sd; n=4; *p<0.05, Wilcoxon signed-rank test) before the arterial blood pressure returned to its baseline. This transient increase was not elicited by placebo injection (see text).

Fig.2B), which was not observed during placebo experiments (same volume of 1:1 polyethylene glycol:NaCl; data not shown).

Intravenous injection of mGluR$_5$ antagonists leads to high levels of receptor occupancy

Next, we verified that the administration of MPEP and M-MPEP did indeed significantly block mGluR$_5$ in our protocol. To this end, we conducted a series of concurrent optical/radiotracer experiments to quantify cortical mGluR$_5$ occupancy and its effect on the hemodynamic response (n=5). Using ^{11}C-ABP688, both MPEP and M-

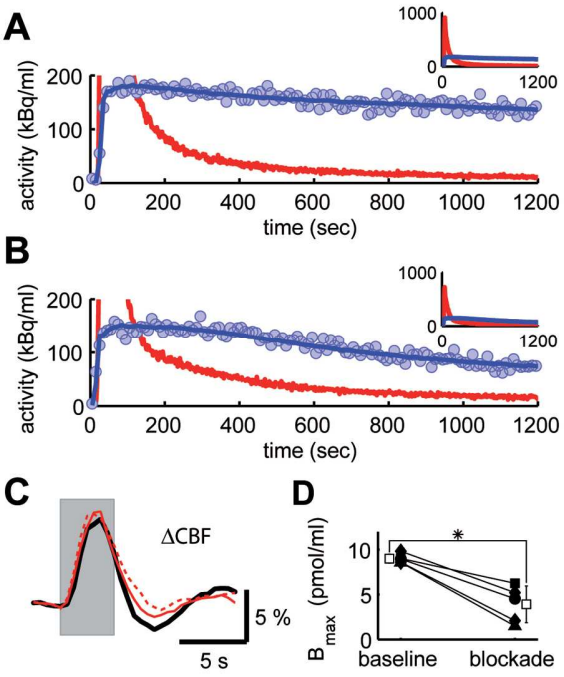

Paper 1 Figure 3. Delivery of M-MPEP leads to blockage of mGluR5 in the rat somatosensory cortex but fails to attenuate the hemodynamic response.

After the injection of M-MPEP (4 mg/kg), the washout of radiolabel from tissue was increased (B) compared to baseline condition (A) as represented by the decay-corrected tissue time-activity curves (blue circles). The model curve (blue line) and the radioactivity concentration in plasma (i.e. input curve; red line) are also shown. The full range of data is displayed in the insets (same axes legends). In this example, the estimated mGluR$_5$ blockage amounted to 47%. (C) Hemodynamic response upon stimulation (gray area) before (black line), 10 minutes (red line) and 30 minutes (broken red line) after delivery of M-MPEP (same experiment as in A and B) was unaffected by mGluR$_5$ blockage. In (D), the density of receptors in the tissue (B_{max}) is shown for all individual beta-probe experiments before and after blockage (square: 1.2 mg/kg MPEP/LY367385; circle: 1 mg/kg M-MPEP; diamond: 4 mg/kg M-MPEP; triangle: 8 mg/kg M-MPEP). White boxes represent mean ± sd (*p<0.05, Wilcoxon signed-rank test).

MPEP were found to significantly reduce radiolabel binding to the tissue compared to baseline condition, without having a noticeable effect on the hemodynamic response (Fig. 3). Radiotracer activity was recorded for a period of 20 minutes, beginning 10 minutes after MPEP or M-MPEP injection. On average, a 57% reduction in the density of free receptors in the tissue was measured (B_{max}; Fig. 3D).

Evoked neuronal activity in the somatosensory cortex is transiently reduced by mGluR$_5$ blockage

In order to assess the potential impact of mGluR$_5$ blockage upon neuronal activity, and in particular to control for changes in the spatiotemporal dynamics of cortical brain activity upon mGluR$_5$ blockage by M-MPEP, VSD experiments were performed. VSD imaging provides a visualization of the cortical activity of a large neuronal population in the upper cortical layers with high spatial and temporal resolution (Chemla and Chavane 2010). VSD fluorescent signals evoked by a single whisker deflection were recorded in control conditions and after M-MPEP i.v. injection (4 mg/kg, n=6). The VSD signal was slightly decreased, on average by 27% 5 minutes after M-MPEP injection (Fig. 4). Measurements at later time points revealed this effect to be completely reversible, indicating a transient reduction in neuronal activity in response to mGluR$_5$ block.

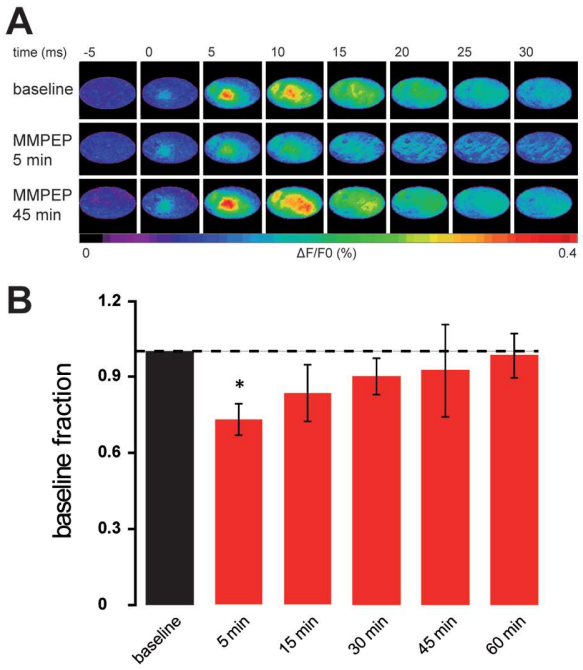

Paper 1 Figure 4. Neuronal activity slightly decreases during the first 30 minutes after mGluR5 blockage.

(A) Maps of a single VSD imaging experiment performed before (top), 5 minutes (middle) and 45 minutes (bottom) after injection of M-MPEP (4 mg/kg). Single frames are 5 ms apart from each other. The series starts 5 ms before single whisker stimulation evoked at time 0. (B) Summary of VSD results in six animals. After only 5 minutes following the injection of M-MPEP (4 mg/kg), the amplitude of the VSD signal significantly decreased by, on average, 27%. At later time points, the signal was not significantly different from baseline level; *p<0.05, Wilcoxon signed-rank test).

Discussion

Recent years have seen a surge in research on the physiology of astrocytes, and the regulation of local CBF is one of the areas where a relatively comprehensive model involving astrocytes has been suggested (Attwell et al. 2010). This model proposes that the activation of astrocytic metabotropic glutamate receptor $mGluR_5$ by neuronal activity triggers intracellular Ca^{2+} transients, leading to the activation of phospholipase A_2. Phospholipase A_2, in turn, activates a variety of pathways that ultimately lead to the release of possibly multiple vasoactive agents by astrocytes. The work presented here contradicts this model. More specifically, it contradicts the involvement of $mGluR_5$ in triggering this complex chain of events. We have reported here that, even though antagonists of $mGluR_5$ delivered intravenously cross the blood-brain barrier and block up to 80% of the receptors (Fig. 3), they fail to induce a reduction of the hemodynamic response upon brief 4- and 24-second whisker stimulation (Figs. 1 and 2). However, it was found that $mGluR_5$ antagonists provoke a transient increase in mean arterial blood pressure (Fig. 2) and a transient reduction of neuronal activity (Fig. 4). Additionally, injection of $mGluR_5$ antagonists did not significantly affect the baseline cerebral blood flow which could have interacted with the hemodynamic response following the stimulation (data not shown).

As mentioned above, several studies have reported a reduction of the hemodynamic response upon blockage of $mGluR_5$ (Petzold et al. 2008; Takano et al. 2006; Zonta et al. 2003). Activation of $mGluR_5$ has also been reported to elicit Ca^{2+} transients in astrocytes (Wang et al. 2006). The present study differs from these studies in three ways. First, we used relatively brief whisker stimulations (4 and 24 seconds), whereas a 60-second stimulation was normally applied in these studies. Secondly, we used a thinned skull preparation to keep the system as intact and healthy as possible. Finally, we used a combination of intrinsic optical imaging and laser speckle imaging, whereas in the earlier studies CBF was measured with a laser Doppler probe. This last point, however, should not affect the results. Despite the fact that laser speckle imaging maps CBF in two dimensions and laser Doppler flowmetry is normally a point measurement, both techniques essentially rely on the same physical principles.

It is important to note that we probed the system in a time frame comparable to the one used in other studies. For example, Zonta et al. (2003) measured the effect of MPEP injection on CBF 15 to 20 minutes after injection. Our results show a very significant receptor occupancy 10 to 30 minutes after MPEP or M-MPEP injection (Fig. 3), yet still no reduction in the hemodynamic response. In principle, the transient decrease in neural activity reflected by the decrease in VSD signal amplitude (Fig. 4) should lead to a detectable reduction of the hemodynamic signal in the first few minutes after injection. One possible explanation of the absence of a hemodynamic effect is an interaction with the observed transient increase in systemic arterial blood pressure. A limitation of the present study is the fact that the stimulation protocols used for the VSD and hemodynamic imaging were not identical. Further investigation of this phenomenon will require a simultaneous acquisition of both signals to detect possible interactions on the single trial level.

Blockage of $mGluR_5$ by injection of the potent M-MPEP slightly but significantly increased the evoked CBF response (Fig. 1C). It is difficult to give a simple explanation for this result as $mGluR_5$ plays a role in a variety of physiological processes, some of them of systemic nature, as reflected by the transiently elevated blood pressure.

Part, but not all, of the apparent contradiction between our data and previous reports could be explained by regional differences in the expression pattern of $mGluR_5$, e.g. the study by Petzold and colleagues (Petzold et al. 2008) focused on the olfactory bulb. However, the question remains open whether or not astrocytic $mGluR_5$ plays a role in NVC. We note that the literature does not unequivocally support a key physiological role for astrocytic $mGluR_5$ in functional hyperemia. The arguments are as follows.

First, it appears that expression of $mGluR_5$ is mostly neuronal but that it can also be highly expressed in reactive glia. $mGluR_5$ immunoreactivity has been reported in neurons, in axons or in vesicles (Jia et al. 1999), and the receptor is indeed widely expressed by neurons in adult rodents (Ferraguti and Shigemoto 2006). In support of these results, knocking out $mGluR_5$ only in cortical excitatory neurons strongly reduces its overall expression level in the cortex (Ballester-Rosado et al. 2010). Moreover, in the

cerebral cortex, all non-neuronal cells were found to be negative for $mGluR_5$ by Mudo and colleagues (2007). Even though $mGluR_5$ has been reported in hypothalamic (Van Den Pol et al. 1995) and cultured (Biber et al. 1999) astrocytes, high levels of astrocytic $mGluR_5$ expression have been observed in reactive glia and are thus often associated with non-physiological conditions (Aronica et al. 2000; Notenboom et al. 2006). Consistent with this view, $mGluR_5$ expression is increased *in vitro* in the presence of growth factors, such as transforming growth factor α and epidermal growth factor, in the extracellular environment (Miller et al. 1995).

Secondly, GPCRs are in general responsible for slow postsynaptic signaling. In a recent review, Cauli and Hamel (2010) discuss the temporal sequence of astrocytic and neuronal contributions to CBF control. In both neurons and astrocytes, intracellular Ca^{2+} increases code neuronal activity and elicit several cascades of events. Neurons express ionotropic receptors more frequently and abundantly than astrocytes and consequently are able to evoke quick changes in membrane potential, inducing rapid intracellular Ca^{2+} increases in a time window of about 10–12 ms. On the contrary, due to their signal trasduction pathways, metabotropic receptors in general elicit responses of slower onset and longer duration, from seconds to potentially hours, although GPCR mediated synaptic responses can occur at relatively fast timescales of 1 to 2 seconds upon strong stimulation (Charpak and Gahwiler 1991). Even though these faster responses are compatible with functional hyperemia, it seems more likely that group I mGluRs expressed in either neurons and/or astrocytes are responsible for the slow components of Ca^{2+} dynamics (Cauli and Hamel 2010). In different *in vivo* studies (Devor et al. 2008; Takano et al. 2006; Weber et al. 2004) and in the data reported here, a hemodynamic delay of about 500 ms was observed, indicating that the transient phase of the hemodynamic response, if it is Ca^{2+}-induced, is likely to be initiated by cells with fast Ca^{2+} dynamics. Astrocytes, which only in a small portion exhibit Ca^{2+} responses as fast as in neurons (Winship et al. 2007), potentially contribute to NVC regulation only in the later response phase.

Finally, other groups have also reported findings contradicting the $mGluR_5$ astrocytic model. Takata and Hirase have reported that astrocytic spontaneous Ca^{2+} surges are

not affected by MPEP systemic injection or pyridoxalphosphate-6-azophenyl-2',4'-disulfonic acid (PPADS, a non-selective P2 purinergic antagonist) topical application in L1 and L2/3 of the somatosensory cortex of anesthetized rats (Takata and Hirase 2008), indicating that the spontaneous astrocytic Ca^{2+} surges are independent of metabotropic glutamate or purinergic receptors. More recently, the group of A. Devor reported that astrocytic Ca^{2+} increases are infrequent and delayed compared to the onset of vasodilation upon a variety of stimulation types in the rat or mouse somatosensory cortex (Nizar et al. 2010). Taken together, these studies are not supportive of a predominant role for astrocytic $mGluR_5$ in triggering the fast initial hemodynamic response and do not support the notion that the transient neurovascular response is mediated through a Ca^{2+}-related mechanism. However, our results and the literature cited above do not rule out a possible involvement of $mGluR_5$ in the late maintenance phases of the hemodynamic response, which would then explain why other groups have observed a reduction of the neurovascular response upon MPEP delivery after longer periods of stimulation (30–60 seconds). However, at least for the whisker-to-barrel system, such long lasting activity patterns are rather artificial and rapid neuronal adaptation already occurs after a few seconds following stimulation onset.

The results presented here strongly suggest that $mGluR_5$ does not play a crucial role in the transient phase of the hemodynamic response. Thus, the exact mechanism by which astrocytes sense the extracellular glutamate concentration and trigger intracellular events for regulation of the vascular response remains unclear and research on this topic must be continued.

Paper 2

Multimodal imaging reveals impaired neurovascular coupling in sustained hypertension

Novella Calcinaghi, MSc [1]; Matthias T. Wyss, MD, PhD [1,2,*]; Renaud Jolivet, PhD [3 *]; Anand Singh, MSc [1]; Anna L. Keller, PhD [4]; Stephan Winnik, MD [5]; Jean-Marc Fritschy, PhD [1]; Alfred Buck, MD, MSc [2]; Christian M. Matter, MD [5,6,7] and Bruno Weber, PhD [1]

[1] Institute of Pharmacology and Toxicology, University of Zurich, Switzerland
[2] PET Center, Division of Nuclear Medicine, University Hospital Zurich, Switzerland
[3] Neuroscience, Physiology & Pharmacology, University College London, UK
[4] Max Planck Institute for Biological Cybernetics, Tübingen, Germany
[5] Institute of Physiology, University of Zurich, Switzerland
[6] Division of Cardiology, University Hospital Zurich, Switzerland
[7] Zurich Center for Integrative Human Physiology, University of Zurich, Switzerland

Submitted to *Circulation*

Presented in poster form at the following conferences:

- Swiss Society of Neuroscience, Lausanne, (Switzerland), 2010
- Gordon Research Conference in Brain Energy Metabolism and Blood Flow, Andover (NH), 2010
- Pharma Day, Pharmacology and Toxicology Institute, University of Zürich, (Switzerland), 2010
- Brain Pet international congress, Barcelona, (Spain), 2011
- Pharma day, Pharmacology and Toxicology Institute, University of Zürich, (Switzerland), 2011

- Swiss Society for Neuroscience Meeting, Zürich (Switzerland), 2012
- 11th Day of Clinical Research, Zürich University Hospital, Zürich, (Switzerland), 2012.

Presented as talk at the Zürich Center for Integrative Human Physiology (ZIHP) symposium, Zürich University Hospital, Zürich, (Switzerland), 2010.

Abstract

Background – Arterial hypertension is an important risk factor for cerebrovascular disease such as transient ischemic attacks or stroke, and represents a major global health issue. The effects of hypertension on cerebral blood flow (CBF), particularly at the microvascular level, remain unknown.

Methods and Results – Using the spontaneously hypertensive rat (SHR) model, we examined the cortical hemodynamic response upon whisker stimulation applying a multimodal imaging approach (multiwavelength spectroscopy, laser speckle imaging, two-photon microscopy). We assessed the effects in 10-, 20-, and 40-week-old male SHRs and age-matched male Wistar Kyoto rats (CTRL) with regard to hemodynamic, histological, and biochemical parameters. Losartan and verapamil were administered for 10 weeks to test the reversibility of hypertension-induced impairments. Compared with CTRLs, increased arterial blood pressure in SHRs was associated with a progressive decrease in functional hyperemia in 20- and 40-week-old SHRs; baseline capillary red blood cell velocity was increased in 40-week-old SHRs. Antihypertensive treatment reduced baseline capillary CBF almost to CTRL values, while functional hyperemic signals improved only slightly. Structural analyses of the microvascular network revealed no differences between normo- and hypertensive animals, whereas expression analyses of cerebral lysates showed signs of increased oxidative stress in hypertensive rats and signs of impaired endothelial homeostasis upon early hypertension.

Conclusions – Impaired neurovascular coupling in the SHR evolves upon sustained hypertension. Antihypertensive mono-therapy using verapamil or losartan is not sufficient to abolish this functional impairment. These deficits in neurovascular coupling in response to sustained hypertension might contribute to accelerated progression of neurodegenerative diseases in chronic hypertension.

Keywords: Hypertension, brain, rats, neurovascular coupling, multimodal imaging, cerebral blood flow.

Introduction

Arterial hypertension (aHTN) accounts for more than one third of deaths in Western countries (Lawes et al. 2008). High blood pressure strongly affects the brain which depends on the continuous blood-borne supply of oxygen and energy substrates in a timely and localized manner. It constitutes one of the major risk factors for hemorrhagic stroke (Goldstein et al. 2006) and is a leading cause of dementia and cognitive impairments (Dahlof 2007).

At the functional level, high blood pressure disrupts the regulatory mechanisms underlying neurovascular coupling (NVC) (Iadecola and Davisson 2008) and impairs cerebral blood flow (CBF) autoregulation (Paulson et al. 1990). From a structural point of view, aHTN induces a reduction in gray matter thickness as well as an increased ventricular size due to brain atrophy (Jennings and Zanstra 2009). Furthermore, aHTN induces vascular hypertrophy with a consequent reduction of lumen diameters and increased rigidity of the arterial walls. aHTN is also associated with a loss of arterioles and capillaries (Boegehold 2007).

The effects of aHTN on brain hemodynamics have been investigated in several animal studies yielding contradictory results. These may depend on strains, anesthetic conditions, and whether the study assessed evoked signals or resting conditions. For instance, resting CBF in spontaneously hypertensive rats (SHR) has been reported to be similar to (Wei et al. 1992), less than (Katsuta 1997), or greater than (Heinert et al. 1998) that of controls (Wistar Kyoto rats). More recently, no differences in resting CBF were observed between Wistar Kyoto rats and SHRs under α-chloralose anesthesia at either 3 or 10 months of age and in different brain areas (Leoni et al.). In another model where aHTN was induced by systemic injection of angiotensin II (Capone et al. 2012), CBF responses evoked by whisker stimulation were reduced in hypertensive animals in comparison to normotensive mice. In human positron emission tomography studies, aHTN appears to induce a mild dampening in regional CBF response during memory tasks, more pronounced in frontal and subcortical regions (Jennings et al. 2005).

The prevalence of aHTN increases with age, which may also affect CBF and NVC. In human positron emission tomography studies, aging is usually associated with a significant decrease in resting CBF (Bentourkia et al. 2000). In addition, aging is accompanied by a reduction in the blood oxygenation level-dependent response (Ances et al. 2009). Similarly, Dubeau and colleagues have recently reported a reduced hemodynamic response in the somatosensory cortex of aged rats (24 and 40 months) with unaltered metabolic rate of oxygen (Dubeau et al. 2011).

The influence of sustained aHTN on NVC has never been studied by means of a multimodal brain imaging approach in a model of essential genetic aHTN such as the SHR. SHRs provide a unique animal model for studying chronic essential aHTN, superseding pharmacological intervention to increase blood pressure. The animals are normotensive at birth and develop severe systolic and diastolic aHTN in the first 2–4 months of life. At 6 months, they show established sustained aHTN (Amenta et al. 2003).

In the present study, we investigated the effects of sustained aHTN of variable duration on the hemodynamics and structure of the somatosensory cortex in SHRs. In the second phase, we examined the reversibility of alterations by antihypertensive treatment. We found a reduced stimulation-evoked hemodynamic response in the somatosensory cortices of 20- and 40-week-old male SHRs when compared with age-matched and sex-matched normotensive controls. These functional changes of NVC were paralleled by structural changes such as decreased cortical thickness and increased ventricle size, and biochemical alterations such as signs of increased oxidative stress and altered endothelial homeostasis. In contrast, we did not detect any structural changes in the cerebral microvascular system. Antihypertensive treatment using losartan or verapamil decreased blood pressure and normalized baseline capillary blood flow, but did not improve CBF response.

Materials and Methods

Animals

All experimental procedures were reviewed and approved by the local ethical committee and the cantonal veterinary authority. They conform to the guidelines of the Swiss Animal Protection Law, Veterinary Office, Canton Zurich (Act of Animal Protection of December 16, 2005 and Animal Protection Ordinance of April 23, 2008). The animals were provided by Harlan Laboratories (Blackthorn, UK) and were kept in cages in a ventilated cabinet with standardized conditions of light (night/day cycle: 12 h/12 h) and temperature, and free access to food and water was permitted.

Male rats of three different ages were examined in this study: 10, 20, and 40 weeks. At each age, SHRs were compared to age-matched Wistar Kyoto rats serving as normotensive controls (CTRL). In the 10 and 20 weeks groups, SHRs and CTRLs were directly compared. The 40 weeks group was divided into four subgroups: [i] CTRLs, [ii] untreated SHRs, [iii] SHRs treated for 10 weeks with losartan (LOS), and [iv] SHRs treated for 10 weeks with verapamil (VER).

Surgical preparation

All surgical procedures were performed under isoflurane anesthesia (2.5–3.5%). Catheters (PE-50) were inserted into the right femoral artery and vein. Animals were tracheotomized and artificially ventilated. The skull above the left barrel cortex (1 mm caudal and 3 to 6 mm lateral from bregma) was carefully thinned to translucency using a dental drill (Bien-Air Medical Technologies, Bienne, Switzerland). The thinned area was then covered with 2% agarose type III-A (Sigma-Aldrich, Buchs, Switzerland) in Ringer's solution (in g/l: NaCl 8.6, $CaCl_2$ 0.30, KCl 0.30) and a circular glass coverslip of 5 mm diameter. The animal's temperature was kept constant at 37℃ with a heating blanket and blood gases were maintained within physiological ranges by adjusting the ventilation when necessary. After surgery, isoflurane was discontinued (or reduced to a maximum of 0.4% when necessary) and anesthesia was maintained with an initial subcutaneous injection of α-chloralose (44 mg/kg; Sigma-Aldrich) followed by continuous subcutaneous infusion (22 mg/kg/h). This anesthetic regime is considered

ideal for studies of neurovascular and neurometabolic coupling (Bonvento et al. 1994). Intrinsic optical imaging experiments were performed after a post-operative recovery period of at least one hour in order to achieve a stable level of α-chloralose anesthesia and stable imaging signals.

Sensory stimulation

Following a baseline of 2 seconds, a single vibrissa contralateral to the thinned skull was deflected for 4 seconds at a frequency of 4 Hz.

Intrinsic optical imaging

Data were acquired following the method previously described by our group (Calcinaghi et al. 2011). Cortical surface images were acquired using two 12-bit CCD cameras (Pixelfly VGA, PCO Imaging, Kelheim, Germany) attached to a motorized epifluorescence stereomicroscope (Leica MZ16 FA, Leica Microsystems, Heerbrugg, Switzerland) focused 0.5 mm below the cortical surface, as previously described in (Calcinaghi et al. 2011; Goldstein et al. 2006). Two-dimensional optical spectroscopy was performed using the method described by Dunn and colleagues (Dunn et al. 2003b; Dunn et al. 2005). The six wavelengths (560, 570, 580, 590, 600 and 610 nm, 10 nm full width at half maximum) were produced with a monochromator (Polychrome V, Till Photonics, Grafelfing, Germany) and coupled in the microscope using an optical fiber. Images were acquired at 30 Hz and the monochromator was synchronized with the image acquisition (each frame was acquired with a different illumination wavelength). The second camera was used to simultaneously measure CBF employing dynamic laser speckle imaging. The method is described in details elsewhere (Zakharov et al. 2009). 785-nm laser light (TuiOptics, Munich, Germany) was shone onto the cortex and images were acquired at 30 Hz with an exposure time of 10 ms per image. A scheme of the intrisic optical set up is reproduced in Figure 1C.

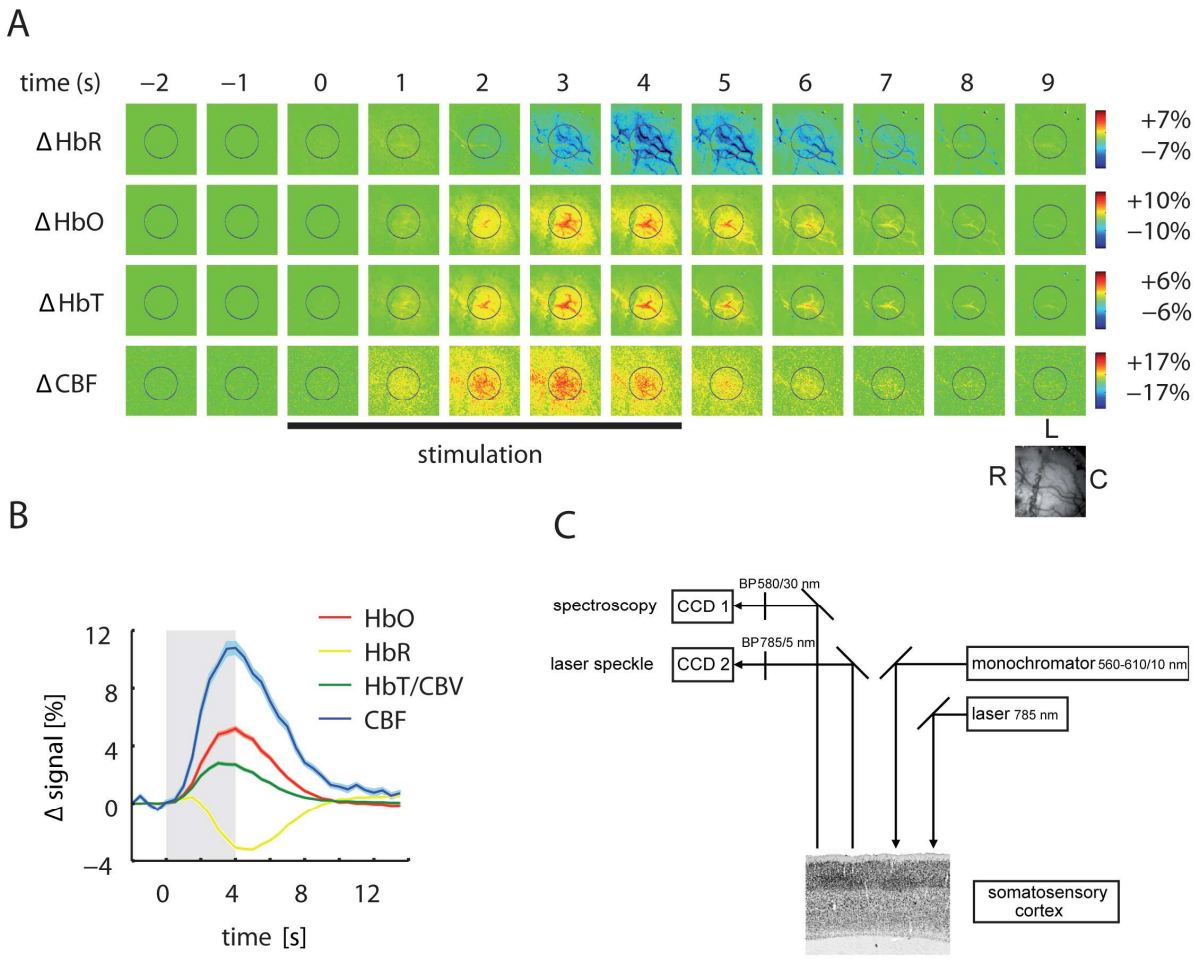

Paper 2 Figure 1. Example images and signals obtained by Intrinsic optical imaging and laser specke.

A, Activation maps of deoxy- (HbR), oxy- (HbO), and total hemoglobin (HbT) as well as cerebral blood flow (CBF) upon single whisker stimulation (4 Hz during 4s). Hemoglobin reflectance changes were measured by optical spectroscopy while CBF was measured by laser speckle imaging. **B,** Typical relative changes in HbR, HbO, HbT and CBF corresponding to the ROI in A (gray bar marks the stimulation period). **C,** Schematic of the setup for multiwavelength spectroscopy and laser speckle imaging.

Two-photon laser scanning microscopy

Following the camera-based optical imaging session, the skull and dura mater above the activated cortical area were removed. The cortex was stained for 5 minutes with the fluorescent astrocyte marker sulforhodamine 101 (Sigma-Aldrich). The barrel cortex was then washed with saline for 10 minutes and covered with 2% agarose type III-A in Ringer's solution and with a circular glass coverslip. Two-photon laser scanning microscopy was performed using a custom-built microscope equipped with a 16× objective (Haiss et al. 2009). Blood plasma was labeled with a 0.5 ml bolus of 5% fluoresceinisothiocyanate-labeled dextran (10 kDa; Sigma-Aldrich) dissolved in physiological saline. Line scans of straight capillary segments were acquired at 800 Hz.

Drug treatment

Antihypertensive treatment was administered to SHRs at the age of 30 weeks for a period of 10 weeks, either with VER (80 mg/kg/day (Fortepiani et al. 1999); Sigma-Aldrich) or LOS (30 mg/kg/day (Gohlke et al. 1996); Sigma-Aldrich). Both drugs were dissolved in the drinking water and solutions were freshly prepared each day. During the treatment period, blood pressure was monitored by regular tail cuff measurements (data not shown).

Immunohistochemistry

After the functional imaging measurements, rats were deeply anesthetized with pentobarbital (pentobarbital-Na; 60 mg/kg, i.p.) and perfused transcardially with ice-cold fixative (0.15 M sodiumphosphate buffer, 4% paraformaldehyde, pH 7.4). Brains were removed immediately after perfusion, post-fixed for 2 hours at 4℃, and impregnated overnight with 30% sucrose in PB (Phosphate Buffer) for cryoprotection. Transverse 40-µm-thick sections were cut from frozen blocks with a sliding microtome and collected in PBS (Phosphate-buffered Saline). Sections were then stored in antifreeze solution (50 mM PB, 15% glucose, 30% ethylene glycol, sodium azide, pH 7.4) at –20℃ until use.

Nissl staining. A 1:6 series of sections was Nissl stained with cresyl violet to measure lateral ventricle sizes and cortical thicknesses within the different animal groups.

Immunoperoxidase staining. Immunoperoxidase staining was performed to visualize microglia activation, as described in (Fritschy and Mohler 1995). Sections were incubated overnight at 4℃ with primary antibodies diluted in Tris buffer, pH 7.4, containing 2% normal goat serum and 0.2% Triton X-100 (Iba-1, 1:3000). Sections were washed and incubated for 30 minutes in biotinylated secondary antibodies (1:300; Jackson ImmunoResearch, Newmarket, UK), followed by ABC complex for 30 minutes (Vectastain Elite kit; Vector Laboratories, Peterborough, UK) and reaction with diaminobenzidine tetrahydrochloride (Sigma-Aldrich) for 5–15 minutes in Tris, pH 7.7. Finally, sections were washed thoroughly, mounted on gelatin-coated slides, air-dried overnight, dehydrated, and coverslipped with Eukitt (Erne Chemie, Dällikon, Switzerland).

Fluorescein-labeled-albumin intravascular filling. Following the perfusion protocol described above, a subgroup of animals was perfused with 1% fluorescein-labeled albumin (Sigma-Aldrich) and 3% porcine skin gelatin type A (Sigma-Aldrich) in PBS (Tsai et al. 2009). The head of the animal was then cooled with ice water to aid solidification of the gelatin. For details regarding the gel composition and protocol, see Tsai et al. (Tsai et al. 2009). The brain was extracted from the skull and stored for cryoprotection in 30% sucrose until it sank. Then, 60-µm-thick frozen sections were cut on a sliding microtome (HM 440E; Microm, Walldorf, Germany). Selected sections were washed 3 × 5 minutes in 0.1 M PB and incubated for 5 minutes in 0.4×10^{-4}% DAPI (4',6-diamidino-2-phenylindole dihydrochloride; Sigma-Aldrich) in dH_2O to stain the cell nuclei for later anatomical orientation. Following another series of three rinses in 0.1 M PB, the sections were mounted on glass slides and coverslipped with polyvinyl alcohol (Mowiol 4-88; Hoechst, Frankfurt, Germany) containing 4% 1,4-diazabicyclooctane (Merck, Darmstadt, Germany) to preserve the fluorescence of the FITC-labeled gelatin and the DAPI-labeled cell nuclei. Double-channel (FITC and DAPI) images of the whole rat brain sections were taken with a fluorescence microscope (AxioImager.Z1, 5× objective; Carl Zeiss, Göttingen, Germany) equipped with a monochrome CCD camera (AxioCam HRm, controlled by AxioVision 4.8; Carl Zeiss).

RNA isolation, reverse transcription, and quantitative PCR

Total RNA was isolated from somatosensory cortices of 20- and 40-week-old rats using TRIzol® Reagent (Invitrogen, Carlsbad, CA, USA). Reverse transcription was performed using Ready-To-Go You-Prime First-Strand Beads (Amersham, Buckinghamshire, UK).

Quantitative PCR was performed in a Stratagene Mx 3000 P™ machine (Stratagene, La Jolla, CA, USA) using the Stratagene MxPro sequence detection system and software. SYBR green reagents were used as supplied in the SYBR® Green JumpStart™ Taq Ready Mix™ (Sigma, St. Louis, MO, USA). Expression was calculated using the ΔΔCT method. Primers were: superoxide dismutase 1 (SOD1): forward: 5'-GTG TGC GTG CTG AAG GGC GA-3', reverse: 5'-CGT GGA CCA CCA TAG TAC GGC CA-3'; superoxide dismutase 2 (SOD2): forward: 5'-TCG TGG GCG CCT CAG CAA TG-3', reverse: 5'-AAC ATC TCC CTT GGC CAG CGC-3'; superoxide dismutase 3 (SOD3): forward: 5'-TGG GAG AGC TTG TCA GGT GTG GAA C-3', reverse: 5'-CGG CCC AAG ATC GAG TGC GG-3'; endothelial nitric oxide synthase (eNOS): forward: 5'-GGC ACC TAC CAG CTC CGG GA-3', reverse: 5'-GGG GTC AGG CTG GTA GCG GA-3'; p47/phox: forward: 5'-ATG ACC GTG GCG ACG GGA GA-3', reverse: 5'-TTG CGG ATG GTC GAC CTG CG-3'; catalase (cat): forward: 5'-ACC GGA GGC GGG AAC CCA AT-3', reverse: 5'-GGC GGC CCT GGA GCA TCT TG-3'; GAPDH: forward: 5'-TGC CAA GTA TGA TGA CAT CAA GAA G-3', reverse 5'-AGC CCA GGA TGC CCT TTA GT-3'. Relative gene expression was normalized to GAPDH. PCR conditions were: 95℃ for 10 minutes, followed by 40 cycles of 95℃ for 30 seconds, 60℃ for 1 minute, and 72℃ for 1 minute, followed by one cycle of 95℃ for 1 minute, 55℃ for 30 seconds, and 95℃ for 30 second s.

Data analysis

Image analysis was performed using custom-written Matlab routines and the software package PMOD (Mikolajczyk et al. 1998a).

Optical imaging. Data were analyzed as recently reported by our group (Calcinaghi et al. 2011). The analysis of the multiwavelength spectroscopy followed the protocol of Dunn and colleagues (Dunn et al. 2005). Baseline values for total hemoglobin

concentrations were set to 100 µM with 70% oxygen saturation, which implies $C_0^{\mathrm{HbO}} = 70$ µM and $C_0^{\mathrm{HbR}} = 30\,\mu\mathrm{M}$. To quantify CBF, speckle images were processed as described recently (Zakharov et al. 2009) using 5x5 spatial and 25 temporal binning. Circular regions of interest (0.5 mm^2) were drawn manually over the area of maximal stimulation-induced signal increase to extract the signal time courses. 10 trials carried out within 12 minutes in each animal were averaged. All data represent the mean ± standard error of the mean used for each experimental condition. Maximal amplitude, area under the curve (AUC) and the full width at 25% of the maximum were determined for instrinsic optical imaging data.

Two-photon laser scanning microscopy. Line scan data were analyzed using the Radon transform approach as described in Drew et al.(Drew et al. 2010a).

Histological image acquisition and processing. Digital images of cresyl violet staining were taken and analysis was performed with MCID™ software (InterFocus Imaging Ltd, Cambridge, UK). Immunoperoxidase staining analysis was performed using bright-field microscopy (Zeiss AxioScope) and images acquired with an 8-bit digital color camera (Zeiss AxioCam) controlled by AxioVision 4.5 (Zeiss).

Analysis of vascular density. Image processing was performed with Matlab (Mathworks, Natick, MA, USA). The FITC images were filtered, thresholded, and eroded to yield single-pixel-wide traces of the vessels. Layer-specific ROIs of the somatosensory cortex were defined manually on the DAPI images and transferred to the respective vessel trace from the same location. The length density, mean vessel caliber, and volume fraction were then computed stereologically for each cortical layer and the white matter (for more details see Weber et al. (2008)).

Statistics. Differences between hemodynamic responses between different groups were statistically analyzed using the Mann-Whitney U test. Data are presented as mean ± sem.

Results

Mean arterial blood pressure, heart rate and body weight in SHRs and CTRLs

During the *in vivo* multimodal imaging experiments, mean arterial blood pressure (MAP; mmHg) and heart rate (HR; beats/min) of animals were continuously monitored via a catheter inserted into the femoral artery (Fig. 2). SHR start to develop aHT between 5 and 10 weeks of age (Okamoto and Aoki 1963). Fig. 2A shows that MAP is significantly higher in SHR than in CTRL in all age groups (Box plot of MAP values, Mann-Whitney U-test, **p<0.005) and that HT is manifest in SHRs already at 10 weeks of age. In contrast to that, HR is significantly higher in SHR than in CTRL only at 40 weeks of age (Fig. 2B; Box Plot of HR data, Mann-Whitney U-test, **p<0.005; data not available for animals in the 10 weeks group). Additionally, all animals were weighted before anesthesia was induced. SHR aged 20 and 40 weeks have a smaller body weight than CTRL. No body weight difference was observed in the 10 weeks group (Fig. 2C; Box plot of weight data, Mann-Whitney U-test, **p<0.005).

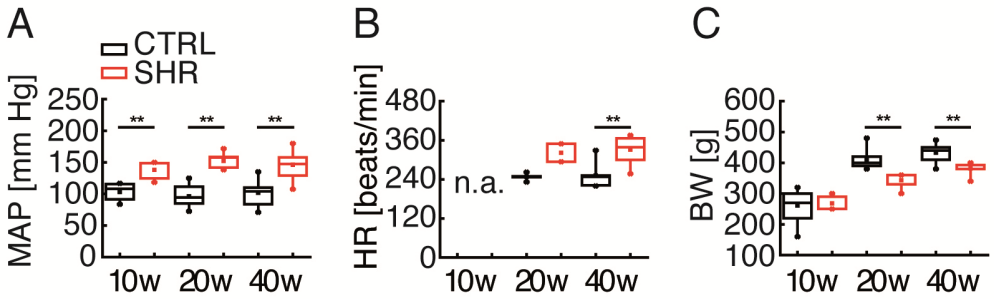

Paper 2 Figure 2. Mean Arterial Blood Pressure, Heart rate and Body Weight for CTRL and SHR at 10-, 20-, 40 weeks.

A, Box plot of mean arterial blood pressure values (MAP) for CTRL (10, 20 and 40 weeks, N=7, 13, 14, respectively) and SHR (10, 20 and 40 weeks, N=5, 9, 14, respectively). **B**, Box plot of heart rate values for CTRL (20 and 40 weeks, N=5, 8) and SHR (20 and 40 weeks, N=8, 7). **C**, Box plot of body weight values at the time of the experiment for CTRL (10, 20 and 40 weeks, N=8, 14, 15) and SHR (N=6, 9, 13). Stars indicate significance level p<0.005 (Mann-Whitney U-test).

Hemodynamic responses are impaired in SHRs in the 20 and 40 weeks groups

Hemodynamic responses were evoked in the somatosensory cortex by single whisker stimulation and imaged using multiwavelength spectroscopy combined with laser speckle imaging (Fig. 1). Rats of 10, 20, and 40 weeks of age were imaged (CTRL: n=5, 8, 11; SHR: n=5, 7, 12, respectively) and relative changes in total hemoglobin or cerebral blood volume (CBV) and CBF were measured.

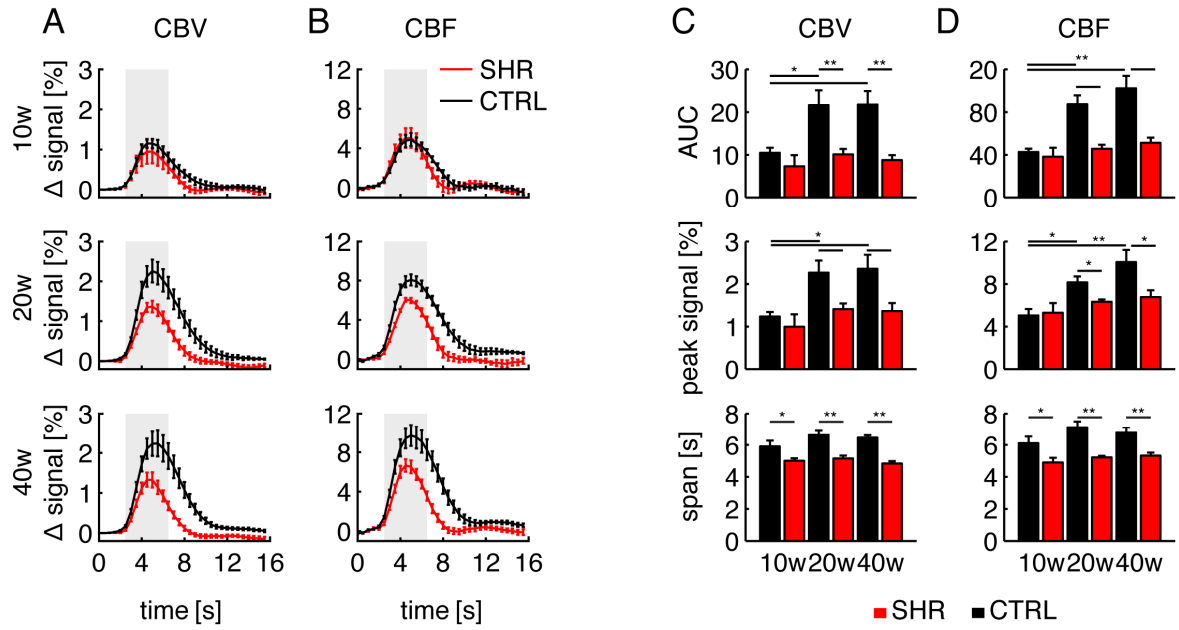

Paper 2 Figure 3. Impairment of the hemodynamic response increases with duration of aHTN.
CBV (**A**) and CBF (**B**) relative signal changes for CTRLs (black) and SHRs (red). Rats were imaged at 10, 20, and 40 weeks of age (CTRL: n=5, 8, 11; SHR: n=5, 7, 12, respectively). Area under the curve (AUC), peak signal, and time span of CBV (**C**) and CBF (**D**) (mean ± s.e.m.; Mann-Whitney U test, * p<0.05, ** p<0.005).

Fig. 3 shows that in the CTRL group, both CBV (panel A) and CBF (panel B) evoked signals increased with age. The area under the curve (AUC) and peak response exhibited a significant increase from 10 to 20 weeks and remained high in the 40 weeks group. In contrast, the time span of the responses was unaltered at 10, 20 and 40 weeks (Fig. 3C and D). When comparing the 10-week CTRL group with the respective age-matched SHR group, we observed very similar hemodynamic responses (peak value and AUC) despite the difference in MAP (Fig. 2A). However, as the SHRs aged, the evoked responses remained stable until 40 weeks, not displaying any significant changes in time span, amplitude, or AUC. Finally, the time span of evoked responses

was always slightly but significantly longer in the CTRL group than in the SHR group, already apparent at 10 weeks of age.

10-week treatment with LOS or VER does not normalize hemodynamic responses in SHRs

Next, we investigated whether antihypertensive treatment would restore NVC in SHRs. Two separate groups of SHRs were treated, one with the angiotensin II receptor 1 blocker losartan, the other with the calcium channel blocker verapamil from weeks 30 to 40 and imaged at 40 weeks of age. The drugs were administered in the drinking water at 30 and 80 mg/kg/day, respectively. The MAP of SHRs treated with LOS was significantly lowered compared to the MAP of untreated SHRs and reached the level of the CTRL group at the time of imaging, indicating that the LOS treatment normalized blood pressure values. In the VER treated group, the MAP was significantly lowered compared to the SHR group, but did not reach the level observed in CTRL animals (Fig. 5.E). Treatment with either LOS or VER did not alter body weight nor heart rate in comparison to untreated SHRs (Fig. 4).

Despite a reduction in MAP, the stimulation-evoked hemodynamic responses of the LOS and VER groups were not significantly different from those observed in untreated SHRs (Fig. 5A and B). None of the parameters used to characterize the responses, i.e. AUC, peak response, and time span, was found to be significantly different when compared to untreated SHRs (Fig. 5C and D).

Interestingly, for both CBV and CBF, the peak hemodynamic response and the MAP correlated significantly in SHRs (treated and untreated); this correlation was absent in CTRL animals (Fig. 5F). Although neither of the treatments affected the evoked responses, both treatments did push the animals closer to the region corresponding to CTRL animals in these MAP versus peak hemodynamic response graphs, with LOS being more effective than VER in line with the reduction in MAP (Fig. 5E and F).

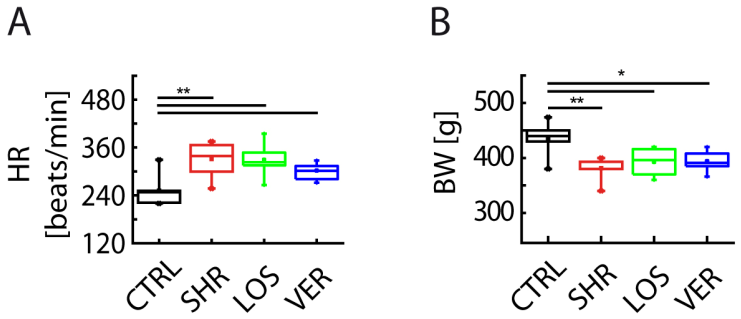

Paper 2 Figure 4. SHR untreated and treated have significant different Heart Rate and Body Weight in comparison to CTRL.

A. Box plot of heart rate (HR; beats/min) in the 40 weeks CTRL group (N=8), in the 40 weeks SHR group (N=7) and in both 40 weeks SHR groups treated with Losartan (LOS; N=9) or Verapamil (VER; N=8). Stars indicate significance with p-values * $p<0.05$, ** $p<0.005$ or *** $p<0.0005$ (Mann-Whitney U-test). **B.** Same as in A, but for body weights (g). N=13, 13, 10 and 10, respectively.

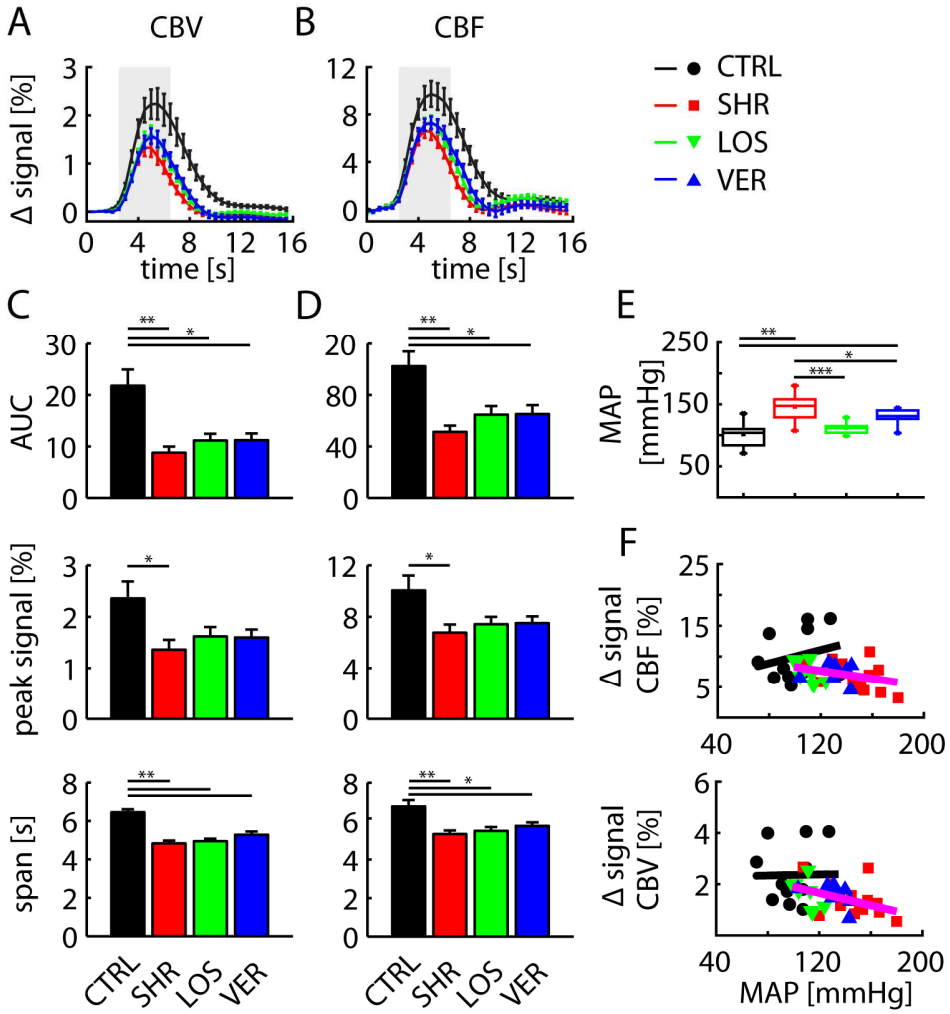

Paper 2 Figure 5. Antihypertensive treatment does not recover hemodynamic response.

Average evoked CBV (A) and CBF (B) responses in the 40-week-old animals (mean ± s.e.m.): CTRL group (n=11), SHR group (n=12), losartan treated group (LOS; n=9), and verapamil treated group (VER; n=8). (C), Area under the curve (AUC), peak signal, and time span corresponding to CBV traces in panel A (Mann-Whitney U test, * $p<0.05$, ** $p<0.005$). (D), Same as in panel C for CBF. (E), Box plot of MAP values for 40-week-old rats (CTRL: n=14, SHR: n=14, LOS: n=10, VER: n=9, Mann-Whitney U test, * $p<0.05$, ** $p<0.005$). (F), Correlation between peak CBF and MAP (top; pink line, R=0.451, $p<0.05$) and peak CBV and MAP (bottom; pink line, R=0.382, $p<0.05$) in all hypertensive groups (SHR, LOS, and VER). In both cases, no significant correlation was observed to MAP for the CTRL group (black lines).

Capillary red blood cell velocity correlates with the duration of aHTN

In order to assess the impact of aHTN and of the LOS and VER treatments on baseline microcirculation, we quantified capillary red blood cell (RBC) velocity in all groups aged 40 weeks. Two-photon *in vivo* imaging experiments were conducted and RBC velocity was measured in resting conditions from selected straight capillaries in layers 2/3 of the somatosensory cortex using the line scan technique (Kleinfeld et al. 1998) (Fig. 6A). The two-photon experiments were conducted on the same animals used for the intrinsic optical imaging experiments and the capillaries were chosen in the same barrel cortex area as previously imaged. Fig. 6 shows that RBC velocity in SHRs measured during resting conditions was significantly higher than in CTRL animals. Treatment with LOS reduced RBC velocity back to CTRL values, whereas treatment with VER reduced RBC velocity without reaching statistical significance (Fig. 6B).

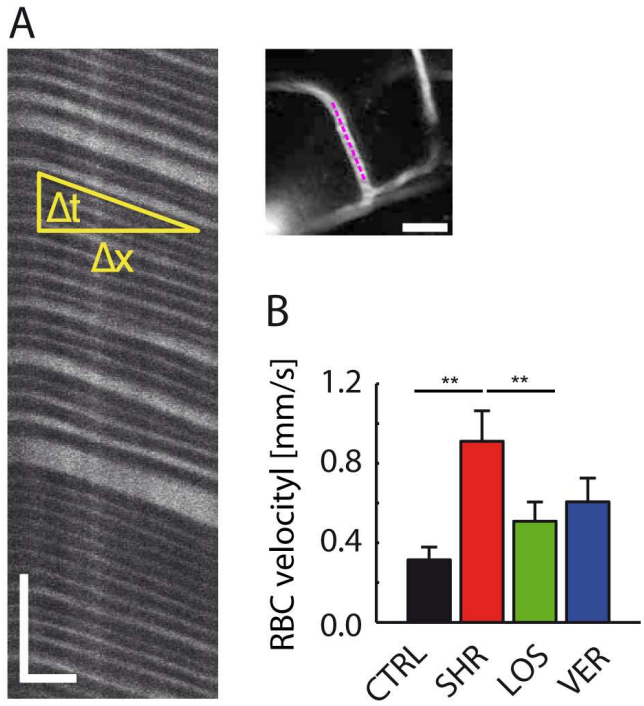

Paper 2 Figure 6. Baseline capillary flow is increased in SHRs.

(**A**), Line scans were repeatedly acquired along a capillary segment (magenta line; right panel; scale bar 20 µm) while the plasma was loaded with a fluorescent dye, yielding stripes when individual RBCs passed through the capillary (left panel; vertical scale bar 100 ms; horizontal scale bar 10 µm). (**B**), RBC baseline velocity (mean ± sem) for CTRL (n=17), SHR (n=12), LOS (n=27), and VER (n=24) (Mann-Whitney U test, ** $p<0.005$).

SHRs exhibit brain atrophy but no changes in microvascular density or vessel diameter

Cerebral atrophy was evaluated in all 40 weeks groups. Compared with CTRL animals, SHRs exhibited larger lateral ventricles and a thinner cortex in the occipital region (Nissl stained sections; Fig. 8A and B). Both are signs of progressive cerebral atrophy (Amenta et al. 2003).

Detailed analysis of the microvascular network such as volume fraction, length density, and vessel diameters revealed no differences between the subgroups at 40 weeks. In addition, they did not differ from age-matched CTRL animals (Fig. 8C and D).

No inflammatory reactions observed in the brains of CTRLs, SHRs, and treated animals

Microglial cells are responsive defense cells (Graeber 2010) and can sense pathological changes in the central nervous system, exhibiting morphological adjustments from a resting 'ramified' to an activated state (i.e. still ramified but with thicker cell processes) (Graeber 2010). The ionized calcium-binding adaptor molecule 1 (Iba1) is a macrophage/microglia-specific calcium-binding protein. It has been shown to be upregulated during an inflammation process because it is involved in the activation pathway (Imai and Kohsaka 2002). In all four groups of 40 weeks of age (CTRL, SHR, LOS, and VER), tipical Iba1 staining was observed and no morphological changes triggered by inflammation in microglia were detected (Fig. 8A)

Expression analyses of brain lysates reveal increased levels of eNOS and catalase in hypertensive rats

Expression analyses of brain lysates detected a blood pressure-dependent increase in endothelial nitric oxide synthase **(**eNOS) expression in 20-week-old rats (Fig. 8E), indicating an impairment of endothelial homeostasis. Expression levels did not rise further in older hypertensive animals. Moreover, we observed an age- and blood pressure-dependent increase in cerebral catalase expression, suggestive of enhanced levels of oxidative stress upon both aging and sustained hypertension (Fig. 8F). A trend towards a blood pressure-dependent increase in ncf1 (active subunit of NADPH

oxidase) from 1.08 ± 0.21 to 1.43 ± 0.24 (40 weeks CTRL vs. 40 weeks SHR; n=5, p=0.31, Fig. 7A) may contribute to increased generation of reactive oxygen species (ROS) in sustained hypertension.

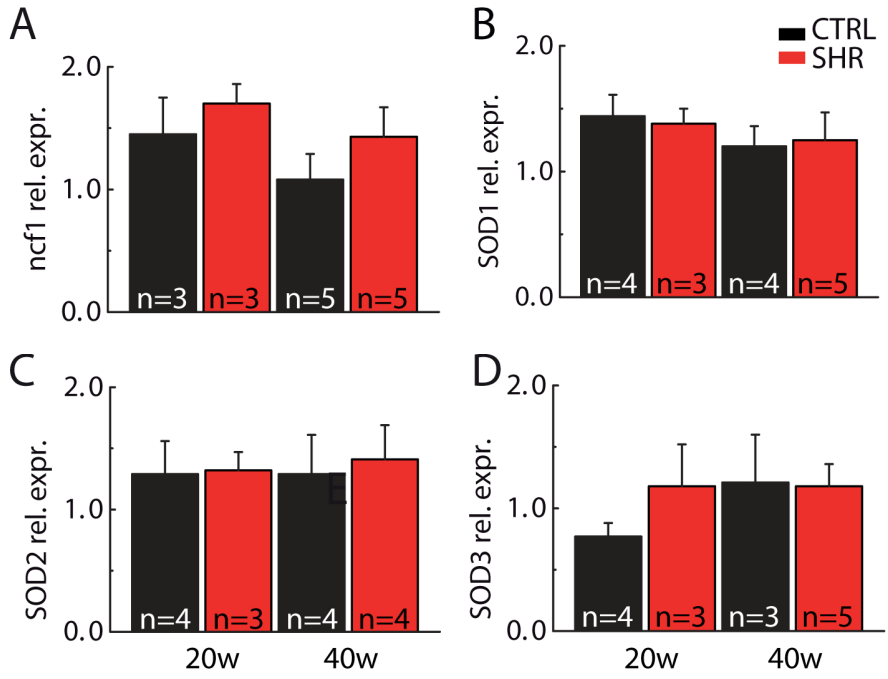

Paper 2 Figure 7. Expression analyses of brain lysates for CTRL and SHR.

Relative expression histograms of ncf1 (A), SOD1 (B), SOD2 (C), SOD3 (D). Mean ± s.e.m.

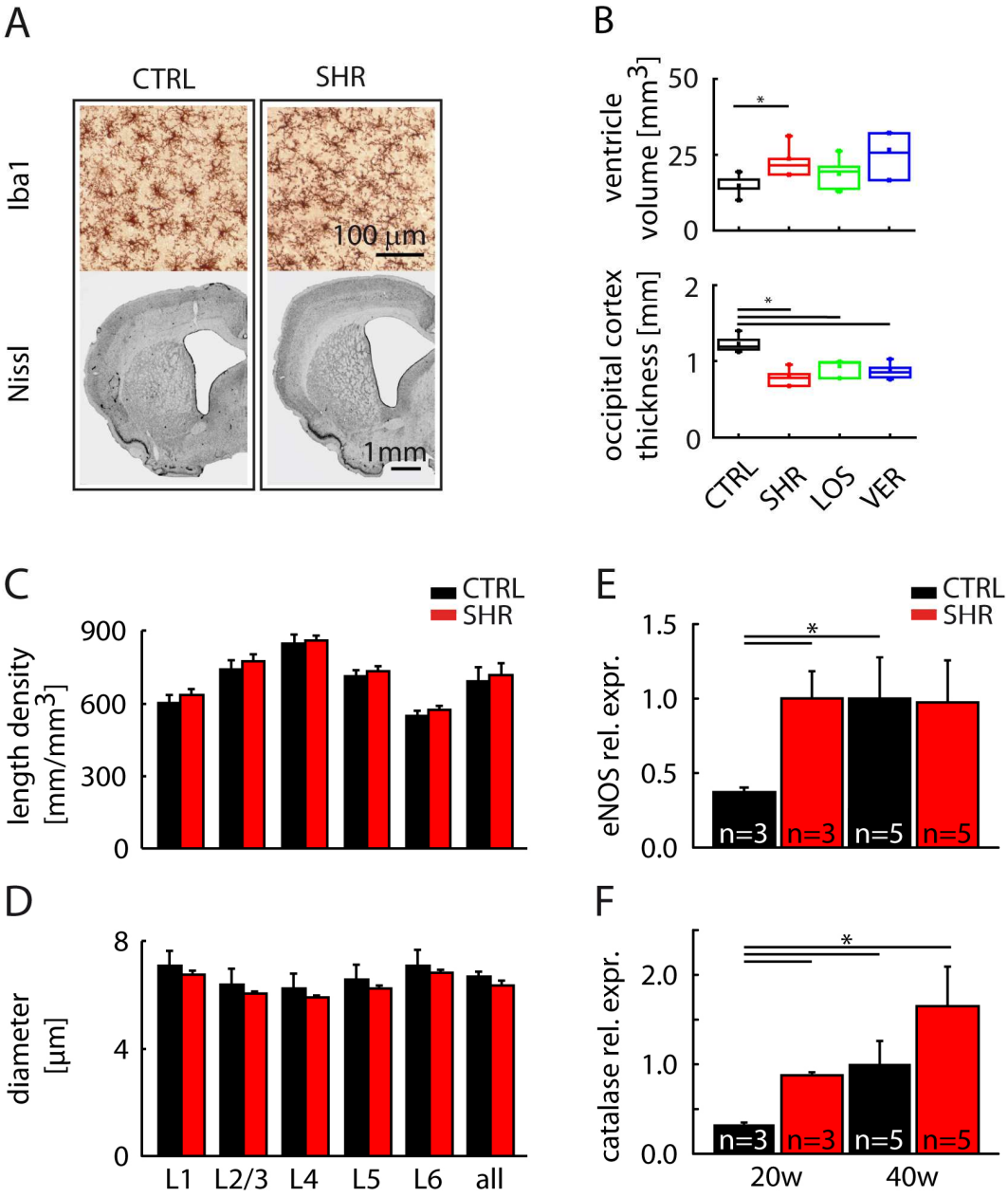

Paper 2 Figure 8. Structural and biochemical analyses reveal brain atrophy in 40-week-old SHRs without active inflammatory reactions and increased anti-oxidant defense.

(**A**), Representative example of Iba1 staining (upper panel) and Nissl staining (lower panel) from CTRLs and SHRs. 4 brains from every group at 40 weeks age (CTRL, SHR, LOS, VER) were stained for Iba1. (**B**), Box plot of lateral ventricle volumes (mm^3, upper panel) and occipital cortex thickness (mm, lower panel) measured from Nissl stained sections of 40-week-old rats: CTRL (N=5), SHR (N=4). LOS (N=4) and VER (N=5) with the same color code as in Fig. 3. Statistical analysis: asterisks indicate significant difference according to Mann-Whitney U test, * $p<0.05$. Microvascular structure analysis was performed from layer 1 to 6 of the barrel cortex: capillary length density (**C**) and diameter (**D**) are reported as mean ± sem (CTRL n=3, SHR n=5). Expression analyses derived from lysates of the somatosensory cortices of 20- and 40-week-old rats were assessed by real-time PCR: endothelial nitric oxide synthase (**E**) and catalase (**F**) (Mean ± sem**,** Mann-Whitney U test, * $p<0.05$).

Discussion

aHTN constitutes a major risk factor for transient ischemic attacks and stroke that represent a major cause of morbidity in Western countries. Several studies have investigated the role of aHTN in the pathogenesis of stroke (Sacco 2001) and assessed the benefit of lowering elevated blood pressure for stroke prevention. Less is known about the impact of aHTN on physiological CBF-related processes such as NVC.

The present work reports five major findings: (1) CBF alterations occurred only after a period of sustained hypertension: 20- and 40- but not 10-week-old SHRs showed reduced hemodynamic responses to somatosensory stimulation despite increased MAP values already being present in animals of 10 weeks of age; (2) baseline capillary blood flow was increased in 40-week-old SHRs compared to age-matched CTRLs; (3) antihypertensive treatment recovered baseline capillary RBC velocity but did not affect evoked hemodynamic responses; (4) the functional changes were not accompanied by structural alterations of the cerebral microvascular network; and (5) sustained hypertension increased oxidative stress and impaired endothelial homeostasis.

A short-term increase in blood pressure is not sufficient to impair NVC

Our results indicate that aHTN alone does not explain the impairment of the neurovascular response. Although increased MAP was already present in 10-week-old SHRs (Fig. 2A), the cerebrovascular dysfunction only became evident at the age of 20 weeks and later (Fig. 3). These results support the notion that the increase in blood pressure in the early phase of aHTN may be compensated for by the brain through autoregulative processes (Claassen et al. 2008) and is not sufficient to lead to the observed functional disturbances in CBF responses. Only at a later stage did we detect functional impairment. This finding is in agreement with the work of Capone et al.(2010) who demonstrated that acute or chronic non-pressor doses of angiotensin II injected into mice induce cerebrovascular dysfunction and increase levels of ROS. Similar to our findings, they reported a >40% attenuation of the blood flow response to whisker stimulation. Biochemical and structural changes triggered by the chronically increased arterial blood pressure may induce a dysfunction in NVC. Higher blood velocity associated with aHTN leads to increased shear stress on the blood vessel wall, which

has been reported to result in the remodeling of cellular and extracellular components in the vessel wall (Baumbach and Heistad 1991; Baumbach et al. 2003).

Apart from inducing structural changes, aHTN alters molecular mechanisms critical for functional integrity at both the neural and vascular level. aHTN is known to favor an imbalance in antioxidant defense systems as well as a disruption of endothelial homeostasis (Chrissobolis and Faraci 2008; Girouard et al. 2007). In a recent paper, Capone and colleagues (2012) demostrated that ROS production in the subfornical organ is involved in the NVC impairment observed in aHTN. Similar events may be reflected in our expression analyses of cerebral lysates in which we observed increased expression levels of the cytosolic active subunit of NADPH oxidase, an important source of ROS in endothelial cells. Increased levels of catalase, an enzyme scavenging free radicals, suggest a blood pressure- and age-dependent enhancement of this antioxidative defense mechanism. Therefore, increased generation of ROS upon aging and sustained hypertension may exceed the cerebral antioxidant defense capacity, and thereby contribute to cerebral endothelial dysfunction.

A key mechanism by which intact endothelial cells communicate with the underlying vascular smooth muscle cells constitutes eNOS-derived nitric oxide (NO) (Faraci 2006; Toda et al. 2009). Endothelial (and neuronal) cell-mediated NO-dependent vascular relaxation of cerebral arteries and arterioles is known to contribute to increased CBF. We found increased levels of eNOS in 20-week-old hypertensive animals; this may reflect a compensatory mechanism in response to reduced CBF. Our finding is in accordance with earlier reports describing an upregulation of cerebral eNOS in SHRs (Hojna et al. 2007). A similar compensatory increase in eNOS has been described in rats upon aging. Van der Loo et al. found an increase in O_2^-, trapping of vasorelaxant NO, and subsequent peroxynitrite formation, followed by nitration and inhibition of manganese superoxide dismutase (van der Loo et al. 2009).

Taken together, these findings may support the notion that insufficient compensation for increased cerebral levels of ROS and impaired endothelial homeostasis contribute to impaired NVC.

Capillary RBC velocity is increased in hypertensive animals

In addition to the spectroscopic assessment of the hemodynamic response, we determined RBC velocity in single capillaries in the somatosensory cortex using two-photon microscopy. We observed a marked increase in baseline RBC velocity in SHRs (40 weeks) compared to normotensive control animals. Our finding is in contrast to the findings of other studies showing maintained (Jennings et al. 2005; Wei et al. 1992) or decreased CBF (Beason-Held et al. 2007; Fujishima et al. 1995). However, our study is the first one to selectively investigate the relationship between blood pressure and CBF at the capillary level using two-photon microscopy. The observed velocity increase was less pronounced in animals on antihypertensive therapy. The linear correlation between MAP and RBC velocity suggests a direct relationship between increased arteriovenous pressure gradient and blood flow velocity. For such a direct relationship to be true, two prerequisites must be fulfilled: (1) impaired cerebral autoregulation and (2) unaltered microvascular density. Both of these prerequisites are discussed in detail below.

Impaired cerebral autoregulation

Cerebral autoregulation maintains a constant perfusion of brain parenchyma within a certain blood pressure range. Intact cerebral autoregulation depends on various mechanisms such as myogenic, neurogenic/sympathetic, and endothelial components (Ohta et al. 1991). In sustained aHTN cerebral autoregulation is altered, mainly due to vascular hypertrophy (Paulson et al. 1990). The reduced hemodynamic response upon activation observed in 20- and 40-week-old SHRs also points to an impaired capacity of precapillary vessels to dilate, as otherwise the stimulation-induced increase in blood flow would be comparable in normotensive and hypertensive animals.

Unchanged microvascular density and diameter

We were unable to detect changes in vascular density and diameter in the somatosensory cortex – even after sustained hypertension. In accordance, other groups have not found consistent differences between SHRs and CTRLs in the cerebral capillary network (Lin et al. 1990) and in arterial luminal diameter (Struijker Boudier et al. 1992). However, this subject requires further study, as diameter changes have been described (Baumbach and Heistad 1988). We are aware that the absence of differences between SHRs and CTRLs in our histological samples does not exclude them. Our histological measurements incompletely reflect the physiological in vivo situation, mainly due to a lack of vascular tone and intraluminal pressure. In addition, our histological approach has a spatial resolution of 0.7 µm (Weber et al. 2008) and as a consequence small differences might remain undetected.

Antihypertensive treatment reduces baseline CBF but does not normalize functional hyperemia in hypertensive animals

Ten weeks of treatment with the angiotensin II type 1 receptor antagonist losartan or with the calcium channel blocker verapamil were not effective in normalizing hemodynamic responses towards control levels (Fig. 5). Notably, MAP was successfully reduced with both therapeutic regimens. Thus, it appears that lowering blood pressure by a 10-week long pharmacological mono-treatment is not sufficient to affect functional hemodynamic signals and to compensate for all the involved pathways such as increased oxidative stress, endothelial imbalance, and brain atrophy. In contrast, we found a significant reduction of the elevated baseline capillary blood flow upon treatment with losartan (Fig. 6B). From a fluid dynamics perspective, blood flow velocity directly depends on the resistance and the pressure gradient between two compartments, which are both increased in hypertension (O'Rourke and Hashimoto 2007; Ritz et al. 2009) and – according to our data – brought back to a normal level by antihypertensive treatment.

On the other hand, regeneration of the impaired CBF response upon whisker stimulation was not accomplished with the applied treatment. However, a non-significant

increase towards the control situation was observed. Fig. 5F illustrates that the measurements obtained in treated animals were shifted towards the left and upwards. There was a change of the hemodynamic response in these animals towards higher hemodynamic signals at lower MAP values. The exact reasons for the incomplete recovery after treatment remain unclear. Insufficient treatment duration could be an important factor. Furthermore, a single pharmacological target might not be sufficient. Indeed, Dupuis and colleagues recently reported that telmisartan – like losartan, an angiotensin II type 1 receptor antagonist – does not have a significant impact on mean cerebral arteriolar pressure in SHRs (Dupuis et al. 2010).

Sabbatini et al. (Sabbatini et al. 2001) treated SHRs for 12 weeks with different antihypertensive drugs: dihydropyridine-type calcium channel blockers (lercanidipine, manidipine, and nimodipine) and hydralazine. The observed loss of frontal, occipital, and hippocampal neurons was partially prohibited by the treatments, with a better performance of hydralazine, although the drugs showed a similar effect on blood pressure. This suggests a neuroprotective effect of hydralazine in hypertensive subjects.

In general, the wide spectrum of different results reported reflects the complex nature of cerebrovascular regulation in the pathophysiology of essential aHTN and underlines the need for further *in vivo* research using multimodal imaging technology.

Limitations

The use of older animals may allow the effects of sustained aHTN and aging on CBF to be specifically addressed. For technical reasons, our two-photon imaging of capillary RBC velocity was limited to 40-week-old animals and only included resting state measurements. Furthermore, the applied antihypertensive treatment protocol could be extended with respect to choice of drugs, dosage, and treatment period.

Conclusions

To the best of our knowledge, this is the first study to investigate the effects of sustained aHTN on cerebral perfusion in SHRs. With increasing duration of aHTN, we

found an increased impairment of the hemodynamic response following sensory stimulation and an elevated baseline capillary RBC velocity. Mono-antihypertensive treatment either with LOS or with VER reduced blood pressure within 10 weeks but was insufficient to normalize the impaired hemodynamic response, indicating the need for alternative or additional treatment strategies to address the cerebrovascular functional impairment in sustained hypertension. Additional research is required to further elucidate possible interactions of sustained aHTN and aging. This will be of particular interest for therapeutic efforts aimed at inhibiting the progression of neurodegenerative diseases, such as Alzheimer's disease or vascular dementia, where the pathophysiology involves impaired blood supply (Iadecola and Davisson 2008).

Chapter 4. Implications and future directions

The aim of this thesis was to contribute to a better understanding of the important aspects of neurovascular coupling. First, we investigated whether $mGluR_5$ activation is the main trigger in the initiation of hemodynamic responses in NVC and whether it is directly involved in CBF regulation in the rat somatosensory cortex upon whisker stimulation. Second, we studied how hemodynamic responses are affected by arterial hypertension in SHR and aged-matched control rats. We also studied whether the impairment in NVC with hypertension is reversed by antihypertensive treatment.

In the following section, I would like to focus on some important implications of our results, highlight the relevance of our data and identify potential approaches for use in answering remaining research questions.

Open questions about the role of astrocytes in functional hyperemia *in vivo*

In the paper, "Metabotropic glutamate receptor $mGluR_5$ is not involved in the early hemodynamic response," it is shown that $mGluR_5$ blockade does not affect the hemodynamic response *in vivo* upon whisker stimulation. Our data challenge a model in which astrocytes are the main initiators and principal mediators of functional hyperemia *in vivo*. Some important and as yet unanswered questions will be discussed below.

A) What is the temporal scale of astrocytic and neuronal signals in the functional hyperemia response?

According to work published to date, the time scales of stimulus-evoked calcium changes in astrocytes and of functional hyperemia do not completely match *in vivo*. In various brain areas in several species (mouse somatosensory cortex, ferret visual cortex, mouse olfactory glomeruli) the onset of astrocytic calcium changes has been described to be in the range of 1-6 seconds (Petzold et al. 2008; Schummers et al. 2008; Takano et al. 2006; Wang et al. 2006), whereas the hyperemic response typically starts about 0.5-1 second after the stimulus onset (Devor et al. 2008; Tian et al. 2010; Weber et al. 2004).

Furthermore, the activation kinetics of a metabotropic receptor might not be compatible with onset of the functional hyperemia response (Perea and Araque 2005). How can $mGluR_5$ activation in astrocytes lead to the production of several vasoactive molecules in less than 1 second? (Attwell et al. 2010) Here, we try to identify the main reasons why *in vivo* astrocytic calcium waves are detected a few seconds after the onset of hyperemia. This delay could possibly be due to some technical issues: (i) the calcium signal could be unspecific because synthetic dyes are taken up by all cells, and (ii) the indicator molecules could be insufficiently sensitive to detect small changes in calcium concentration and may preferentially concentrate in the soma rather than in the astrocytic endfeet (Petzold and Murthy 2011). Alternatively, astrocytic calcium waves could occur a few seconds after onset of the hyperemic response because they are actually involved in the maintenance of the functional hyperemia response, rather than in the initiation process. In this regard, neurons that express ionotropic receptors more abundantly than astrocytes may be good candidates for initiating the functional hyperemia response by means of their fast calcium signal kinetics (Cauli and Hamel 2010; Petersen et al. 2003).

B) Are astrocytes activated by glutamate only via $mGluR_5$?

$mGluR_5$ expression is not restricted to astrocytes. It has been shown that these receptors are more abundant in neurons in the mature brain (Barres 2008). Additionally, $mGluR_5$ is highly expressed in reactive glia, i.e. in non-physiological states. Another important pathway for astrocytic activation by glutamate involves uptake by amino acid transporters. Reduced CBF responses were reported after application of TBOA, a broad-spectrum glutamate transporter inhibitor, in the olfactory bulb (Gurden et al. 2006; Petzold et al. 2008) or in the visual cortex (Schummers et al. 2008). This effect was additionally observed after injection of DHK, a selective inhibitor of the astrocytic glutamate transporter GLT1 (Petzold et al. 2008). However, transport inhibition may increase glutamate concentration in the synaptic space and thereby enhance glutamate receptor stimulation. Therefore, it is still unclear how these two described astrocytic activation pathways are linked or coordinated during the *in vivo* functional hyperemic response. The cellular mechanisms underlying these effects are yet to be investigated

in detail, and further research on these pathways with either selective pharmacological tools or novel approaches (see below) is necessary to address specific questions.

Open questions about hypertension and aging effects on functional hyperemia

In the paper "Multimodal imaging reveals impaired neurovascular coupling after chronic hypertension," a research project was undertaken and reports for the first time the effects of hypertension and disease duration on functional hyperemia by means of a multimodal imaging approach. In addition to functional evidence of the NVC disruption in hypertension, structural analyses were performed on the same rat brains. A better understanding of NVC impairment at the NVU level will provide new insights in the identification of the pathophysiological processes underlying vascular cognitive impairments. However, there remain several questions that need to be specifically addressed.

A) What is the direct effect of oxidative stress on the functional impairment in NVC?

Reactive oxygen species have been identified as key pathogenic effectors of cerebrovascular dysfunction during pathological conditions such as hypertension (Girouard and Iadecola 2006). In our study, some signs of increased oxidative stress have been identified from the rat brain lysates, suggesting that ROS production exceeds the antioxidant defense capacity. Increased oxidative stress might be a factor leading to the observed dysfunction in NVC and requires further investigation. In angiotensin-induced hypertension, peroxynitrite inhibitors abolish the angiotensin-induced impairment of CBF responses (Girouard et al. 2006). Using our multimodal approach applied in SHR and WKR at different ages, it would be useful to better investigate the contribution of ROS on NVC impairment and its reversibility upon pharmacological treatment (for example with peroxynitrite inhibitors). Such experiments would shed light on the responsible mediators of NVC disruption in chronic hypertension and will potentially offer new strategies to curtail cerebrovascular oxidative stress with further clinical implications.

B) When should a successful antihypertensive treatment be started? Is treatment with multiple drugs superior to mono-treatment?

Losartan and verapamil were administered for ten weeks to SHR from age 30 to 40 weeks. In the treated SHRs the evoked hemodynamic responses did not return to control levels whereas RBC velocity responses did. In view of these results, we asked ourselves: should this treatment have been started at the onset of hypertension in SHR (8-10 weeks) and not when hypertension was already fully established (30^{th} week)? Should the treatment period have been longer? Additionally, a mono-therapy was employed. Could a multi-treatment approach reverse the functional hyperemia impairment observed in 40-week-old SHR?

General outlook

NVC process research remains an important area of scientific endeavor with the potential to further understanding and improve treatments in clinical populations. Many questions remain unanswered but nevertheless important for progress in this field. Relevant remaining questions are:

1) Which are the most important pathways involved in the complex regulation of NVC?
2) Are there specific vasoactive messengers for particular phases of the hyperemic response (initiation, maintenance and propagation of vasodilation)?
3) What is the primary target of specific vasoactive molecules (large arterioles, precapillary arterioles, capillaries)?
4) How do different cellular subpopulations - astrocytes, excitatory neurons, inhibitory interneurons - contribute to functional hyperemia?

In attempting to answer these questions, novel techniques and improved understanding will be required. Already newly available techniques are lighting the way to furthering knowledge in this area. In particular:

1. Genetic modifications in animals.

With our experimental approach as for most pharmacological interventions, we were not able to selectively block astrocytic $mGluR_5$. In order to specifically distinguish between astrocytic and neuronal receptor contribution to NVC, genetically engineered mice could be employed with a receptor knocked out (Fiacco et al. 2007) or with an inducible receptor overexpression in a cell specific manner. Additionally, to selectively investigate the contribution of glutamate transporters in the functional hyperemia process, gene targeted mice lacking specific astrocytic glutamate transporters may be used for *in vivo* experiments.

2. Technical development/new methodologies.

   Optogenetics is a new approach that allows selective activation of specific cell populations by optically activated G-protein coupled receptors (OptoXRs), (Airan et al. 2009). This recently introduced technology provides new possibilities for studying *in vivo* intracellular signaling processes with more precise spatio-temporal control. Specific neurons have been manipulated with Channelrhodopsin (ChR2) optogenetic probes, and ChR2 transgenic mice have been generated. By means of this technology, results were published recently: Lee and colleagues (2010) have demonstrated that cortical pyramidal neurons expressing ChR2 evoke changes in fMRI BOLD. Furthermore, Scott and colleagues (2012) reported that deep cortical pyramidal neurons expressing ChR2 by light activation can evoke changes in optical and CBF signals in the somatosensory cortex.

   Following from this work, an interesting idea would be to selectively activate by ChR2 astrocytes or specific interneurons and thus observe the selective contribution of these specific cells to hemodynamic responses.

3. NVC in pathologies.

   In the past, most studies of NVC were performed on the healthy humans and animals. All the questions we should like to answer ought to be considered with regards not only to normal physiological conditions but also to diseases where NVC has been shown to be impaired.

4. Chronic implantation.

A possible technical approach may be to study hypertension effects on NVC in the same animals examined at different ages. Multiple experiments on the same SHR and WKR animals could be performed by employment of an *in vivo* chronic brain imaging approach. Such an approach would allow evaluation of the aging process in the same cohort of animals, reducing the individual variability and providing important longitudinal data.

5. Investigation in awake animals.

   The brain imaging experiments described here were performed under anesthesia. It has been reported that hemodynamic responses to functional stimulation can change according to the anesthetic regime used and between anesthetized and awake animals (Drew et al. 2010b). An evaluation of NVC mechanisms with a combined approach (anesthetized and awake animals) would likely allow identification of artifacts resulting from anesthesia.

In summary, the results described in this thesis provide new insights into understanding the basic principles of NVC in physiological conditions and in the presence of hypertension-aging. Our experimental results contribute to better interpreting the read-out of neuroimaging studies. With regard to the study on hypertension, the inability of the antihypertensive treatment to recover the functional hyperemia impairment in aged SHR may be partially responsible for the onset of vascular cognitive impairment in elderly patients. This finding has important implications for clinical populations and the aged. Further investigation is required to identify dysfunction at the NVU level and to unveil the cerebrovascular component of important cognitive disorders and degenerative diseases such as Alzheimer's disease.

Curriculum Vitae

Name: CALCINAGHI

First Name: Novella

Date of Birth: 25th September 1976, Milan (Italy)

Nationality: Italian (IT)

Education

- High school Liceo Classico "Bartolomeo Zucchi", Monza (Monza e Brianza), year of graduation 1995, Matura.
- Milan University, Pharmacy Faculty, Chemistry and Pharmaceutical Technologies degree (Università degli Studi di Milano, Facolta' di Farmacia, Chimica e Tecnologie Farmaceutiche), from 1995 to 2001, 100/110.

  Master thesis to Neuroprotection Laboratory, Prof. Andrea Volterra, Pharmaceutical Sciences Department, from 2000 to 2001. Thesis Title: "*The chemokine SDF-1α induces glutamate release from astrocytes via TNF-α with effects on synaptic transmission*".
- Employed as PhD student at the University of Zurich since January 2008, Institute of Pharmacology and Toxicology, Functional Imaging and Neurovascular Coupling Laboratory, Prof. Bruno Weber.

Positions:

- PhD student at Universität Zürich (MNF), from 2008 to 2012;
- Scientist at Glaxo Smith Kline (GSK), Drug Discovery Department, In vitro Electrophysiology, Research and Development Center, Verona (Italy) (from 2005 to 2007) and previously Associate Scientist (from 2002 to 2005);
- Internship in the Neuroprotection Laboratory, Prof. Andrea Volterra, Pharmaceutical Sciences Department, Universita' degli Studi di Milano, 2002;
- Internship as pharmacist, Milano, 2001.

Publications

During PhD:

[1] Zakharov P, Völker AC, Wyss MT, Haiss F, **Calcinaghi N**, Zunzunegui C, Buck A, Scheffold F, Weber B. *Dynamic laser speckle imaging of cerebral blood flow*. Opt Express. 2009 Aug 3;17(16):13904-17.

[2] **Calcinaghi, N.,** Jolivet, R., Wyss, M. T., Zunzunegui, C., Gasparini, F., Buck A. and Weber B. *Blockade of the Metabotropic Glutamate Receptor mGluR$_5$ does not affect Neurovascular Coupling in adult Sprague-Dawley rats.* Proceedings of the 9th European Meeting on Glial Cells in Health and Disease**,** Sept 2009 (Paris). GLIA 2009 Vol. 57 (13)**;** S124-S124**.**

[3] **Calcinaghi, N.,** Jolivet, R., Wyss, M. T., Gasparini, F., Ametamey S., Buck A. and Weber B. Metabotropic Glutamate Receptor mGluR$_5$ is not involved in the early neurovascular response. Journal of cerebral blood flow and metabolism, 2011. Vol 31 (9); pag 1967.

[4] **Calcinaghi, N.,** Wyss, M.T., Jolivet, R., Singh A., Keller A., Winnik S., Buck A., Fritschy JM., Matter C. and Weber B. Multimodal imaging reveals impaired neurovascular coupling in sustained hypertension. Submitted.

[5] Chamot, S.R., Migacheva, E.V., **Calcinaghi, N.**, Wyss, M., Weber, B., Rudin, M., Depeursinge, C., Magistretti, P.J., Marquet P. Variations of Cortex Optical Properties During Sustained Neuronal Activity. In preparation.

Before PhD:

[6] Davies, D., Crowe, M., Lucas, N.,Quinn, J., Miller, D., Pritchard, S., Grose, D., Bettini, E., **Calcinaghi, N.**, Virginio, C., Abberley, L., Goldsmith, P., Michel, A., Chessel, I., Kew, J., Milelr, N. and Gunthorpe M. A novel series of benzimidazole NR2B-selective NMDA receptor antagonist. Bioorganic and Medicinal Chemistry Letters. 2012

Poster Presentations

During PhD

[1] **Calcinaghi, N**., Jolivet, R., Wyss, M.T., Zunzunegui, C., Gasparini, F., Buck, A., Weber, B*. Blockade of the metabotropic glutamate receptor mGluR5 does not affect neurovascular coupling in adult Sprague-Dawley rats.* Swiss society of Neuroscience, Fribourg 2009.

[2] **Calcinaghi, N**., Jolivet, R., Wyss, M.T., Zunzunegui, C., Gasparini, F., Buck, A., Weber, B*. Blockade of the metabotropic glutamate receptor mGluR5 does not affect neurovascular coupling in adult Sprague-Dawley rats.* 9th European Meeting on Glial Cells, Paris 2009.

[3] **Calcinaghi, N**., Jolivet, R., Wyss, M.T., Zunzunegui, C., Gasparini, F., Buck, A., Weber, B*. Blockade of the metabotropic glutamate receptor mGluR5 does not affect neurovascular coupling in adult Sprague-Dawley rats.* Gordon Conference in Glial Biology, Ventura (CA).

[4] **Calcinaghi, N**., Jolivet, R., Wyss, M.T., Zunzunegui, C., Gasparini, F., Buck, A., Weber, B*. Blockade of the metabotropic glutamate receptor mGluR5 does not affect neurovascular coupling in adult Sprague-Dawley rats.* Society of Neuroscience (SfN), Chicago (IL), 2009.

[5] **Calcinaghi, N**., Jolivet, R., Wyss, M.T., Zunzunegui, C., Gasparini, F., Buck, A., Weber, B*. Blockade of the metabotropic glutamate receptor mGluR5 does not affect neurovascular coupling in adult Sprague-Dawley rats.* Pharma day, Pharmacology and Toxicology Institute, University of Zürich, 2009.

[6] **Calcinaghi, N.**, Jolivet, R., Wyss, M.T., Matter C., Buck, A., Weber, B*. Imaging Neurovascular Coupling in Normotensive and Spontaneously Hypertensive Rats.* Swiss Society of Neuroscience Meeting, Lausanne, 2010.

[7] **Calcinaghi, N.**, Jolivet, R., Wyss, M.T., Matter C., Buck, A., Weber, B*. Imaging Neurovascular Coupling in Normotensive and Spontaneously Hypertensive Rats.*

Gordon Research Conference in Brain energy metabolism and blood flow, Andover (NH), 2010.

[8] **Calcinaghi, N.**, Jolivet, R., Wyss, M.T., Matter C., Buck, A., Weber, B*. Imaging Neurovascular Coupling in Normotensive and Spontaneously Hypertensive Rats.* Pharma Day, Pharmacology and Toxicology Institute, University of Zürich, 2010.

[9] **Calcinaghi, N**., Jolivet, R., Wyss, M.T., Gasparini, F., Buck, A., Weber, B*. Metabotropic glutamate receptor mGluR5 is not involved in the initiation of the hemodynamic response.* 10th European Meeting on Glial Cells in Health and Disease, Prague, Sept 2011.

[10] S.R. Chamot, E.V. Migacheva, **N. Calcinaghi**, M.Wyss, B.Weber, M. Rudin, C. Depeursinge, P.J.Magistretti, P. Marquet. *Variations of Cortex Optical Properties During Sustained Neuronal Activity*. Optical society Meeting, Optics in Neuroscience Topical Meeting, Monterey, California, 2011.

[11] S.R. Chamot, E.V. Migacheva, **N. Calcinaghi**, M.Wyss, B.Weber, M. Rudin, C. Depeursinge, P.J.Magistretti, P. Marquet. *Variations of Cortex Optical Properties During Sustained Neuronal Activity*. Brain Pet international congress, Barcelona (Spain), 2011.

[12] **Calcinaghi, N.**, Wyss, M.T., Jolivet, R., Singh A., Keller, A.L., Winnik, S., Fritschy, J-M., Buck, A., Matter C., Weber, B*. Neurovascular coupling impairment increases with age in Spontaneous Hypertensive Rats (SHR).* Brain Pet international congress, Barcelona, May 2011.

[13] **Calcinaghi, N.**, Wyss, M.T., Jolivet, R., Singh A., Keller, A.L., Winnik, S., Fritschy, J-M., Buck, A., Matter C., Weber, B*. Neurovascular coupling impairment increases with age in Spontaneous Hypertensive Rats (SHR).* Pharma day, Pharmacology and Toxicology Institute, University of Zürich, 2011.

[14] **Calcinaghi, N.**, Wyss, M.T., Jolivet, R., Singh A., Keller, A.L., Winnik, S., Fritschy, J-M., Buck, A., Matter C., Weber, B*. Neurovascular coupling impairment*

increases with age in Spontaneous Hypertensive Rats (SHR). Swiss Society of Neuroscience Meeting, Zürich 2012.

[15] **Calcinaghi, N.**, Wyss, M.T., Jolivet, R., Singh A., Keller, A.L., Winnik, S., Fritschy, J-M., Buck, A., Matter C., Weber, B*. Neurovascular coupling impairment increases with age in Spontaneous Hypertensive Rats (SHR).* 11th Day of Clinical Research, Zürich University Hospital, Zürich, 2012.

Before PhD

[1] **Calcinaghi N.**, Virginio C. and Jarolimek W. *Biophysical characterisazion of NMDA 1A/2B receptor antagonists in transiently transfected HEK293T cells (A079.2*). FENS, Lisbon, 2004.

[2] **Calcinaghi N.**, Virginio C. and Jarolimek W. *Alpha1-nAChR: Profiling of Neuromuscular blockers and marketed drugs by electrophysiology (A044.2)*. FENS, Wien, 2006.

References

Airan RD, Thompson KR, Fenno LE, Bernstein H, Deisseroth K. (2009) Temporally precise in vivo control of intracellular signalling. *Nature* 458:1025-1029

Amenta F, Antonietta M, Tullio D, Tomassoni D. (2003) Arterial hypertension and brain damage - Evidence from animal models (Review). *Clinical and Experimental Hypertension* 25:359-380

Ances BM, Liang CL, Leontiev O, Perthen JE, Fleisher AS, Lansing AE, Buxton RB. (2009) Effects of aging on cerebral blood flow, oxygen metabolism, and blood oxygenation level dependent responses to visual stimulation. *Hum Brain Mapp* 30:1120-1132

Aronica E, van Vliet EA, Mayboroda OA, Troost D, da Silva FH, Gorter JA. (2000) Upregulation of metabotropic glutamate receptor subtype mGluR3 and mGluR5 in reactive astrocytes in a rat model of mesial temporal lobe epilepsy. *Eur J Neurosci* 12:2333-2344

Attwell D, Buchan AM, Charpak S, Lauritzen M, MacVicar BA, Newman EA. (2010) Glial and neuronal control of brain blood flow. *Nature* 468:232-243

Attwell D, Laughlin SB. (2001) An energy budget for signaling in the grey matter of the brain. *J Cereb Blood Flow Metab* 21:1133-1145

Ballester-Rosado CJ, Albright MJ, Wu CS, Liao CC, Zhu J, Xu J, Lee LJ, Lu HC. (2010) mGluR5 in cortical excitatory neurons exerts both cell-autonomous and -nonautonomous influences on cortical somatosensory circuit formation. *J Neurosci* 30:16896-16909

Barres BA. (2008) The mystery and magic of glia: a perspective on their roles in health and disease. *Neuron* 60:430-440

Baumbach GL, Heistad DD. (1988) Cerebral circulation in chronic arterial hypertension. *Hypertension* 12:89-95

Baumbach GL, Heistad DD. (1991) Adaptive changes in cerebral blood vessels during chronic hypertension. *J Hypertens* 9:987-991

Baumbach GL, Sigmund CD, Faraci FM. (2003) Cerebral arteriolar structure in mice overexpressing human renin and angiotensinogen. *Hypertension* 41:50-55

Bayliss WM. (1902) On the local reactions of the arterial wall to changes of internal pressure. *J Physiol* 28:220-231

Beason-Held LL, Moghekar A, Zonderman AB, Kraut MA, Resnick SM. (2007) Longitudinal changes in cerebral blood flow in the older hypertensive brain. *Stroke* 38:1766-1773

Bell RD, Winkler EA, Sagare AP, Singh I, LaRue B, Deane R, Zlokovic BV. (2010) Pericytes control key neurovascular functions and neuronal phenotype in the adult brain and during brain aging. *Neuron* 68:409-427

Bentourkia M, Bol A, Ivanoiu A, Labar D, Sibomana M, Coppens A, Michel C, Cosnard G, De Volder AG. (2000) Comparison of regional cerebral blood flow and glucose metabolism in the normal brain: effect of aging. *Journal of the Neurological Sciences* 181:19-28

Berwick J, Johnston D, Jones M, Martindale J, Martin C, Kennerley AJ, Redgrave P, Mayhew JEW. (2008) Fine detail of neurovascular coupling revealed by spatiotemporal analysis of the hemodynamic response to single whisker stimulation in rat barrel cortex. *Journal of Neurophysiology* 99:787-798

Biber K, Laurie DJ, Berthele A, Sommer B, Tolle TR, Gebicke-Harter PJ, van Calker D, Boddeke HWGM. (1999) Expression and signaling of group I metabotropic glutamate receptors in astrocytes and microglia. *Journal of Neurochemistry* 72:1671-1680

Boegehold M. (2007) Vascular remodeling and rarefaction in hypertension. In: *Comprehensive Hypertension.* (HLip GH, JE., ed), Philadelphia: Mosby/Elsevier, pp 157-166

Bonvento G, Charbonne R, Correze JL, Borredon J, Seylaz J, Lacombe P. (1994) Is Alpha-Chloralose Plus Halothane Induction a Suitable Anesthetic Regimen for Cerebrovascular Research. *Brain Research* 665:213-221

Brayden JE, Earley S, Nelson MT, Reading S. (2008) Transient receptor potential (TRP) channels, vascular tone and autoregulation of cerebral blood flow. *Clin Exp Pharmacol Physiol* 35:1116-1120

Bushong EA, Martone ME, Jones YZ, Ellisman MH. (2002) Protoplasmic astrocytes in CA1 stratum radiatum occupy separate anatomical domains. *Journal of Neuroscience* 22:183-192

Calcinaghi N, Jolivet R, Wyss MT, Ametamey SM, Gasparini F, Buck A, Weber B. (2011) Metabotropic glutamate receptor mGluR5 is not involved in the early hemodynamic response. *J Cereb Blood Flow Metab*

Capone C, Faraco G, Anrather J, Iadecola C. (2010) The Neurovascular Dysfunction Induced by Angiotensin II Requires Activation of EP1 Receptors by Cyclooxygenase 1-Derived Prostaglandin E2. *Stroke* 41:E243-E244

Capone C, Faraco G, Peterson JR, Coleman C, Anrather J, Milner TA, Pickel VM, Davisson RL, Iadecola C. (2012) Central cardiovascular circuits contribute to the neurovascular dysfunction in angiotensin II hypertension. *J Neurosci* 32:4878-4886

Cauli B, Hamel E. (2010) Revisiting the role of neurons in neurovascular coupling. *Front Neuroenergetics* 2:9

Cauli B, Tong XK, Rancillac A, Serluca N, Lambolez B, Rossier J, Hamel E. (2004) Cortical GABA interneurons in neurovascular coupling: relays for subcortical vasoactive pathways. *J Neurosci* 24:8940-8949

Chaigneau E, Tiret P, Lecoq J, Ducros M, Knopfel T, Charpak S. (2007) The relationship between blood flow and neuronal activity in the rodent olfactory bulb. *Journal of Neuroscience* 27:6452-6460

Charpak S, Gahwiler BH. (1991) Glutamate Mediates a Slow Synaptic Response in Hippocampal Slice Cultures. *Proceedings of the Royal Society of London Series B-Biological Sciences* 243:221-226

Chemla S, Chavane F. (2010) Voltage-sensitive dye imaging: Technique review and models. *J Physiol Paris* 104:40-50

Chen BR, Bouchard MB, McCaslin AF, Burgess SA, Hillman EM. (2010) High-speed vascular dynamics of the hemodynamic response. *Neuroimage* 54:1021-1030

Chrissobolis S, Faraci FM. (2008) The role of oxidative stress and NADPH oxidase in cerebrovascular disease. *Trends Mol Med* 14:495-502

Cipolla MJ. (2009) The cerebral circulation

Claassen JAHR, van Beek AHEA, Rikkert MGMO, Jansen RWMM. (2008) Cerebral autoregulation: an overview of current concepts and methodology with special focus on the elderly. *Journal of Cerebral Blood Flow and Metabolism* 28:1071-1085

Cohen Z, Bonvento G, Lacombe P, Hamel E. (1996) Serotonin in the regulation of brain microcirculation. *Prog Neurobiol* 50:335-362

Dahlof B. (2007) Prevention of stroke in patients with hypertension. *Am J Cardiol* 100:17J-24J

Devor A, Hillman EM, Tian P, Waeber C, Teng IC, Ruvinskaya L, Shalinsky MH, Zhu H, Haslinger RH, Narayanan SN, Ulbert I, Dunn AK, Lo EH, Rosen BR, Dale AM, Kleinfeld D, Boas DA. (2008) Stimulus-induced changes in blood flow and 2-deoxyglucose uptake dissociate in ipsilateral somatosensory cortex. *J Neurosci* 28:14347-14357

Devor A, Sakadzic S, Saisan PA, Yaseen MA, Roussakis E, Srinivasan VJ, Vinogradov SA, Rosen BR, Buxton RB, Dale AM, Boas DA. (2011) "Overshoot" of O is required to maintain baseline tissue oxygenation at locations distal to blood vessels. *J Neurosci* 31:13676-13681

Devor A, Sakadzic S, Srinivasan VJ, Yaseen MA, Nizar K, Saisan PA, Tian P, Dale AM, Vinogradov SA, Franceschini MA, Boas DA. (2012) Frontiers in optical imaging of cerebral blood flow and metabolism. *J Cereb Blood Flow Metab*

Diamond ME, von Heimendahl M, Knutsen PM, Kleinfeld D, Ahissar E. (2008) 'Where' and 'what' in the whisker sensorimotor system. *Nat Rev Neurosci* 9:601-612

Drew PJ, Blinder P, Cauwenberghs G, Shih AY, Kleinfeld D. (2010a) Rapid determination of particle velocity from space-time images using the Radon transform. *J Comput Neurosci* 29:5-11

Drew PJ, Shih AY, Driscoll JD, Knutsen PM, Blinder P, Davalos D, Akassoglou K, Tsai PS, Kleinfeld D. (2010b) Chronic optical access through a polished and reinforced thinned skull. *Nat Methods* 7:981-984

Dubeau S, Ferland G, Gaudreau P, Beaumont E, Lesage F. (2011) Cerebrovascular hemodynamic correlates of aging in the Lou/c rat: A model of healthy aging. *Neuroimage* 56:1892-1901

Duchemin S, Boily M, Sadekova N, Girouard H. (2012) The complex contribution of NOS interneurons in the physiology of cerebrovascular regulation. *Front Neural Circuits* 6:51

Dunn AK, Bolay H, Moskowitz MA, Boas DA. (2001) Dynamic imaging of cerebral blood flow using laser speckle. *J Cereb Blood Flow Metab* 21:195-201

Dunn AK, Devor A, Bolay H, Andermann ML, Moskowitz MA, Dale AM, Boas DA. (2003a) Simultaneous imaging of total cerebral hemoglobin concentration, oxygenation, and blood flow during functional activation. *Opt Lett* 28:28-30

Dunn AK, Devor A, Bolay H, Andermann ML, Moskowitz MA, Dale AM, Boas DA. (2003b) Simultaneous imaging of total cerebral hemoglobin concentration, oxygenation, and blood flow during functional activation. *Optics Letters* 28:28-30

Dunn AK, Devor A, Dale AM, Boas DA. (2005) Spatial extent of oxygen metabolism and hemodynamic changes during functional activation of the rat somatosensory cortex. *Neuroimage* 27:279-290

Dupuis F, Vincent JM, Liminana P, Chillon JM, Capdeville-Atkinson C, Atkinson J. (2010) Effects of suboptimal doses of the AT1 receptor blocker, telmisartan, with the angiotensin-converting enzyme inhibitor, ramipril, on cerebral arterioles in spontaneously hypertensive rat. *J Hypertens* 28:1566-1573

Faraci FM. (2006) Protecting the brain with eNOS: run for your life. *Circ Res* 99:1029-1030

Fernandez-Klett F, Offenhauser N, Dirnagl U, Priller J, Lindauer U. (2010) Pericytes in capillaries are contractile in vivo, but arterioles mediate functional hyperemia in the mouse brain. *Proc Natl Acad Sci U S A* 107:22290-22295

Ferraguti F, Shigemoto R. (2006) Metabotropic glutamate receptors. *Cell and Tissue Research* 326:483-504

Fiacco TA, Agulhon C, Taves SR, Petravicz J, Casper KB, Dong X, Chen J, McCarthy KD. (2007) Selective stimulation of astrocyte calcium in situ does not affect neuronal excitatory synaptic activity. *Neuron* 54:611-626

Filosa JA, Bonev AD, Straub SV, Meredith AL, Wilkerson MK, Aldrich RW, Nelson MT. (2006) Local potassium signaling couples neuronal activity to vasodilation in the brain. *Nat Neurosci* 9:1397-1403

Fortepiani LA, Rodrigo E, Ortiz MC, Cachofeiro V, Atucha NM, Ruilope LM, Lahera V, Garcia-Estan J. (1999) Pressure natriuresis in nitric oxide-deficient hypertensive rats: effect of antihypertensive treatments. *J Am Soc Nephrol* 10:21-27

Fox PT, Raichle ME. (1986) Focal Physiological Uncoupling of Cerebral Blood-Flow and Oxidative-Metabolism during Somatosensory Stimulation in Human-Subjects. *Proceedings of the National Academy of Sciences of the United States of America* 83:1140-1144

Fritschy JM, Mohler H. (1995) GABAA-receptor heterogeneity in the adult rat brain: differential regional and cellular distribution of seven major subunits. *J Comp Neurol* 359:154-194

Fujishima M, Ibayashi S, Fujii K, Mori S. (1995) Cerebral blood flow and brain function in hypertension. *Hypertens Res* 18:111-117

Gasparini F, Andres H, Flor PJ, Heinrich M, Inderbitzin W, Lingenhohl K, Muller H, Munk VC, Omilusik K, Stierlin C, Stoehr N, Vranesic I, Kuhn R. (2002) [(3)H]-M-MPEP, a potent, subtype-selective radioligand for the metabotropic glutamate receptor subtype 5. *Bioorg Med Chem Lett* 12:407-409

Gasparini F, Lingenhöhl K, Stoehr N, Flor PJ, Heinrich M, Vranesic I, Biollaz M, Allgeier H, Heckendorn R, Urwyler S, Varney MA, Johnson EC, Hess SD, Rao SP, Sacaan AI, Santori EM, Veliçelebi G, Kuhn R. (1999) 2-Methyl-6-(phenylethynyl)-pyridine (MPEP), a potent, selective and systemically active mGlu5 receptor antagonist. *Neuropharmacology* 38:1493–1503

Girouard H, Bonev AD, Hannah RM, Meredith A, Aldrich RW, Nelson MT. (2010) Astrocytic endfoot Ca2+ and BK channels determine both arteriolar dilation and constriction. *Proc Natl Acad Sci U S A* 107:3811-3816

Girouard H, Iadecola C. (2006) Neurovascular coupling in the normal brain and in hypertension, stroke, and Alzheimer disease. *Journal of Applied Physiology* 100:328-335

Girouard H, Park L, Anrather J, Zhou P, Iadecola C. (2006) Angiotensin II attenuates endothelium-dependent responses in the cerebral microcirculation through Nox-2-derived radicals. *Arteriosclerosis Thrombosis and Vascular Biology* 26:826-832

Girouard H, Park L, Anrather J, Zhou P, Iadecola C. (2007) Cerebrovascular nitrosative stress mediates neurovascular and endothelial dysfunction induced by angiotensin II. *Arteriosclerosis Thrombosis and Vascular Biology* 27:303-309

Gohlke P, Linz W, Scholkens BA, Wiemer G, Unger T. (1996) Cardiac and vascular effects of long-term losartan treatment in stroke-prone spontaneously hypertensive rats. *Hypertension* 28:397-402

Golanov EV, Reis DJ. (1996) Cerebral cortical neurons with activity linked to central neurogenic spontaneous and evoked elevations in cerebral blood flow. *Neurosci Lett* 209:101-104

Goldstein LB, Adams R, Alberts MJ, Appel LJ, Brass LM, Bushnell CD, Culebras A, Degraba TJ, Gorelick PB, Guyton JR, Hart RG, Howard G, Kelly-Hayes M, Nixon JV, Sacco RL. (2006) Primary prevention of ischemic stroke: a guideline from the American Heart Association/American Stroke Association Stroke Council: cosponsored by the Atherosclerotic Peripheral Vascular Disease Interdisciplinary Working Group; Cardiovascular Nursing Council; Clinical Cardiology Council; Nutrition, Physical Activity, and Metabolism Council; and the Quality of Care and Outcomes Research Interdisciplinary Working Group: the American Academy of Neurology affirms the value of this guideline. *Stroke* 37:1583-1633

Gordon GR, Choi HB, Rungta RL, Ellis-Davies GC, MacVicar BA. (2008) Brain metabolism dictates the polarity of astrocyte control over arterioles. *Nature* 456:745-749

Graeber MB. (2010) Changing Face of Microglia. *Science* 330:783-788

Grinvald A, Frostig RD, Siegel RM, Bartfeld E. (1991) High-resolution optical imaging of functional brain architecture in the awake monkey. *Proc Natl Acad Sci U S A* 88:11559-11563

Gurden H, Uchida N, Mainen Z. (2006) Sensory-Evoked Intrinsic Optical Signals in the Olfactory Bulb Are Coupled to Glutamate Release and Uptake. *Neuron* 52:335-345

Haiss F, Jolivet R, Wyss MT, Reichold J, Braham NB, Scheffold F, Krafft MP, Weber B. (2009) Improved in vivo two-photon imaging after blood replacement by perfluorocarbon. *Journal of Physiology-London* 587:3153-3158

Halassa MM, Fellin T, Takano H, Dong JH, Haydon PG. (2007) Synaptic islands defined by the territory of a single astrocyte. *J Neurosci* 27:6473-6477

Hamel E. (2006) Perivascular nerves and the regulation of cerebrovascular tone. *J Appl Physiol* 100:1059-1064

Hamilton NB, Attwell D, Hall CN. (2010) Pericyte-mediated regulation of capillary diameter: a component of neurovascular coupling in health and disease. *Front Neuroenergetics* 2

Heinert G, Casadei B, Paterson DJ. (1998) Hypercapnic cerebral blood flow in spontaneously hypertensive rats. *J Hypertens* 16:1491-1498

Hojna S, Kadlecova M, Dobesova Z, Valouskova V, Zicha J, Kunes J. (2007) The participation of brain NO synthase in blood pressure control of adult spontaneously hypertensive rats. *Mol Cell Biochem* 297:21-29

Hyder F, Patel AB, Gjedde A, Rothman DL, Behar KL, Shulman RG. (2006) Neuronal-glial glucose oxidation and glutamatergic-GABAergic function. *J Cereb Blood Flow Metab* 26:865-877

Iadecola C. (2004) Neurovascular regulation in the normal brain and in Alzheimer's disease. *Nature Reviews Neuroscience* 5:347-360

Iadecola C, Davisson RL. (2008) Hypertension and cerebrovascular dysfunction. *Cell Metabolism* 7:476-484

Imai Y, Kohsaka S. (2002) Intracellular signaling in M-CSF-induced microglia activation: role of Iba1. *Glia* 40:164-174

Jennings JR, Muldoon MF, Ryan C, Price JC, Greer P, Sutton-Tyrrell K, van der Veen FM, Meltzer CC. (2005) Reduced cerebral blood flow response and compensation among patients with untreated hypertension. *Neurology* 64:1358-1365

Jennings JR, Zanstra Y. (2009) Is the brain the essential in hypertension? *Neuroimage* 47:914-921

Jia H, Rustioni A, Valtschanoff JG. (1999) Metabotropic glutamate receptors in superficial laminae of the rat dorsal horn. *J Comp Neurol* 410:627-642

Jolivet R, Magistretti PJ, Weber B. (2009) Deciphering neuron-glia compartmentalization in cortical energy metabolism. *Front Neuroenergetics* 1:4

Jones EG. (1970) On the mode of entry of blood vessels into the cerebral cortex. *J Anat* 106:507-520

Katsuta T. (1997) Decreased local cerebral blood flow in young and aged spontaneously hypertensive rats. *Fukuoka Igaku Zasshi* 88:65-74

Kleinfeld D, Mitra PP, Helmchen F, Denk W. (1998) Fluctuations and stimulus-induced changes in blood flow observed in individual capillaries in layers 2 through 4 of rat neocortex. *Proc Natl Acad Sci U S A* 95:15741-15746

Kocharyan A, Fernandes P, Tong XK, Vaucher E, Hamel E. (2008) Specific subtypes of cortical GABA interneurons contribute to the neurovascular coupling response to basal forebrain stimulation. *J Cereb Blood Flow Metab* 28:221-231

Lawes CM, Vander Hoorn S, Rodgers A. (2008) Global burden of blood-pressure-related disease, 2001. *Lancet* 371:1513-1518

Lecrux C, Hamel E. (2011) The neurovascular unit in brain function and disease. *Acta Physiol (Oxf)* 203:47-59

Lecrux C, Kocharyan A, Sandoe CH, Tong XK, Hamel E. (2012) Pyramidal cells and cytochrome P450 epoxygenase products in the neurovascular coupling response to basal forebrain cholinergic input. *J Cereb Blood Flow Metab*

Lecrux C, Toussay X, Kocharyan A, Fernandes P, Neupane S, Levesque M, Plaisier F, Shmuel A, Cauli B, Hamel E. (2011) Pyramidal neurons are "neurogenic hubs" in the neurovascular coupling response to whisker stimulation. *J Neurosci* 31:9836-9847

Lee JH, Durand R, Gradinaru V, Zhang F, Goshen I, Kim DS, Fenno LE, Ramakrishnan C, Deisseroth K. (2010) Global and local fMRI signals driven by neurons defined optogenetically by type and wiring. *Nature* 465:788-792

Lee RM. (1995) Morphology of cerebral arteries. *Pharmacol Ther* 66:149-173

Leoni RF, Paiva FF, Henning EC, Nascimento GC, Tannus A, de Araujo DB, Silva AC. Magnetic resonance imaging quantification of regional cerebral blood flow and cerebrovascular reactivity to carbon dioxide in normotensive and hypertensive rats. *Neuroimage* 58:75-81

Lieke EE, Frostig RD, Arieli A, Ts'o DY, Hildesheim R, Grinvald A. (1989) Optical imaging of cortical activity: real-time imaging using extrinsic dye-signals and high resolution imaging based on slow intrinsic-signals. *Annu Rev Physiol* 51:543-559

Lin SZ, Sposito N, Pettersen S, Rybacki L, McKenna E, Pettigrew K, Fenstermacher J. (1990) Cerebral capillary bed structure of normotensive and chronically hypertensive rats. *Microvasc Res* 40:341-357

Lindauer U, Leithner C, Kaasch H, Rohrer B, Foddis M, Fuchtemeier M, Offenhauser N, Steinbrink J, Royl G, Kohl-Bareis M, Dirnagl U. (2010) Neurovascular coupling in rat brain operates independent of hemoglobin deoxygenation. *Journal of Cerebral Blood Flow and Metabolism* 30:757-768

Lindauer U, Megow D, Matsuda H, Dirnagl U. (1999) Nitric oxide: a modulator, but not a mediator, of neurovascular coupling in rat somatosensory cortex. *Am J Physiol* 277:H799-811

Liu X, Li C, Falck JR, Harder DR, Koehler RC. (2012) Relative contribution of cyclooxygenases, epoxyeicosatrienoic acids, and pH to the cerebral blood flow response to vibrissal stimulation. *Am J Physiol Heart Circ Physiol* 302:H1075-1085

Lloyd-Fox S, Blasi A, Elwell CE. (2010) Illuminating the developing brain: the past, present and future of functional near infrared spectroscopy. *Neurosci Biobehav Rev* 34:269-284

Logothetis NK, Pauls J, Augath M, Trinath T, Oeltermann A. (2001) Neurophysiological investigation of the basis of the fMRI signal. *Nature* 412:150-157

Lubke J, Feldmeyer D. (2007) Excitatory signal flow and connectivity in a cortical column: focus on barrel cortex. *Brain Struct Funct* 212:3-17

Mathiisen TM, Lehre KP, Danbolt NC, Ottersen OP. (2010) The perivascular astroglial sheath provides a complete covering of the brain microvessels: an electron microscopic 3D reconstruction. *Glia* 58:1094-1103

McCaslin AF, Chen BR, Radosevich AJ, Cauli B, Hillman EM. (2010) In vivo 3D morphology of astrocyte-vasculature interactions in the somatosensory cortex: implications for neurovascular coupling. *J Cereb Blood Flow Metab* 31:795-806

Metea MR, Newman EA. (2006) Glial Cells Dilate and Constrict Blood Vessels: A Mechanism of Neurovascular Coupling. *Journal of Neuroscience* 26:2862-2870

Mikolajczyk K, Szabatin M, Rudnicki P, Grodzki M, Burger C. (1998a) A JAVA environment for medical image data analysis: initial application for brain PET quantitation. *Med Inform (Lond)* 23:207-214

Mikolajczyk K, Szabatin M, Rudnicki P, Grodzki M, Burger C. (1998b) A JAVA environment for medical image data analysis: Initial application for brain PET quantitation. *Medical Informatics* 23:207-214

Milicevic Sephton S, Mu L, Schweizer WB, Schibli R, Kramer SD, Ametamey SM. (2012) Synthesis and evaluation of novel alpha-fluorinated (E)-3-((6-methylpyridin-2-yl)ethynyl)cyclohex-2-enone-O-methyl oxime (ABP688) derivatives as metabotropic glutamate receptor subtype 5 PET radiotracers. *J Med Chem* 55:7154-7162

Miller S, Romano C, Cotman CW. (1995) Growth-Factor up-Regulation of a Phosphoinositide-Coupled Metabotropic Glutamate-Receptor in Cortical Astrocytes. *Journal of Neuroscience* 15:6103-6109

Mosso A. (1881) Ueber den Kreislauf des Blutes im Menschlichen Gehirn. *Leipzig.*

Mudo G, Trovato-Salinaro A, Caniglia G, Cheng QZ, Condorelli DF. (2007) Cellular localization of mGluR3 and mGluR5 mRNAs in normal and injured rat brain. *Brain Research* 1149:1-13

Mulligan SJ, MacVicar BA. (2004) Calcium transients in astrocyte endfeet cause cerebrovascular constrictions. *Nature* 431:195-199

Nizar KW, Reznichenko L, Cheng Q, Sakadzic S, Boas DA, Masliah E, Dale AM, Silva GA, Devor A. (2010) Unreliable and delayed astrocytic calcium response does not support the hypothesis of calcium-dependent astrocytic regulation of blood flow. In: *Program No. 192.9/FFF13. 2010 Neuroscience Meeting Planner. San Diego, CA: Society for Neuroscience, 2010. Online* (Planner. NM, ed

Notenboom RG, Hampson DR, Jansen GH, van Rijen PC, van Veelen CW, van Nieuwenhuizen O, de Graan PN. (2006) Up-regulation of hippocampal metabotropic glutamate receptor 5 in temporal lobe epilepsy patients. *Brain* 129:96-107

O'Rourke MF, Hashimoto J. (2007) Mechanical factors in arterial aging: a clinical perspective. *J Am Coll Cardiol* 50:1-13

Oberheim NA, Wang XH, Goldman S, Nedergaard M. (2006) Astrocytic complexity distinguishes the human brain. *Trends in Neurosciences* 29:547-553

Ohta K, Gotoh F, Shimazu K, Amano T, Komatsumoto S, Hamada J, Takahashi S. (1991) Locus coeruleus stimulation exerts different influences on the dynamic changes of cerebral pial and intraparenchymal vessels. *Neurol Res* 13:164-167

Okamoto K, Aoki K. (1963) Development of a strain of spontaneously hypertensive rats. *Jpn Circ J* 27:282-293

Orbach HS, Cohen LB, Grinvald A. (1985) Optical mapping of electrical activity in rat somatosensory and visual cortex. *J Neurosci* 5:1886-1895

Paulson OB, Strandgaard S, Edvinsson L. (1990) Cerebral autoregulation. *Cerebrovasc Brain Metab Rev* 2:161-192

Pellerin L, Magistretti PJ. (1994) Glutamate Uptake into Astrocytes Stimulates Aerobic Glycolysis - a Mechanism Coupling Neuronal-Activity to Glucose-Utilization. *Proceedings of the National Academy of Sciences of the United States of America* 91:10625-10629

Peppiatt CM, Howarth C, Mobbs P, Attwell D. (2006) Bidirectional control of CNS capillary diameter by pericytes. *Nature* 443:700-704

Perea G, Araque A. (2005) Properties of synaptically evoked astrocyte calcium signal reveal synaptic information processing by astrocytes. *Journal of Neuroscience* 25:2192-2203

Perea G, Navarrete M, Araque A. (2009) Tripartite synapses: astrocytes process and control synaptic information. *Trends Neurosci* 32:421-431

Petersen CCH, Hahn TTG, Mehta M, Grinvald A, Sakmann B. (2003) Interaction of sensory responses with spontaneous depolarization in layer 2/3 barrel cortex. *Proceedings of the National Academy of Sciences of the United States of America* 100:13638-13643

Petzold GC, Albeanu DF, Sato TF, Murthy VN. (2008) Coupling of neural activity to blood flow in olfactory glomeruli is mediated by astrocytic pathways. *Neuron* 58:897-910

Petzold GC, Murthy VN. (2011) Role of astrocytes in neurovascular coupling. *Neuron* 71:782-797

Purves D, Augustine GL, Fitzpatrick D, Hall CW, LaMantia A, McNamara JO, Williams SM. (2004) Neuroscience:Third edition. Sinauer Associates, Inc.,Publishers Sunderland, Massachusetts U.S.A.

Raichle ME, Mintun MA. (2006a) Brain work and brain imaging. *Annu Rev Neurosci* 29:449-476

Raichle ME, Mintun MA. (2006b) Brain work and brain imaging. *Annual Review of Neuroscience* 29:449-476

Ritz MF, Fluri F, Engelter ST, Schaeren-Wiemers N, Lyrer PA. (2009) Cortical and Putamen Age-Related Changes in the Microvessel Density and Astrocyte Deficiency in Spontaneously Hypertensive and Stroke-Prone Spontaneously Hypertensive Rats. *Current Neurovascular Research* 6:279-287

Roy CS, Sherrington MB. (1890) On the regulation of the blood-supply of the brain. *Journal of Physiology London* 11:85-108

Sabbatini M, Tomassoni D, Amenta F. (2001) Hypertensive brain damage: comparative evaluation of protective effect of treatment with dihydropyridine derivatives in spontaneously hypertensive rats. *Mechanisms of Ageing and Development* 122:2085-2105

Sacco RL. (2001) Newer risk factors for stroke. *Neurology* 57:S31-34

Sakadzic S, Yuan S, Dilekoz E, Ruvinskaya S, Vinogradov SA, Ayata C, Boas DA. (2009) Simultaneous imaging of cerebral partial pressure of oxygen and blood flow during functional activation and cortical spreading depression. *Appl Opt* 48:D169-177

Schummers J, Yu H, Sur M. (2008) Tuned responses of astrocytes and their influence on hemodynamic signals in the visual cortex. *Science* 320:1638-1643

Scott NA, Murphy TH. (2012) Hemodynamic responses evoked by neuronal stimulation via channelrhodopsin-2 can be independent of intracortical glutamatergic synaptic transmission. *PLoS One* 7:e29859

Shimizu H, Watanabe E, Hiyama TY, Nagakura A, Fujikawa A, Okado H, Yanagawa Y, Obata K, Noda M. (2007) Glial Nax channels control lactate signaling to neurons for brain [Na+] sensing. *Neuron* 54:59-72

Sokoloff L. (1960) The metabolism of the central nervous system in vivo. *Handbook of Physiology, Section I, Neurophysiology* 3:1843-1864

Sokoloff L. (1989) Circulation and energy metabolism of the brain. *New York: Raven Press.*

Struijker Boudier HA, le Noble JL, Messing MW, Huijberts MS, le Noble FA, van Essen H. (1992) The microcirculation and hypertension. *J Hypertens Suppl* 10:S147-156

Takano T, Tian GF, Peng WG, Lou NH, Libionka W, Han XN, Nedergaard M. (2006) Astrocyte-mediated control of cerebral blood flow. *Nature Neuroscience* 9:260-267

Takata N, Hirase H. (2008) Cortical layer 1 and layer 2/3 astrocytes exhibit distinct calcium dynamics in vivo. *PLoS One* 3:e2525

Tian P, Teng IC, May LD, Kurz R, Lu K, Scadeng M, Hillman EM, De Crespigny AJ, D'Arceuil HE, Mandeville JB, Marota JJ, Rosen BR, Liu TT, Boas DA, Buxton RB, Dale AM, Devor A. (2010) Cortical depth-specific microvascular dilation underlies laminar differences in blood oxygenation level-dependent functional MRI signal. *Proc Natl Acad Sci U S A* 107:15246-15251

Toda N, Ayajiki K, Okamura T. (2009) Cerebral blood flow regulation by nitric oxide: recent advances. *Pharmacol Rev* 61:62-97

Tsai PS, Kaufhold JP, Blinder P, Friedman B, Drew PJ, Karten HJ, Lyden PD, Kleinfeld D. (2009) Correlations of neuronal and microvascular densities in murine cortex revealed by direct counting and colocalization of nuclei and vessels. *J Neurosci* 29:14553-14570

Van Den Pol AN, Romano C, Ghosh P. (1995) Metabotropic Glutamate Receptor mGluR5 Subcellular Distribution and Developmental expression in Hypothalamus. *The Journal of Comparative Neurology* 362:134-150

van der Loo B, Schildknecht S, Zee R, Bachschmid MM. (2009) Signalling processes in endothelial ageing in relation to chronic oxidative stress and their potential therapeutic implications in humans. *Exp Physiol* 94:305-310

Vannucci SJ, Maher F, Simpson IA. (1997) Glucose transporter proteins in brain: delivery of glucose to neurons and glia. *Glia* 21:2-21

Vaucher E, Hamel E. (1995) Cholinergic Basal Forebrain Neurons Project to Cortical Microvessels in the Rat - Electron-Microscopic Study with Anterogradely Transported Phaseolus-Vulgaris-Leukoagglutinin and Choline-Acetyltransferase Immunocytochemistry. *Journal of Neuroscience* 15:7427-7441

Wang XH, Lou NH, Xu QW, Tian GF, Peng WG, Han XN, Kang J, Takano T, Nedergaard M. (2006) Astrocytic Ca2+ signaling evoked by sensory stimulation in vivo. *Nature Neuroscience* 9:816-823

Weber B, Burger C, Biro P, Buck A. (2002) A femoral arteriovenous shunt facilitates arterial whole blood sampling in animals. *European Journal of Nuclear Medicine and Molecular Imaging* 29:319-323

Weber B, Burger C, Wyss MT, von Schulthess GK, Scheffold F, Buck A. (2004) Optical imaging of the spatiotemporal dynamics of cerebral blood flow and oxidative metabolism in the rat barrel cortex. *European Journal of Neuroscience* 20:2664-2670

Weber B, Keller AL, Reichold J, Logothetis NK. (2008) The microvascular system of the striate and extrastriate visual cortex of the macaque. *Cereb Cortex* (in press)

Wei L, Lin SZ, Tajima A, Nakata H, Acuff V, Patlak C, Pettigrew K, Fenstermacher J. (1992) Cerebral glucose utilization and blood flow in adult spontaneously hypertensive rats. *Hypertension* 20:501-510

Winship IR, Plaa N, Murphy TH. (2007) Rapid astrocyte calcium signals correlate with neuronal activity and onset of the hemodynamic response in vivo. *Journal of Neuroscience* 27:6268-6272

Wyss MT, Ametamey SM, Treyer V, Bettio A, Blagoev M, Kessler LJ, Burger C, Weber B, Schmidt M, Gasparini F, Buck A. (2007) Quantitative evaluation of ^{11}C-ABP688 as PET ligand for the measurement of the metabotropic glutamate

receptor subtype 5 using autoradiographic studies and a beta-scintillator. *Neuroimage* 35:1086-1092

Wyss MT, Jolivet R, Buck A, Magistretti PJ, Weber B. (2010) In vivo evidence for lactate as a neuronal energy source. *J Neurosci* 31:7477-7485

Wyss MT, Obrist NM, Haiss F, Eckert R, Stanley R, Burger C, Buck A, Weber B. (2009) A beta-scintillator for surface measurements of radiotracer kinetics in the intact rodent cortex. *Neuroimage* 48:339-347

Yamanishi S, Katsumura K, Kobayashi T, Puro DG. (2006) Extracellular lactate as a dynamic vasoactive signal in the rat retinal microvasculature. *Am J Physiol Heart Circ Physiol* 290:H925-934

Yemisci M, Gursoy-Ozdemir Y, Vural A, Can A, Topalkara K, Dalkara T. (2009) Pericyte contraction induced by oxidative-nitrative stress impairs capillary reflow despite successful opening of an occluded cerebral artery. *Nat Med* 15:1031-1037

Zakharov P, Volker AC, Wyss MT, Haiss F, Calcinaghi N, Zunzunegui C, Buck A, Scheffold F, Weber B. (2009) Dynamic laser speckle imaging of cerebral blood flow. *Opt Express* 17:13904-13917

Zhang ET, Inman CB, Weller RO. (1990) Interrelationships of the pia mater and the perivascular (Virchow-Robin) spaces in the human cerebrum. *J Anat* 170:111-123

Zlokovic BV. (2005) Neurovascular mechanisms of Alzheimer's neurodegeneration. *Trends Neurosci* 28:202-208

Zlokovic BV. (2008) The blood-brain barrier in health and chronic neurodegenerative disorders. *Neuron* 57:178-201

Zonta M, Angulo MC, Gobbo S, Rosengarten B, Hossmann KA, Pozzan T, Carmignoto G. (2003) Neuron-to-astrocyte signaling is central to the dynamic control of brain microcirculation. *Nature Neuroscience* 6:43-50